uOttawa

L'Université canadienne
Canada's university

FACULTÉ DES ÉTUDES SUPÉRIEURES ET POSTOCTORALES

uOttawa

L'Université canadienne
Canada's university

FACULTY OF GRADUATE AND POSDOCTORAL STUDIES

Garfield Downes
AUTEUR DE LA THÈSE / AUTHOR OF THESIS

M.A.Sc. (Electrical Engineering)
GRADE / DEGREE

School of Information Technology and Engineering
FACULTÉ, ÉCOLE, DÉPARTEMENT / FACULTY, SCHOOL, DEPARTMENT

Characterisation and Performance Prediction of Narrowband MIMO Channels

TITRE DE LA THÈSE / TITLE OF THESIS

T. Willink
DIRECTEUR (DIRECTRICE) DE LA THÈSE / THESIS SUPERVISOR

C. D`Amours
CO-DIRECTEUR (CO-DIRECTRICE) DE LA THÈSE / THESIS CO-SUPERVISOR

EXAMINATEURS (EXAMINATRICES) DE LA THÈSE / THESIS EXAMINERS

Y. Mao

A. Banihashemi

Gary W. Slater
Le Doyen de la Faculté des études supérieures et postdoctorales / Dean of the Faculty of Graduate and Postdoctoral Studies

Characterisation and Performance Prediction of Narrowband MIMO Channels

by

Garfield Orlando Downes, B.A.Sc.

Thesis submitted to the
Faculty of Graduate and Postdoctoral Studies
In partial fulfillment of the requirements
For the M.A.Sc. degree in
Electrical and Computer Engineering

School of Information Technology and Engineering
Faculty of Engineering
University of Ottawa

Your file Votre référence
ISBN: 978-0-494-18413-4
Our file Notre référence
ISBN: 978-0-494-18413-4

Acknowledgements

I would like to extend my sincere thanks to my supervisor, Associate Professor Claude D'Amours for letting me dictate the pace of my research, giving me freedom to a large extent on the choice of topics, his invaluable guidance and encouragement, and for giving me invaluable insight into my research in coding systems.

I would also like to extend my thanks to Dr. Tricia Willink of the Communications Research Centre (CRC) for supervising my research and experiments. Her input and supervision have greatly refined the scope of this work including a paper presented at Wireless 2005 summarising preliminary results. The work in this thesis was supported by the Radio Communications Technologies section under the Defence Communications Program, to which Dr. Tricia Willink, Geoff Colman, and Chris Squires have contributed a significant amount of research including their efforts in undertaking an extensive measurement campaign.

I would also like to thank: Dr. Colin Brown and Dr. Yvo DeJong for their discussions and input on the results presented in this work including making my experiences at CRC pleasant; Stephan Chan (Masters student, University of Ottawa), Jeffery Wells (co-op student, Memorial University), Luis Gurrieri (Masters Student, University of Manitoba) for being great office mates; Professor Abbas Yongaçoglu, and Professor Derek McNamara for answering my queries.

My sincere thanks to CRC for their support under the Spectrum Research Program and use of facilities, data, and research presentations. My thanks to the Department of Electrical Engineering, School of Information and Technology and Engineering (SITE) as well for supporting this research through various research fellowships and teaching assistantships.

Finally, I would like to thank my parents and sisters who have always encouraged me in my quest for higher education and especially my girlfriend and friend of many years Jacy

Cormier for encouraging me and listening to my occasional laments and for supporting my many decisions.

Abstract

Wireless communication using multiple-input multiple-output (MIMO) technology enables increased spectral efficiency. The successful deployment of commercial MIMO systems requires a strong understanding of the channel conditions to achieve desired BER performance. A simple channel model that is frequently used in MIMO research assumes i.i.d.complex Gaussian distributed channel gains to describe the channel links. However, this model ignores common propagation effects present in outdoor environments. On the other hand, the wireless channel is very complex to describe using closed-form expressions.

The objective of the work presented in this thesis is to parameterise the wireless channel using metrics and use these to predict the bit-error rate (BER) performance for different simulated MIMO techniques. The data measurements were obtained in Ottawa, Ontario at approximately 2 GHz, using the CRC MIMO testbed. Communications systems employing spatial multiplexing or space-time block coding (STBC) are mainly designed for operation under ideal channel characteristics. We consider 1) Vertical-Bell Labs Layered Space-Time (V-BLAST) architecture and 2) a QPSK-based quasi-orthogonal STBC.

The measured data exhibit different location-specific characteristics. In some regions, the spatial correlation is low resulting in high diversity and high available mutual information. In others, spatial correlation is higher. Of all the metrics considered, we have identified six that provide useful information to describe the wireless channel. These include effective channel rank, correlation and diversity. The impact of signal power has also been investigated.

It has been found that the performance spatial multiplexing is dominantly dependent on the smallest eigenvalue of the spatial correlation matrix. It is not, however, as useful in predicting the performance of STBC. Spatial correlations appear to improve the BER performance of STBC by improving the effective average SNR. It is important to note this trend is opposite to

that found in spatial multiplexing. The largest eigenvalue also appears to have an impact on STBC performance. Also, it is shown that mutual information is sufficient enough to describe channel behaviour. These metrics give insight into the dominant propagation mechanisms in the environment and demonstrate the effectiveness of this kind of measurements in characterising the behaviour of the mobile radio channel.

Contents

List of Tables

List of Figures

List of Symbols

$\alpha(\mathcal{H})$ Path-loss estimate

χ Effective degrees of freedom estimate

γ Average signal-to-noise ratio

$\hat{e}$ Normalised mean-squared error

κ Coefficient of correlation

λ Eigenvalue

$\theta_d(\rho)$ Kronecker correlation matrix

$\mathrm{C}(\mathrm{s})$ Space-time code matrix

G Nulling matrix

Q Signal covariance matrix

R Correlation matrix of vectorised **H**

$\overline{CC}(\mathcal{H})$ Normalised parallel channel capacity

$\overline{CG}(\mathcal{H})$ Normalised parallel channel gain

$\overline{I}(\mathcal{H})$ Average mutual information

$\overline{I}_s(\mathcal{H})$ Normalised average mutual information

$\overline{R}(\mathcal{H})$ Effective rank

$\mathbf{\Phi}_M$ Transmitter correlation matrix

$\mathbf{\Phi}_N$ Receive correlation matrix

$\Phi(\mathbf{R})$ Correlation measure estimate

$\mathbf{\Phi}_S$ Scatterer correlation matrix

$\Psi(\mathbf{R})$ Diversity measure estimate

ρ Correlation coefficient

σ Singular value

φ Multipath richness

G Fraction of the maximum singular value σ_{max}

I_{outage} Outage mutual information

K Number of narrowband channel realisation subsets

M Number of transmit antennas

N Number of receive antennas

$P(\mathcal{H})$ Average signal strength

q Reference outage ratio

T Number of transmitted symbols

V Number of time slots in a data block

s Spatially-multiplexed transmitted symbol vector

S Number of effective scatterers

List of Abbreviations

AB20	Route AB20 in Rural Ottawa
AB35	Route AB35 in Suburban Ottawa
AOA	Angle of Arrival
BER	Bit-Error Rate
CC25	Route CC25 in Suburban Ottawa
CDF	Cumulative Distribution Function
CG	Complex Gaussian
CRC	Communications Research Centre
CSI	Channel State Information
DD15	Route DD15 in Suburban Ottawa
DFL	David Florida Laboratory
EDOF	Effective Degrees of Freedom
EF0	Route EF0 in Suburban Ottawa
FA20	Route FA20 in Urban Ottawa

FFT	Fast Fourier Transform
GPS	Global Positioning System
IFFT	Inverse Fast Fourier Transform
IR	Impulse Response
LOS	Line-of-Sight
MA	Multiple Access
MIMO	Multiple Input Multiple Output
MQ30	Route MQ30 in Suburban Ottawa
ML	Maximum Likelihood
MMSE	Minimum Mean-Squared Error
NMSE	Normalised Mean-Squared Error
OFDM	Orthogonal Frequency Division Multiplex
OSDM	Orthogonal Space Division Multiplex
PFA	Probability of False Alarm
PN	Pseudo-Noise
PSD	Power Spectrum Density
QPSK	Quadrature Phase Shift Keying
SISO	Single Input Single Output

SITE	School of Information Technology and Engineering
SNR	Signal-to-nose ratio
STBC	Space-Time Block Code
TIRE	Thresholded Impulse Response Estimate
UIRE	Unthresholded Impulse Response Estimate
V-BLAST	Vertical-Bell Labs Layered Space-Time
ZF	Zero Forcing

List of Notations

Throughout this thesis, we use the following notations. Matrices and vectors are denoted as boldface upper case and lower case, respectively. Commonly used operations and definitions are defined below.

$N \times M$	Denotes a matrix with N nows and M columns
$x_{i,j}$	If **X** is a matrix, $x_{i,j}$ refers to the element at the i^{th} row and the j^{th} column
x_i	If **x** is a vector, x_i indicates the i^{th} element of **x**
$\mathcal{E}\{\cdot\}$	Denotes the Expectation operator
$\|\|\cdot\|\|_F$	Denotes the Frobenius norm operator
$\mathbf{I}_n$	Denotes an $n \times n$ identity matrix
$\otimes$	Denotes the Kronecker operator
$\max_{X,Y}$	Denotes the maximum of X subject to the constraint Y
$\log_x(\cdot)$	Denotes the base x logarithmic operator
$\det(\cdot)$	Denotes the determinant operator
$(\cdot)^H$	The superscript denotes the Hermitian transpose operator
$\mathbf{x}_i$	If **X** is a matrix, $\mathbf{x}_i$ indicates the i^{th} column vector of **X**

$\min(X, Y)$	Denotes the minimum of the pair X, Y
$\text{vec}(\mathbf{H})$	Denotes a vector formed by stacking all columns of matrix $\mathbf{H}$ into a single column vector
$\text{tr}(\mathbf{X})$	If $\mathbf{X}$ is a square matrix, $\text{tr}(\mathbf{X})$ is the sum of the diagonal elements
$(\cdot)^T$	The superscript denotes the transpose operator
$\mathcal{R}\text{e}(x)$	Denotes the real part of x where x is complex
$(\cdot)^*$	Denotes the complex conjugate operator
$\mathcal{I}\text{m}(x)$	Denotes the imaginary part of x where x is complex
$\text{var}(\mathbf{x})$	If $\mathbf{x}$ is a vector, $\text{var}(\mathbf{x})$ is the variance of $\mathbf{x}$
$\text{cov}(\mathbf{x}, \mathbf{y})$	If $\mathbf{x}$ and $\mathbf{y}$ are vectors, $\text{cov}(\mathbf{x}, \mathbf{y})$ is the covariance of $\mathbf{x}$ and $\mathbf{y}$

Chapter 1

Overview of Thesis

1.1 Introduction

In wireless communications systems, there is an endless demand for increased capacity and improved quality. Researchers have studied ways to address these issues by using multiple antennas in an effort to improve performance of the wireless link.

Performance, which depends on the application, is often measured as the spectral efficiency (bps/Hz) that the channel can provide. The capacity of wireless channels can be increased without using additional bandwidth or power by using multiple-input multiple-output (MIMO) technology. MIMO configurations exploit the spatial diversity of the multipath channel by using arrays of M and N antenna elements at the transmitter and receiver, respectively. The bit-error rate (BER) performance is a feature of the signal processing and describes how much information can be reliably transmitted through the channel. For a given channel and processing technique, maximum BER performance and reliability is desired the most.

A typical wireless channel as encountered by a mobile device is depicted in Figure 1.1. The presence of scattering objects, terrain, and the dynamic nature of the mobile all affect the response of the wireless channel and can potentially degrade system performance.

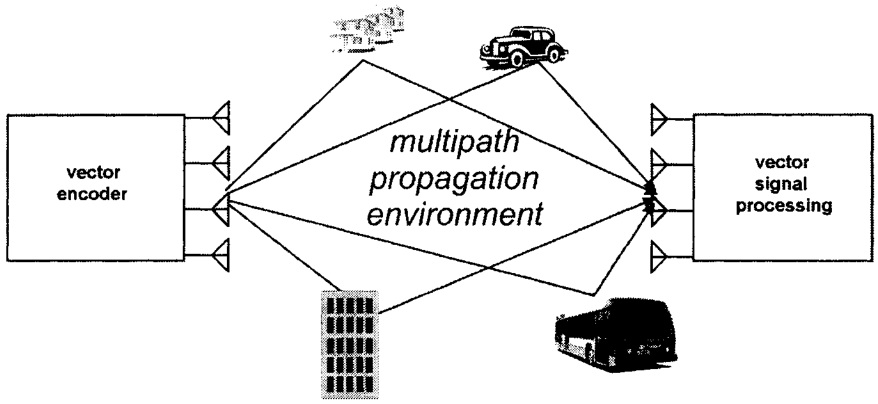

Figure 1.1: Illustration of a local multipath environment.

For a system designer, the utilisation of MIMO technology requires an understanding of the site-specific behaviour of the mobile radio channel. Industry Canada is interested in seeing the real capacity gains using a given MIMO technique in different microcells. The appropriate bandwidths need to be properly assigned to achieve an acceptable level of operation.

To date, there are many publications that study the parameterisation of narrowband MIMO communications channels using channel models developed that emulate propagation conditions. However, these models ignore typical propagation effects such as refraction, diffraction and reflection or correlations between the different channel links, all of which are present in the outdoor channel. The most accurate method to determine channel behaviour at a given site is through analysis of channel measurements and few research studies use these results to predict BER performances reliably. Most research uses less accurate empirical methods.

1.2 Literature Review

There has been considerable amount of literature devoted to the characterisation/parameterisation of the mobile radio channel. A review of outdoor measurement and theoretical modeling literature is given next.

1.2.1 Wireless Channel Studies

An interest in understanding the behaviour of wireless MIMO systems has prompted many field measurement campaigns within the last 10 years [1–5]. Wallace and Jensen [1] report on the development of an experimental 4×4 platform designed to measure the channel matrix for indoor and outdoor MIMO channels. This system allows the characterisation of multipath MIMO channels without the need for lengthly statistical analysis and difficult ray tracing methods. In 2002, Ling *et al.* surveyed narrowband MIMO channel measurements in downtown Manhattan using a 16×16 system [2] and obtained results similar to those predicted by theory for full scattering channels.

Statistical studies of MIMO channels in [3] use channel impulse response estimates to model paths with different delays and associated correlation matrices. This system, different from [1], allows for the extraction of paths to determine correlation coefficients using varying antenna polarisations to help observe resolvable multipath behaviour.

In [4], the effect of scattering clusters in outdoor MIMO channels is investigated. Results summarise the impact of the number of scattering clusters on system performance based on correlation coefficients, channel capacity, and angular spread distributions.

Six measurement campaigns are reported [6–10] that determine the angular spread of signals arriving at the mobile receiver. Measurements in Frankfurt, Germany, which has a strong resemblance to American cities with mountainous profiles (high-rise center, surrounded by low-rise buildings) are described in [6]. In [7], measurements in Paris, France, use direction-of-arrival at the mobile to identify how a far scatterer cluster affects delay dispersion. In [8], measurements in Mulhouse, France demonstrate the phenomenon of a rank deficient channel. However, the lack of scattering clusters, small angular spread, and little received signal energy from the direction of the mobile are opposite to that expected in a poor channel due to low rank. Measurements in Helsinki, Finland [9] characterise scattering clusters and their associated power distributions. The power distributions for a given location are useful in modeling signal interactions specific to the local environment. In Stockholm, Sweden [10] rank deficient behaviour was observed in urban areas characterised by multiple clusters. However, the low rank typical of a simple channel was present in a rich-scattering environment.

Measurements in [5] helped in establishing a model that describes the capacity behaviour of the outdoor channel accurately by determining the key propagation parameters and the conditions needed to establish a high-rank MIMO channel where system throughput is high.

1.2.2 Theoretical Studies

The mobile radio channel has been extensively studied using theoretical models such as Rayleigh. Foschini and Gans [11] and Teletar [12] examined the theoretical limits of the capacity of wireless MIMO communications systems. A fading environment is used to demonstrate the effects on capacity, receiver/transmitter diversity, and mutual information in an ideal Rayleigh-fading case. In [13], Goldsmith *et al.* summarised capacity limits of MIMO systems in multiple access (MA) channels by first exploring single-user channels and then exploiting MIMO technologies to enable multiple access, thereby increasing spectral efficiency. Sklar [14] presented a tutorial describing small-scale and large-scale fading in a wireless communications system. Biglieri [15] presents a complete review of wireless communications systems including statistical models of fading channels, the impact of fading channels on code design, and the effect of fading on mutual information, described as the important figures of merit.

Other theoretical studies on wireless MIMO communications include [11, 16–21] which study the effect of fading correlations on the performance of MIMO systems primarily using mutual information and outage probability as performance descriptors.

With respect to spatial channel correlations and geometric scattering models, research in [22] and [23] serves to characterise and model scattering in wireless channels linked by correlation through the diagonal entries of the covariance matrix. In [22] we find geometrical scattering models such as one-ring, combined-elliptical-ring, one-disk and double-bounce that closely describe real signal interactions in an outdoor wireless channel. They demonstrate the positive impact of diagonal correlations on channel capacity and compensate for receive and transmit correlations. Shin and Lee [23] study MIMO fading channels by observing fading correlations using double scattering propagation models. By controlling the effective number of scatterers and correlation parameters at the transmitter/receiver, they demonstrate the impact on mutual information and channel rank. For outdoor environments, models presented in [24] help explain the rank deficient behaviour of channels where correlation in the channel matrix is zero yet only a single degree of freedom exists.

The orientation of the receive/transmit antenna arrays is often omitted in research on the performance of wireless channels. The MIMO scattering model in [25] looks theoretically at the impact of antenna array orientation on channel spatial correlation and mutual information. Orientation affects the observed angle of arrival distributions and the average spread of incoming signals. For the purposes of this thesis, we do not consider array orientation since such information is contained within measurements and is not easily extracted.

There are a number of studies that present a means of quantifying channels [26–32]. Ivrlač and Nossek [26] quantify the amount of diversity and correlation present in a fading MIMO channel separable at the transmitter, receiver or combined. Environmental issues for MIMO systems are discussed in [27] where information theoretic capacity is the main performance metric using an informed/uninformed transmitter and varying levels of channel complexity, for example, interferers.

Burel [28] uses random matrix theory to perform a statistical analysis on the smallest singular value in MIMO transmission systems relating to the minimum distance of received vectors; an important factor in the performance of certain types of MIMO techniques. Heath and Dandekar [29], [30] illustrate various characterisation metrics for narrowband MIMO channels and present results for a 7×7 system operating in an outdoor urban area through simulation. In total, 4 possible metrics are presented, each fulfilling a different set of requirements. Recognising the need for performance using site-specific data, they simulate downtown Austin, Texas, using electromagnetic ray-tracing software. Characterisation in [31] of MIMO channels is done using Euclidean distances to quantify spatial multiplexing and diversity. In analysing high-rank line-of-sight MIMO channels in [32] a description for the effective degrees of freedom quantifies the number of spatial data pipes available in the channel, thus mirroring the result of mutual information.

1.3 Objective of Thesis

This thesis focuses on the characterisation of outdoor narrowband MIMO channels using metrics and the performance prediction of different techniques operating on these channels. Chapter 3 through Chapter 6 contain the main contributions which can be summarised as follows:

- We describe the behaviour of a wireless MIMO channel using a suitable set of channel metrics obtained from measured channel responses;
- Using metrics introduced by Irvlač and Nossek [26], we evaluate the amount of diversity and correlation present in the wireless channel using measured channel responses;
- We simulate the BER performance of spatial multiplexing and space-time block coding using measured channel responses;

- We evaluate the BER performance of spatial multiplexing and space-time block coding over spatially correlated MIMO channels using Monte-Carlo simulation techniques;
- We analyse complex impulse response data from extensive outdoor urban, suburban, and rural measurement campaigns performed in Ottawa;
- We compare the simulated BER performance of spatial multiplexing and space-time block coding to the parameterised channel metrics;
- We obtain a first-order BER performance prediction using the above results;
- We use measured channel data to show that the channel eigenvalues are preferred over mutual information as the best performance measure for a MIMO channel; and
- We show that the channel eigenvalues are an important performance indicator for system design and is independent of location;

Furthermore, there are many potential applications to which the measured channel responses can be applied [33]. Bandwidth allocation is an important design criteria for wireless system designers. The bandwidth assigned to each user in a MIMO communications system must not be large enough to cause frequency selective fading. System planners and academic researchers can use the information presented in this thesis to properly develop a system capable of operating in an outdoor environment. Such systems designed with theoretical models for propagation may fail in a given scenerio, leaving the operator and end user to cope with poor system performance.

1.4 Content of Thesis

This thesis is divided into 7 major chapters, as follows. In Chapter 2, we introduce MIMO for mobile radio channels. The propagation characteristics and types of mathematical channel models available are discussed. Channel paramaterisation using quantitative metrics are given to characterise the mobile channel. Lastly, we briefly discuss space-time architecture and coding schemes.

In Chapter 3, we introduce the MIMO testbed used in this work, our channel model, methods for impulse extraction, noise effects on mutual information estimates, and reasoning for metric subset selection.

In Chapter 4, we present our outdoor channel measurement campaign in urban, suburban and rural Ottawa, Ontario and include a description of the test, measurement setup, and site local to the mobile receiver.

In Chapter 5, we present the parameterised channel results and BER performance for urban, suburban and rural Ottawa using different MIMO techniques. The chapter concludes with a site analysis to correlate metric results with location.

In Chapter 6, we introduce the methodology used to predict performance of MIMO techniques in the mobile channel. Linear regression and the coefficient of correlation are used to evaluate BER versus metric results to determine a suitable predictor. The chapter concludes by showing prediction results using the best predictor the measurement campaign.

In Chapter 7, the contributions of the previous chapters are summarised and conclusions based on 1) MIMO technique, 2) location, and 3) channel metric are presented. The chapter concludes by describing future work that could be undertaken.

Chapter 2

MIMO for Mobile Radio Channels

In this chapter we review the propagation characteristics of mobile radio channels. We then discuss MIMO channel models and define a collection of metrics used to parameterise them. We then highlight current space-time technologies that employ MIMO techniques.

MIMO systems employ multiple antennas at both the transmitter and receiver. This enables the use of spatial multiplexing and/or diversity gains through space-time coding techniques. In general, research on MIMO systems assume the following:

1. The power and angular spread of the signals follow a Rayleigh distribution with wide, often uniform angular distribution;
2. There exists sufficient richness of multipath components; and
3. The transmit/receive antennas are identical and arranged to achieve decorrelation and low mutual coupling between elements.

Teletar [12], Foschini and Gans [11] used these assumptions to determine the limits, trends and performance of a MIMO communication channel. However, the behaviour of a radio system in an outdoor environment does not necessarily conform to these assumptions.

2.1 The Mobile Radio Channel

The modeling and characterisation of the propagation channel are important to understanding and deploying mobile communication systems. The mobile radio channel is the main contributor to many of the limitations of mobile communication. In the context of interest here, characterisation involves classification of the terrain and making conclusions that are used with other locations with similar characteristics.

The three basic mechanisms which govern radio propagation are attributed to reflection, diffraction, and scattering [34]. Consider, for example, a mobile communication system deployed in a large urban center. The receiver is well below the maximum height of the local structures, where most communication is due to scattering of electromagnetic waves from surfaces and diffraction at the edges of the structures. Reflection occurs when the electromagnetic wave bounces off a structure with dimensions much larger than the wavelength of the signal. The angle of reflection is determined by Snell's law. More objects will cause reflection at high frequency than lower frequencies. Diffraction is the phenomenon where signals travel around an obstacle. Thus, propagation into regions with no line-of-sight (LOS) can be attributed to diffraction. Scattering occurs when the signal interacts with objects having dimensions on the order of a wavelength or less, causing signal energy to be reradiated in different directions, and is the most difficult mechanism to predict. These three mechanisms combined cause the original signal to be dispersed and the received signal is the vector sum of signals from many distinct paths [35].

In an environment with many objects, such as an urban center, each multipath component arrives from a different direction with different time delay[1], amplitude and phase. Once at the receiver, these components combine constructively or destructively due to varying path lengths.

[1]The path length is invariably linked to the time delay.

The received signal is also attenuated due to large-scale fading between the transmitter and receiver pair [36] and suffers from losses including absorption and dispersion. The trajectories of the signal paths are determined by the location of scatterers. If the scatterers are mobile, a fixed reference point in space will experience a received signal that varies in time[2]. Thus, an appropriate radio channel model must take into account these mechanisms.

2.2 Mathematical Channel Model

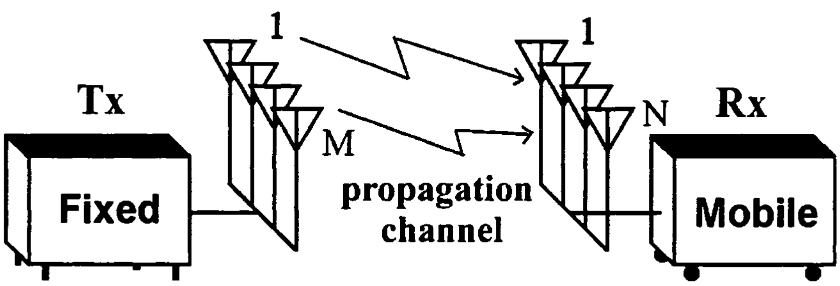

Figure 2.1: Illustration of a MIMO system with M transmit and N receive antennas.

Consider the MIMO communication system illustrated in Figure 2.1 with M transmit antennas and N receive antennas. To describe the behaviour of the wireless propagation channel, narrowband channel estimates are used to define a channel matrix, $\mathbf{H}$, determined by the site-specific scattering environment. In MIMO systems, the channel is divided into many narrowband flat fading subchannels for each user, without the need for channel equalisation and minimising bandwidth consumption.

For narrowband MIMO systems, the channel gains between the receiver and transmitter for each sample in time can be modeled using

$$\mathbf{x} = \mathbf{H}^{(k)}\mathbf{s} + \mathbf{n} \tag{2.1}$$

[2]Different locations in three dimensional space receive different signals due to the different vector phase relationships between signals [34].

where

$\mathbf{x}$	complex receive signal output vector;
$\mathbf{H}$	$N \times M$ complex channel matrix where $h_{i,j}$, $i = 1,2,...,N$ and $j = 1,2,...,M$ are the complex channel gains encountered by the signal that is transmitted by transmit antenna j and received by receive antenna i with $\mathcal{E}\{\|h_{ij}\|^2\} = \sigma_h^2 = 1$ and the superscript denotes the index of the matrix sample at time k;
$\mathbf{s}$	complex transmitted QPSK signal vector; and
$\mathbf{n}$	zero mean complex Gaussian noise.

The received signal (2.1) is a linear transformation of the transmitted information and therefore recovery can be performed using, for example, maximum likelihood (ML) or minimum mean-squared error (MMSE) detection.

Since the actual received signal power varies as a function of location, some type of channel normalisation is necessary to make the average signal-to-noise ratio, γ, independent of location in the environment, i.e. correcting for path loss. A common normalisation used in practice is to scale the channel matrices such that on average, the power transfer between a single transmit-receive pair is unity. Consider the following, let $\hat{\mathbf{H}}^{(k)}$ and $\mathbf{H}^{(k)}$ represent the measured and normalised matrices, respectively. The normalisation operation is given by

$$\mathbf{H}^{(k)} = A\hat{\mathbf{H}}^{(k)} \tag{2.2}$$

where

$$A = \left(\frac{1}{KMN} \sum_{k=1}^{K} \sum_{i=1}^{N} \sum_{j=1}^{M} |\mathbf{H}_{ij}^{(k)}|^2 \right)^{-\frac{1}{2}} \tag{2.3}$$

where K is the total number of matrix samples. By choosing the appropriate number of K samples, the normalisation in (2.3) allows the effect of path loss on the channel behaviour to be analysed without the need of a model.

Researchers often use simplistic models such as the Rayleigh fading model to generate $N \times M$ dimensional channels with mutually independent links to describe outdoor environments.

Real-world measurements differ from those predicted using models such as these. In [23], researchers take into account realistic propagation environments by including spatial fading correlations and scattering around the transmitter/receiver pair. The two most relevant models are discussed next.

2.2.1 Spatially Correlated Model

In a spatially correlated MIMO channel, the channel matrix $\mathbf{H}$ may be modeled using the following form, called the Kronecker model,

$$\mathbf{H} = \mathbf{\Phi}_N^{1/2}\mathbf{H}_w\mathbf{\Phi}_M^{1/2} \tag{2.4}$$

where $\mathbf{H}_w$ is complex Normal[3], and $\mathbf{\Phi}_N$ and $\mathbf{\Phi}_M$ are receive and transmit correlation matrices which may have the form

$$\theta_d(\rho) = \begin{bmatrix} 1 & \rho & \rho & \cdots & \rho \\ \rho & 1 & \rho & \cdots & \rho \\ \vdots & \vdots & \vdots & \ddots & \vdots \\ \rho & \rho & \rho & \cdots & 1 \end{bmatrix}_{d\times d} \tag{2.5}$$

where $\theta_d(\rho)$ is a d^{th}-order ($d \times d$) positive definite matrix with correlation coefficient ρ [23]. This is not the only form of correlation matrix that is used [26]. The Kronecker model is widely used and in general describes a channel with effective correlation at the receiver and transmitter with little effect from scatterers. Thus, it does not accurately describe the properties of a outdoor environment which would typically include scattering clusters [24]. In order to simulate the conditions observed in an outdoor wireless channel, we use a worst-case (uniformly distributed) Rayleigh-fading channel with parameters $\mathbf{\Phi}_M = \theta_M(\rho)$ and $\mathbf{\Phi}_N = \theta_N(\rho)$. By worst-case, the off-diagonals in the correlation matrix Φ are all the same.

[3]This is usually denoted as $\mathcal{CN}(0, \sigma_h^2\mathbf{I}_B)$, where $\mathbf{I}_B = \mathbf{I}_N \otimes \mathbf{I}_M$ is a scaled identity matrix using the Kronecker tensor product.

2.2.2 Double Scattering Model

The previous model (2.4) assumed that there was only a single scattering process ($\mathbf{H}_w$) and cannot explain the low rank[4] behaviour of some MIMO channels. Gesbert *et al.* in [5] proposed a double scattering channel model that exhibited rank-deficient effects including spatial fading correlation given by

$$\mathbf{H} = \frac{1}{\sqrt{S}} \mathbf{\Phi}_N^{1/2} \mathbf{H}_1 \mathbf{\Phi}_S^{1/2} \mathbf{H}_2 \mathbf{\Phi}_M^{1/2} \tag{2.6}$$

where $\mathbf{H}_1 \sim \mathcal{CN}(0, \mathbf{I}_N \otimes \mathbf{I}_S)$ and $\mathbf{H}_2 \sim \mathcal{CN}(0, \mathbf{I}_S \otimes \mathbf{I}_M)$, S is the number of effective scatterers, and correlation matrices $\mathbf{\Phi}_N$, $\mathbf{\Phi}_M$, and $\mathbf{\Phi}_S$ are the receive, transmit and scatterer correlation matrices, respectively. The matrix (2.6) is similar to that found in [24] and uses scattering to realistically model a wireless channel. It has been verified through simulation [23] that by increasing ρ, the channel matrix in (2.6) becomes ill-conditioned. Similarly, S has the same effect reported by Shin and Lee [23] who assert that the rank of the MIMO channel matrix is primarily controlled through the effective number of scatterers, S.

2.3 Parameterisation using Metrics

In this thesis, we study the impact of site-specific environments on MIMO system performance. Therefore we need a general performance metric, which is a function of $\mathbf{H}$, that conveys some information about the quality of the MIMO channel. In the case $N = M = 1$, "good" channels have large amplitude gains. For MIMO channels, large amplitude gains are not necessarily a sufficient condition of the channel to be considered good. The goodness of the channel depends on choice of MIMO technique, the channel characteristics, as well as other factors. Determining the quality of the MIMO channel realisation is necessary for predicting MIMO

[4]The rank of a matrix is the maximum number of independent rows (or, the maximum number of independent columns).

BER performance in a given environment. Bliss *et al.* [37] introduced a simple channel parameterisation for a set of experiments that is a function of the decomposed channel matrix, the importance of which will become clear later.

Research [30] indicates that the most popular performance metric, ergodic channel capacity, for a MIMO communications link is very difficult to apply directly when analysing site-specific channel measurements. In [12], the ergodic capacity of a MIMO communications link with perfect channel state information (CSI) at the transmitter is given by

$$\hat{C}(\gamma) = \max_{Q,\mathrm{tr}(Q)=1} \mathcal{E}\left\{\log\det(\mathbf{I}_N + \frac{\gamma}{M}\mathbf{H}\mathbf{Q}\mathbf{H}^H)\right\} \tag{2.7}$$

where γ is the signal-to-noise ratio (SNR) and $\mathbf{Q}$ is the signal covariance matrix that optimises $\hat{C}(\gamma)$ [38]. Using site-specific (measured) channel information with (2.7) is difficult since the distribution of the measured channel $\mathbf{H}$ is unknown.

From a set of channel realisations given by $\mathcal{H} = \left\{\mathbf{H}^{(k)}\right\}|_{k=0,1,\ldots,K-1}$, where $\mathbf{H}^{(k)}$ is the channel matrix measured at time k, and K identifies the cardinality of the set which is assumed to be ergodic, we need to find a simple function that indicates channel quality according to some performance metric [29]. Radio channel modeling in [39] identified the lengths over which the angles of arrival, amplitudes and phases of the incoming radio waves remained approximately constant in the channel. Collectively we refer to them as the angular spectra (power versus angle of arrival) over a consistency length given in samples. Based on these results, we determine the necessary sample size, or consistency length, to be $K = 60$ using the following

- consistency of measured angular spectra $\sim$2 m;
- vehicular velocity of 30 km/hr (8.333 m/s) in urban areas; and
- sampling rate of 250 samples/sec. [40]

A sample size of $K = 45$ was reported in [41] using similar measurement data, corresponding to a distance of 2 m at 40 km/hr and used in analysis of an urban microcell. The above sample size is not suited to all environments. The data analysis in [39, 42] would have to be carried out again to determine the necessary sample size for a rural and suburban environment. In Table 2.1, the sample sizes for a particular environment are estimated based on mobile speed.

Table 2.1: Consistency Length (K) Sample Summary

Urban	Suburban	Rural
45 - 60	80	200

A rural environment has a larger length compared to urban and suburban. To maintain our assumptions, we select $K = 60$ and remain consistent throughout all measurement analysis. There are many possible measures for MIMO communication channels. A collection of possible metrics found in literature is described next.

2.3.1 Average Signal Strength

Average signal strength, $P(\mathcal{H})$, is given by

$$P(\mathcal{H}) = \frac{1}{K} \sum_{k=0}^{K-1} \|\mathbf{H}^{(k)}\|_F^2 \tag{2.8}$$

where H has been normalised using (2.2). The operation introduces an effective power control and corrects for path-loss, independent of location in the environment.

2.3.2 Path-loss

The path loss estimate, $\alpha(\mathcal{H})$, is given by

$$\alpha(\mathcal{H}) = \frac{1}{KNM} \sum_{k=0}^{K-1} \|\mathbf{H}^{(k)}\|_F^2. \tag{2.9}$$

The normalisation above corresponds to assuming that the system implements slow power control to correct for path-loss, i.e. removing the effect of large-scale fading [29, 38].

2.3.3 Average Mutual Information

The average mutual information, $\overline{I}(\mathcal{H})$, gives an upper-limit estimate of the throughput that can be achieved with no knowledge of the channel. It is given by:

$$\overline{I}(\mathcal{H}) = \frac{1}{K}\sum_{k=0}^{K-1}\log_2\det\left(\mathbf{I}_N + \frac{\gamma}{M}\mathbf{H}^{(k)}{\mathbf{H}^{(k)}}^H\right) \tag{2.10}$$

If the statistics in the local area over which $\mathcal{H}$ is collected are constant, we obtain an estimate of the average mutual information [29]. If $\mathbf{H}^{(k)}$ is i.i.d., then the expression in (2.10) converges to (2.7) as K increases if the channel statistics are stationary [30, 38].

Although $\overline{I}(\mathcal{H})$ is an estimate, no effort has been made in this thesis to determine its bounds. Exact expressions for mutual information for small [43] and large [44, 45] numbers of antennas, have been obtained and are very tight to those in [12].

2.3.4 Outage Mutual Information

Mutual information, defined previously in (2.10), is instantaneous for a given realisation of the channel matrix $\mathbf{H}$. Since the channel matrix changes randomly, mutual information is also random. Outage mutual information is related to outage probability, which is the fraction of the time the mutual information falls below a given threshold I_{outage} [27], i.e.,

$$P_{out}(I_{outage}) = P_r\{I \leq I_{outage}\}. \tag{2.11}$$

For example, a mutual information of 20 bits/s/Hz with 1 percent outage probability means that the mutual information will remain at least 20 bits/s/Hz for 99 percent of the time.

2.3.5 Channel Decomposition

The singular value (σ) decomposition of $\mathbf{H}$, or the related eigenvalue (λ) decomposition of $\mathbf{H}\mathbf{H}^H$, is a useful metric for understanding the expected performance of a MIMO wireless communication system. Consider the following decomposition given by

$$\mathbf{HH}^H = \mathbf{U}\Lambda\mathbf{U}^H = \sum_{i=1}^{N} \lambda_i \mathbf{u}_i \mathbf{u}_i^H \tag{2.12}$$

where $\mathbf{U} = [\mathbf{u}_1 \dots \mathbf{u}_N]$ is any unitary matrix of eigenvectors and Λ is a diagonal matrix of eigenvalues λ of $\mathbf{HH}^H$. In this definition we use $\lambda_1 \leq \lambda_2 \leq \lambda_3 \leq \lambda_4$ for $N = M = 4$.

Due to the fading encountered in realistic channels, it is possible that the ratio $\lambda_{max}/\lambda_{min}$ $\mathbf{HH}^H$ is large [34], i.e. one or more of $\lambda_1, ..., \lambda_N$ could be small. It can be seen that mutual information in (2.10) is a function of the eigenvalues of $\mathbf{HH}^H$. Therefore, a channel with relatively small eigenvalues produces a small average mutual information. The optimum condition would be when all the eigenvalues are equal and large, but in complex Gaussian (CG) channels they are not.

The BER performance of MIMO systems in different types of fading channels were shown in [46,47]. Research in [47] utilised the largest eigenmodes corresponding to the largest eigenvalue to perform eigenbeamforming to exploit the existence of scatterers in an urban environment. However, such a technique requires perfect CSI at the transmitter and receiver. It was demonstrated in [48] that the feedback of CSI to the transmitter can result in self-interference of the eigenbeams and is often omitted [47] in the selection of modes for transmission.

2.3.6 Multipath Richness

In [49] Andersen describes a measure of the richness of the MIMO scattering environment, φ. The well-known formula for capacity in [12] is expanded to obtain the richness curve defined as the sum of the log of the eigenvalues

$$\varphi = \sum_{i=1}^{U} \log_2(\lambda_i) \tag{2.13}$$

where λ_i is the i^{th} eigenvalue of $\mathbf{HH}^H$ and $U = \min(M, N)$. For a given location it is a measure of the intrinsic multipath richness of the environment and is independent of power or SNR. This metric reveals a significant amount of information about the channel, in that the number and angular spread of the multipath components affect the eigenvalues of $\mathbf{H}^{(k)}$ [49]. It is also important to note that richness is the same regardless of which direction the signal energy propagates through the channel.

2.3.7 Normalised Average Mutual Information

If we want to compare the average mutual information of two different locations, it is proposed in [29] to remove the average path-loss to determine the normalised average mutual information, $\overline{I}_s(\mathcal{H})$, given by

$$\overline{I}_s(\mathcal{H}) = \frac{1}{K}\sum_{k=0}^{K-1}\log_2 \det\left(\mathbf{I}_N + \frac{E_s}{N_0}\frac{1}{\alpha}\mathbf{H}^{(k)}\mathbf{H}^{(k)^H}\right) \tag{2.14}$$

where α is an estimate of the path-loss and normalised using (2.8). This is necessary to determine if the differences in $\overline{I}_s(\mathcal{H})$ are due to differences in path-loss or to differences in channel quality (rank, etc.) [29]. The above re-derives (2.10) as a function of small-scale variations. This metric was used in [50] to analyse data from a MIMO measurement campaign.

2.3.8 Normalised Parallel Channel Gain

Eggers [51] stated that the independent parallel links provided by a MIMO technology can be exploited to split the information transmitted into multiple low bandwidth channels. It is referred to as an equivalent orthogonal space division multiplex (OSDM) providing subchannels in the spatial/angular domain; a parallel to orthogonal frequency division multiplex (OFDM) which provides subchannels in the frequency domain.

OSDM can, like OFDM, mitigate against fading and time dispersion. However, OSDM's spatial subchannels have different power gains whereas OFDM has equal average gains and so, only a few OSDM subchannels can be used to effectively convey information reliably.

With interest only in the relative comparison between channels and array configurations [51], we defined the normalised cumulative eigen channel gain, $\overline{CG}(\mathcal{H})$, given by

$$\overline{CG}(\mathcal{H}) = \frac{1}{\lambda_{max,q}} \sum_{i=1}^{U} \lambda_{i,q} \tag{2.15}$$

where q is the specified reference outage ratio $0 < q < 1$, and $\lambda_{i,q} \geq \lambda_{max,q} \times q$. Thus, we have a simple means of describing the multiplexing potential of the environment and array configuration.

2.3.9 Normalised Parallel Channel Capacity

Eggers decomposes the capacity in [12] for a MIMO link with no feedback as follows

$$C \approx \sum_{i=1}^{U} \log_2(\frac{\gamma}{M}\lambda_i) = U \cdot \log_2(\gamma) - U \log_2(M) + \sum_{i=1}^{U} \log_2(\lambda_i) \tag{2.16}$$

for U and λ_i defined previously. The last term describes the multiplexing contribution in the total capacity. Using (2.16), the normalised parallel channel capacity, $\overline{CC}(\mathcal{H})$, is defined as [51]

$$\overline{CC}(\mathcal{H}) = \frac{1}{\log_2(\lambda_{max,q})} \sum_{i=1}^{U} \log_2(1 + \lambda_{i,q}) \tag{2.17}$$

where $\lambda_{max,q} \gg 1$, and q is the reference outage ratio from (2.15).

2.3.10 Effective Rank

The effective rank of a MIMO communications link, $\overline{R}(\mathcal{H})$ [29], is given by

$$\overline{R}(\mathcal{H}) = \frac{1}{K} \sum_{k=0}^{K-1} R(\mathbf{H}^{(k)}) \tag{2.18}$$

where $R(\mathbf{H}^{(k)}) = \sum_{i=1}^{U} I(\sigma_i > G\sigma_{max})$ is the number of singular values of $\mathbf{H}^{(k)}$ greater than a pre-defined fraction G of the maximum singular value σ_{max}, i.e. the effective number of non-negligible singular values, and is an estimate of the number of spatial data pipes that are available in the channel and does not depend on SNR.

2.3.11 Effective Degrees of Freedom

The effective degrees of freedom [32], χ_1, is given by

$$\chi_1(\mathcal{H}) = \sum_{i=1}^{U} \frac{\gamma\lambda_i}{M + \gamma\lambda_i} \tag{2.19}$$

where γ is the average SNR. Equation (2.7) is written as a decomposition of U equivalent SISO channels of matrix $\mathbf{HH}^H$, each with power gain λ_i. When the average SNR and eigenvalues are large, satisfying $\gamma\lambda_i \gg M$, a 3 dB increase in SNR realises ~1 bits/s/Hz increase in capacity for the sub-channel. It also quantifies how many of the equivalent SISO channels effectively exhibit this increase.

An alternative definition given in [52] is $\chi_2(\mathcal{H})$, defined as

$$\chi_2(\mathcal{H}) = \sum_{i=1}^{U} \frac{\sigma_i}{\sigma_{max}} \tag{2.20}$$

where σ_i and σ_{max} are the i^{th} and maximum singular value of **H**, respectively. In both definitions, χ has a range $[1, \min(N, M)]$.

2.3.12 Diversity

The diversity measure, $\Psi(\mathbf{R})$, of a MIMO system operating in Rayleigh fading is described in [26]. Using the correlation matrix[5] $\mathbf{R} = \mathcal{E}\{\text{vec}(\mathbf{H})\text{vec}(\mathbf{H})^H\}$, it is defined as [26]

$$\Psi(\mathbf{R}) = \left(\frac{\text{tr}(\mathbf{R})}{||\mathbf{R}||_F}\right)^2 \tag{2.21}$$

and has the property $1 \leq \Psi(\mathbf{R}) \leq N \cdot M$. The diversity measure quantifies the number of independent paths available to the data propagating between transmitter and receiver. Squires *et al.* demonstrated in [53] the use of the diversity measure in mitigating the effects of interference and jamming sources in a wideband wireless system operating at 2.0375 GHz.

[5]The matrix $\mathbf{R}$ is strictly real for the $\text{vec}(\cdot)\text{vec}(\cdot)^H$ operation.

2.3.13 Correlation

Using the diversity measure, we define the correlation measure for a Rayleigh fading MIMO system. The correlation measure, $\Phi(\mathbf{R})$, of a $NM \times NM$ correlation matrix $\mathbf{R}$ is given by [26]

$$\Phi(\mathbf{R}) = \sqrt{\frac{1 - NM/\Psi(\mathbf{R})}{1 - NM}} \tag{2.22}$$

where $\Psi(\mathbf{R})$ was defined in (2.21). The correlation measure is inversely related to (2.21) and quantifies the amount of spatial correlation present in the channel. Both diversity and correlation are functions of the correlation matrix $\mathbf{R} = \mathcal{E}\{\text{vec}(\mathbf{H})\text{vec}(\mathbf{H})^H\}$ defined in [26]. The statistical analysis of the covariance matrix, $\mathbf{R}$, has been shown to provide a useful metric for describing a physical propagation environment [54,55].

2.4 Space-Time Architecture and Coding Schemes

In this section, we introduce the MIMO space-time architecture and coding schemes used to estimate the bit-error performance using Matlab Simulations. Known channel models are used with V-BLAST and STBC to obtain worst-case BER estimates of performance. Since the characteristics of the channel are unknown, the simulations presented in this thesis assume highly correlated channels [23,24].

2.4.1 V-BLAST

Spatial multiplexing is a popular method employed to increase the throughput of a MIMO channel. However, the trade off may be a decrease in performance. The basic concept of multiplexing is as follows:

- Divide (multiplex) the information to be transmitted; and
- Transmit the parallel data streams into space from different antennas.

To recover the transmitted information, we employ space-time equalisation at the receiver; subject to the constraint $N \geq M$, the data streams can be separated by the receiver if the fading processes of the spatial channels are almost independent.

Vertical Bell Labs Layered Space-Time (V-BLAST) architecture [56] was one of the first spatial multiplexing systems and performs well when channel estimates are good. Figure 2.2 shows the block diagram of a typical V-BLAST implementation over a MIMO communications channel. The V-BLAST system model is represented using (2.1),

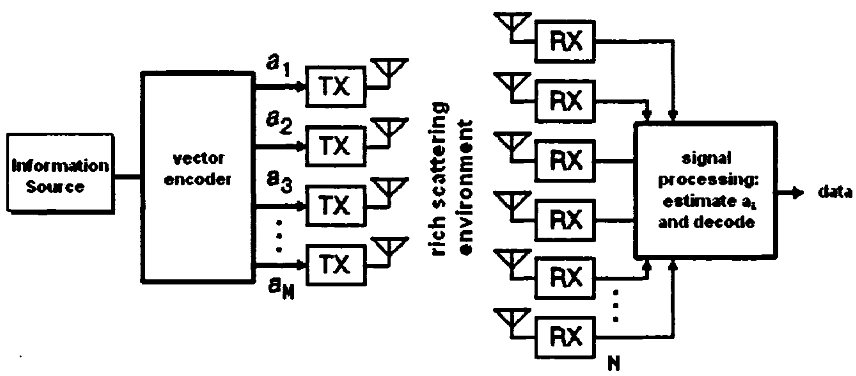

Figure 2.2: Block diagram of an uncoded V-BLAST system.

$$\mathbf{X} = \mathbf{H}\mathbf{s} + \mathbf{N} \tag{2.23}$$

where

$\mathbf{X}$	complex receive signal output;
$\mathbf{H}$	channel matrix;
$\mathbf{s}$	spatially-multiplexed transmitted symbol vector $[s_1, s_2, \ldots, s_F]^T$; and
$\mathbf{N}$	zero mean complex Gaussian noise.

and $F \leq M$ is the length of the vector.

The V-BLAST detection algorithm utilises interference suppression and symbol cancelation to successively detect symbols from each transmit antenna. When detecting the i^{th} symbol, all other symbols are treated as interferers. Linear nulling is used in interference suppression by weighting the received vector to satisfy a performance criterion. Many types of detection are available, of which the most common use minimum mean-squared error (MMSE) or zero-forcing (ZF) weighting. We describe the simplest method, ZF, next.

The nulling matrix for ZF is given by the Moore-Penrose pseudoinverse

$$\mathbf{G} = (\mathbf{H}^H\mathbf{H})^{-1}\mathbf{H}^H. \tag{2.24}$$

The i^{th} ZF nulling vector nulls all the undetected signals except the i^{th} transmitted signal from the received signal, given by

$$\mathbf{w}_i = (\mathbf{G}^H)_i \tag{2.25}$$

where $(\mathbf{G})_i$ is the i^{th} column of the nulling matrix $\mathbf{G}$. The nulling vector multiplied by the received signal vector $\mathbf{X}$ suppresses all layers except the i^{th} layer. A decision statistic, y_i, is calculated from the nulling vector, $y_i = \mathbf{w}_i^T\mathbf{X}$. The ZF estimate, $\tilde{s}_i$, is determined from y_i. The symbol estimate, assumed to be correct, is used for symbol cancelation. Interference from the already detected components of s are subtracted from the received signal vector. The updated received symbol is given by

$$\mathbf{X} = \mathbf{X} - \tilde{s}_i(\mathbf{H})_i. \tag{2.26}$$

The column of H that corresponds to the most recently detected symbol is removed and the nulling matrix is recalculated. The detection process is repeated until all transmitted symbols are detected. Using the optimal detection order, the symbols are detected in order of decreasing signal strength and as a result, the strongest interference is canceled first [34]. In practical V-BLAST systems the overall system performance is limited by the worst substream, which is the first detected one [57].

After each symbol is canceled from x, the number of symbols remaining to be detected is reduced. If less nulling is required, diversity should increase from layer to layer. During the symbol cancelation, all previous decisions are assumed to be free of error. When an incorrect decision is made, interference is added in, rather than being subtracted, resulting in errors propagating into the following layers.

In our benchmark simulations, the burst length is set equal to 250 symbol durations as in [56, 58] and the channel matrix is generated randomly from one burst to the next using (2.6) for 100,000 channel realisations with at least 100 bit-errors. Each channel realisation is generated at each SNR value to obtain the BER with $N = M = 4$. In Figure 2.3, we compare the BER performance of uncoded V-BLAST using these parameters

Channel 1 $\Phi_N(0.1)$, $\Phi_M(0.1)$, $\Phi_S(0.9)$, $S = 6$; and
Channel 2 $\Phi_N(0.1)$, $\Phi_M(0.1)$, $\Phi_S(0.1)$, $S = 6$.

Performance of V-BLAST is poor when severe spatial correlation is introduced using channel 1. Over a wide range of SNRs no useful information can be recovered as the receiver is unable to effectively separate the data streams. With lower correlation in channel 2, the BER performance slowly improves with SNR giving a decade improvement in BER over channel 1 at 16 dB. The performance of V-BLAST is very dependent on correlation and performs well when the fading processes are nearly independent.

To assess the range of performance expected using the V-BLAST detector in real environments, we use measured channel matrices, $\mathbf{H}^{(k)}$, with QPSK modulated data streams and produce BER estimates for a specified average SNR. Results will be presented in Chapter 4.

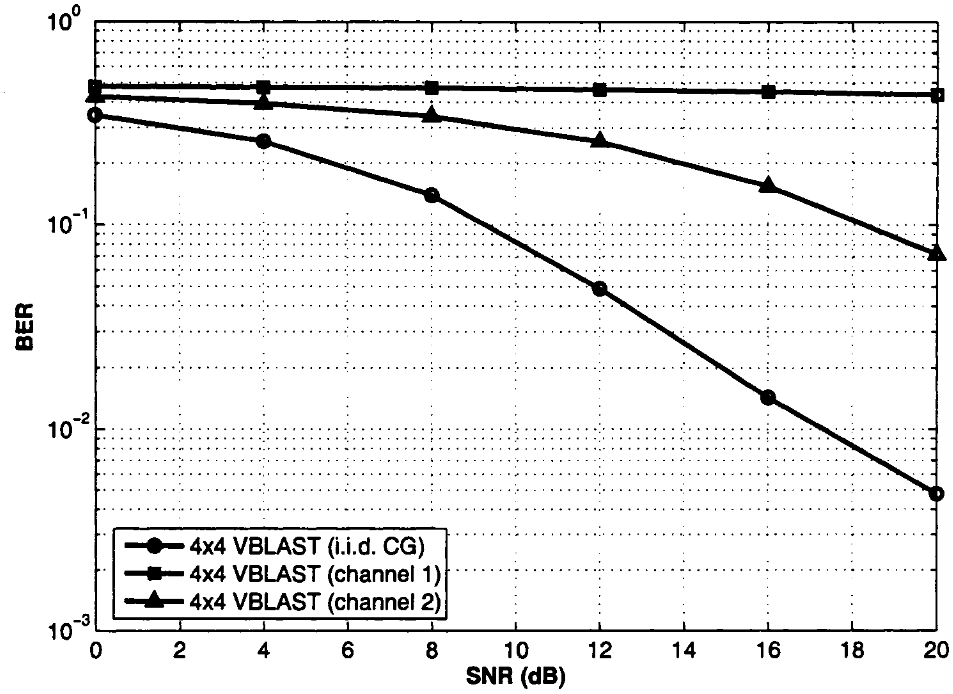

Figure 2.3: Bit-error probability versus SNR for V-BLAST for QPSK with $N = M = 4$ for channels 1 and 2 and i.i.d. complex Gaussian.

2.4.2 Space-Time Coding

Space-time codes for MIMO wireless communications use joint channel symbol encoding over multiple transmit antennas to mitigate the effects of fading by employing redundancy [34]. These codes can be used to minimise the outage probability, increase the degree of statistical independence among transmitted signals, and maximise bit-error rate performance, but do not increase the data rate.

Space-time codes are classified into two types: 1) block and 2) trellis. For a fixed number of transmit antennas, the decoding complexity of space-time trellis codes (measured in terms of trellis states at the decoder) typically increases exponentially as a function of the constellation size [59]. However, the method in [60] maintains a nearly constant complexity per bit. Multiplexing and space-time coding are useful MIMO techniques that help improve the BER performance of a MIMO communications system. A method proposed in [61] combined both techniques for transmission over a correlated channel with a large complexity in operation.

Trellis codes are only practical and useful for a small number of transmit antennas. For a space-time block code, transmission takes place in blocks using a transmission matrix defined by three parameters:

- The number of transmitted symbols, T;
- The number of transmit antennas, M; and
- The number of time slots in a data block, V.

The code rate is hence T/V. Alamouti [62] proposed a simple 2×2 block code with unit code rate. Tarokh [59] *et al.* developed code construction criteria, and studied design trade-offs between constellation sizes, data rates, diversity advantage and complexity. However, only $1/2$ or $1/3$ rate codes are achieved using complex constellations.

Researchers in [63] state that, in 2003, there are no reports of a full-rate full-diversity orthogonal code design that can be used in a system with more than two transmit antennas with complex constellations, and this was proved in [59]. However, other codes for multi-element systems [64, 65] have been developed. He *et al.* proposed a code in [63] for a 4×4 system using nonlinear processing that is full-rate and uses QPSK.

Consider the model of the received data using (2.1)

$$\mathbf{X} = \mathbf{C}(\mathbf{s})\mathbf{H} + \mathbf{N} \tag{2.27}$$

where

$\mathbf{X}$	$V \times N$ complex receive signal output;
$\mathbf{C}(\mathbf{s})$	$V \times M$ space-time code matrix for input symbol vector s;
$\mathbf{H}$	$M \times N$ complex channel matrix; and
$\mathbf{N}$	$V \times N$ zero mean complex Gaussian noise.

The entries of $\mathbf{H}$ have been normalised and entries of $\mathbf{N}$ are mutually independent, zero-mean complex Gaussian variables with variance

$$\sigma_n^2 = \frac{M\sigma_h^2\sigma_s^2}{\gamma} = \frac{M\bar{E}_s}{\gamma} \tag{2.28}$$

where $\sigma_h^2 = 1$, $\sigma_s^2 = \bar{E}_s$ is energy per symbol, γ is the average signal-to-noise ratio, and M is the number of transmitters defined previously.

A maximum-likelihood (ML) exhaustive search [66] is performed at the receiver to search over all QPSK input vectors given the channel matrix $\mathbf{H}$ and received data $\mathbf{X}$, i.e.,

$$\widehat{\mathbf{s}} = \arg\min_{\mathbf{C}(\mathbf{s})} \|\mathbf{X} - \mathbf{C}(\mathbf{s})\mathbf{H}\|^2. \tag{2.29}$$

The ML detection in (2.29) considers all possible input codes $\mathbf{C}$ for all s and chooses the input which minimises the Euclidean distance. Using unit-energy orthogonal design [59] $\mathbf{C}^H\mathbf{C} =$

$\mathbf{I}_{M\times M}$, (2.29) can be re-written as

$$\widehat{\mathrm{s}} = \arg\max_{\mathrm{C(s)}} \mathcal{R}\mathrm{e}\left\{\sum_{m=1}^{M} \mathrm{x}_m^H \mathrm{C(s)} \mathbf{h}_m\right\} \tag{2.30}$$

where $\mathbf{x}_m$ and $\mathbf{h}_m$ are the m^{th} columns of the data matrix **X** and channel matrix **H**, respectively.

The space-time block encoder encodes a vector sequence of input symbols of length T, $\mathrm{s} = [s_1, \ldots, s_T]^T$ into a $V \times M$ transmission matrix $\mathrm{C(s)}$. The QPSK-based nonlinear transmission matrix for $M = T = V = 4$ is given by [63]

$$\mathrm{C(s)} = \frac{1}{\sqrt{2}}\begin{pmatrix} s_1 & s_2 & s_3 & s_4 \\ -s_2^* & s_1^* & -s_4^* & s_3^* \\ -x_1^* & x_2 & s_1^* & -s_2 \\ -x_2^* & -x_1 & s_2^* & s_1 \end{pmatrix} \tag{2.31}$$

where $x_1 = \mathcal{R}\mathrm{e}\{s_3\} + j\mathcal{I}\mathrm{m}\{2s_1s_2s_4^*\}$ and $x_2 = s_1^{*2}s_4 + s_2^2s_4^* + s_1^*s_2s_3 - s_1^*s_2s_3^*$.

A four-dimensional linear quasi-orthogonal STBC was presented by Jafarkhani [67] defined by

$$\mathrm{C(s)} = \begin{pmatrix} s_1 & s_2 & s_3 & s_4 \\ s_2 & s_1^* & -s_4^* & s_3^* \\ s_3 & -s_4^* & s_1^* & -s_2 \\ s_4 & s_3^* & s_2^* & s_1 \end{pmatrix}. \tag{2.32}$$

The nonlinearity of $\mathrm{C(s)}$ in [63] presents a problem when searching over all 4^4 possible combinations of s. A popular decoding technique separates $\mathrm{C(s)}$ into two 4×2 code matrices and eliminates the first two symbols of s by consulting a lookup table of 256×4 QPSK symbols. The efficiency of a simple ML detector is increased by "eliminating" sections of the lookup table by operating over half of the segmented code matrix.

Figure 2.4 provides simulation results for the transmission of 2 bits/s/Hz by four transmit antennas, one and four receiving antennas using (2.31) and (2.32). The simulation parameters are

- Block length size = 120; and

- Number of iterations = 1000

for each defined code matrix. Simulation results show that the BER performance of (2.31) is close to that of (2.32) when SNR is low for i.i.d.CG channels. As the SNR increases, no error floor is apparent. The code given by He in [63] outperforms Jafarkhani's code for one receive antenna. Using the severe correlated channels from Section 2.4.1, the performance of the two codes is similar for one receiver. Using four receivers, the performance of the two codes is also similar on both the i.i.d.and scattering channels[6]. In a spatially correlated channel, both codes still perform well when SNR is low, i.e. at SNR = 9 dB a BER of 10^{-4} is achieved. Therefore, the performance of the two codes is similar in correlated and uncorrelated channels with single or multiple receivers. Correlation boosts signal power and results in a higher effective SNR. The Jafarkhani code will be used since the non-linear terms in (2.31) prevent implementation of a simple ML detector.

[6]Jafarkhani's code produces almost no errors when simulating an i.i.d.channel with 4 receivers.

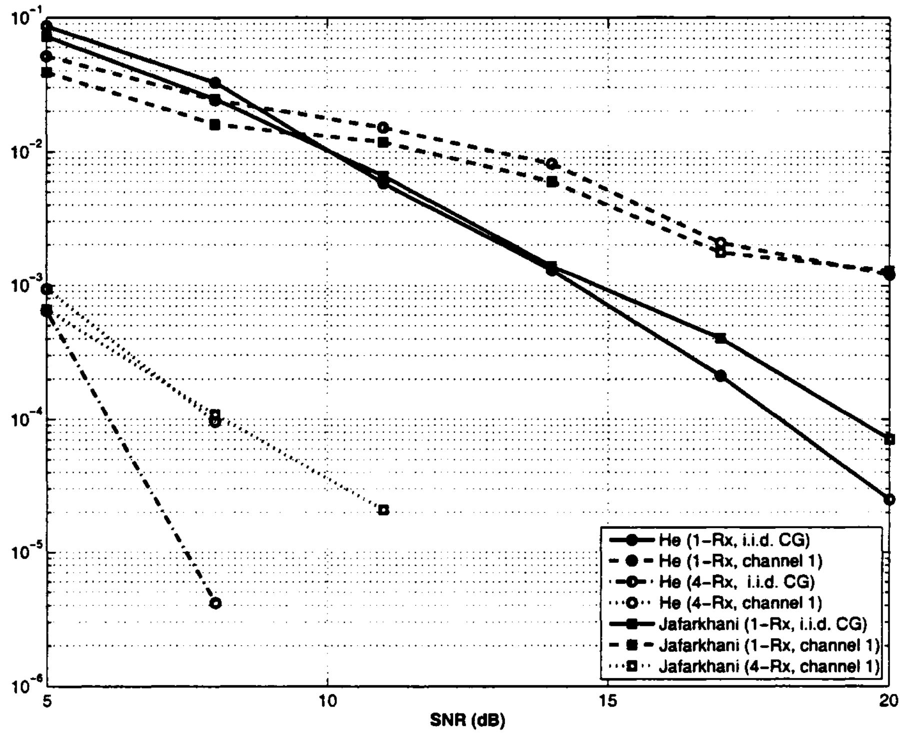

Figure 2.4: Bit-error probability versus SNR for space-time block codes at 2 bits/s/Hz; one and four receive antennas for channel 1 and i.i.d. complex Gaussian channels.

Chapter 3

CRC MIMO Testbed

In order to characterise the radio channel, the properties must be accurately quantified. Outdoor measurements were obtained using the distance-triggered CRC MIMO testbed, described briefly in Section 3.1, developed by the Radio Communications Technologies group at CRC [40, 68]. Other radio channel testbeds are discussed in [69–71]. The channel estimation methods are described in Section 3.2 and metric selection is discussed in Section 3.4.

3.1 System Description

The purposes of the CRC MIMO testbed are to 1) serve as a flexible sounding platform to obtain data for channel characterisation, and 2) be used as a tool for investigating and demonstrating various space-time communications techniques [40].

In this thesis, we consider a point-to-point communications link with M transmit and N receive antennas with $N = M = 4$, operating at 2.0375 GHz. The testbed is shown in Figure 3.1. In all experiments, the transmitter was installed at a static location (i.e. corner window of a building) and used omnidirectional, vertically-polarised monopole antennas spaced 1 wavelength apart.

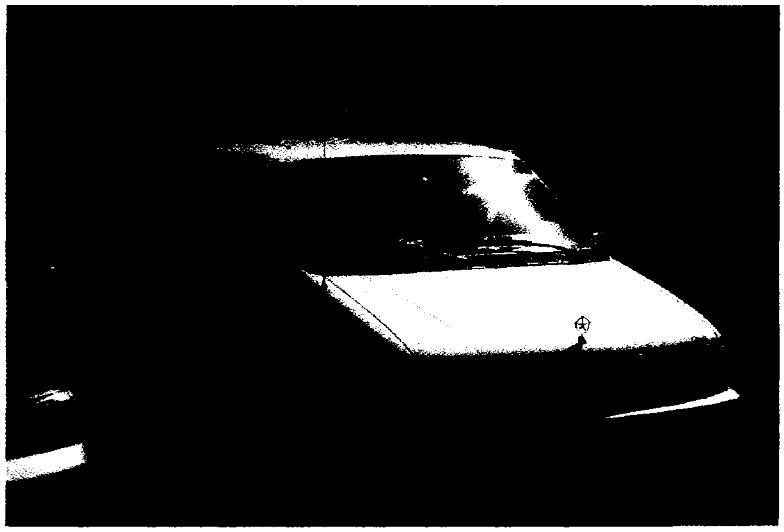

Figure 3.1: CRC MIMO testbed receiver.

Figure 3.2: CRC MIMO testbed transmitter.

The receiver was installed in the measurement minivan, using roof-mounted vertically-polarised omnidirectional monopole antennas (see Figure 3.1). Custom hardware [40] provided amplification, down-conversion, and sampling of an in-phase and quadrature channel at a rate of 250 Hz, while traveling at nominal speed limits.

We omit the technical specifications of the transmitter/receiver assemblies and software utilised by the MIMO testbed. However, these can be found in Section 3 and 4 of [40]. Calibration[1] of the sounder is also omitted.

3.2 Data Measurements

In practical systems, the channel matrix H is not exactly known. The primary function of the CRC MIMO testbed is to provide measurements for estimating properties of the wireless channel. A well-known method for generating the impulse response (IR) of the wireless channel is employed by CRC [40]. Carefully optimised and proprietary pseudo-noise sequences are transmitted from each array element and the received signals are processed to produce estimates of the $N \times M$ channel impulse response. This technique is discussed briefly in the next section.

3.2.1 Channel Impulse Response Estimation

The standard channel model from Chapter 2 applies where the transmitted signals, s, consist of repeated sequences, with chips $c(k)$. The channel sounding process employs a repeating length-L pseudo-noise (PN) sequence, assigned to each transmitter element, up-sampled by 4, each delayed by 177 chips between antenna elements.

Impulse estimation is achieved using following steps:

[1]Calibration ensures that the characteristics measured are due to the propagation environment and not the MIMO transmitter and receiver system assemblies.

1. correlate the received signal $\mathbf{r}(k)$ with the transmitted sequence c;

2. synchronise and average over a large sample size to obtain noise averaging; and

3. apply threshold encapsulation (noise rejection) to extract the IR from noise with a low probability of false detection.

In Step 1, we correlate each received signal $\mathbf{r}(k)$ with the transmitted code sequence c,

$$\mathbf{x}(n) = \sum_{k=0}^{L-1} \mathbf{c}(k)\mathbf{r}(n+k) \tag{3.1}$$

where $\mathbf{r}(k)$ was defined in Chapter 2. The design criterion for obtaining PN sequences to provide the capability to extract good channel response estimates is discussed in [40, 72].

3.2.2 Preliminary Measurements

Initial measurements were made with the MIMO sounder during a measurement campaign in downtown Ottawa [58] in 2004. Figure 3.3 shows the impulse magnitude response for the transmitter/receiver pair[2]. Coded Matlab routines average over 19 consecutive IR samples (data blocks) as defined in Step 2. Analysis in [72] showed that the probability of selecting incorrect multipath components in 160 IRs was 0.008. This method is called Probability of false alarm (PFA) analysis and employed by CRC.

The desired signal is extracted from noise by applying a threshold statistic $\hat{x}_t$, given by [72]

$$\hat{x}_t = \eta\hat{\sigma}_n \tag{3.2}$$

where $\hat{x}_t$ is the threshold level estimate, $\hat{\sigma}_n$ is the standard deviation of the averaged data set, and $\eta = 3.11$ assumes the noise envelope follows a Rayleigh distribution for $N = 4$. In Step

[2] We defined the notation (i, j) to describe the complex channel gain between transmitter element i and receiver element j.

3, threshold bins which are a function of $\hat{x}_t$ encapsulate the desired signal, and 'brick wall' the noise.

In this thesis, only narrowband channels are of interest. Here, we have assumed that the system undergoes flat fading. The bandwidth occupied to each antenna should not be large enough to cause frequency selective fading. If the underlying data rate is large enough to cause frequency selective fading, techniques such as orthogonal frequency-division multiplexing could be used at the receiver[3].

Once an IR is identified within a (vertical) bin, a 512-point fast Fourier transform (FFT) is applied to the data set producing the channel frequency response. Figure 3.4 shows the spectra of the IR at receiver 1 from all transmitters[4]. A single spectral line at index 230, corresponding to a frequency of 2.035 GHz, is taken to obtain the complex channel coefficients $h_{i,j}$ at time sample k.

Figure 3.5 shows a consecutive set of unthresholded[5] impulse response estimates (UIREs) at receiver 1 from all transmitters over 3 blocks. The corresponding thresholded impulse response estimates (TIREs) is shown in Figure 3.6 using the first recorded impulse.

Results in [58] indicated that mutual information could be artificially inflated by increasing the area contained within the vertical (bin) limits. It is clear from Figure 3.5 that our measured data is noisy. Therefore, our TIREs and mutual information will be affected by noise. The effect of noise is discussed in the next section.

[3]This removes the need for complicated equalisation techniques.
[4]The phase plots were intentionally omitted.
[5]This is prior to Step 2 being executed on the IR data.

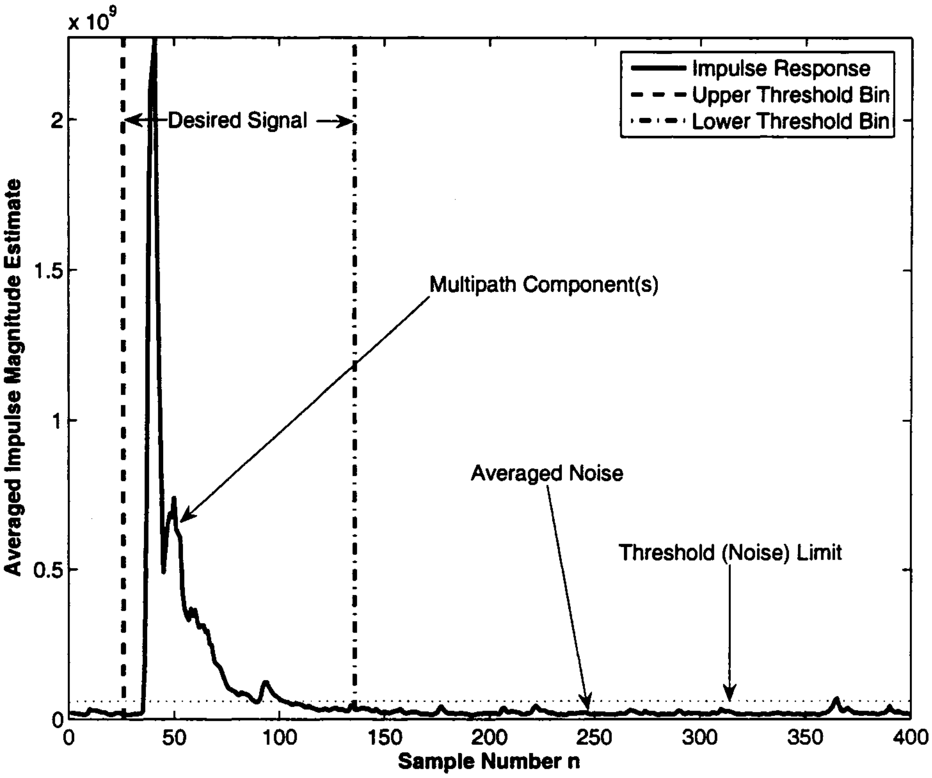

Figure 3.3: Single impulse response estimate with averaged noise contained within thresholding bins.

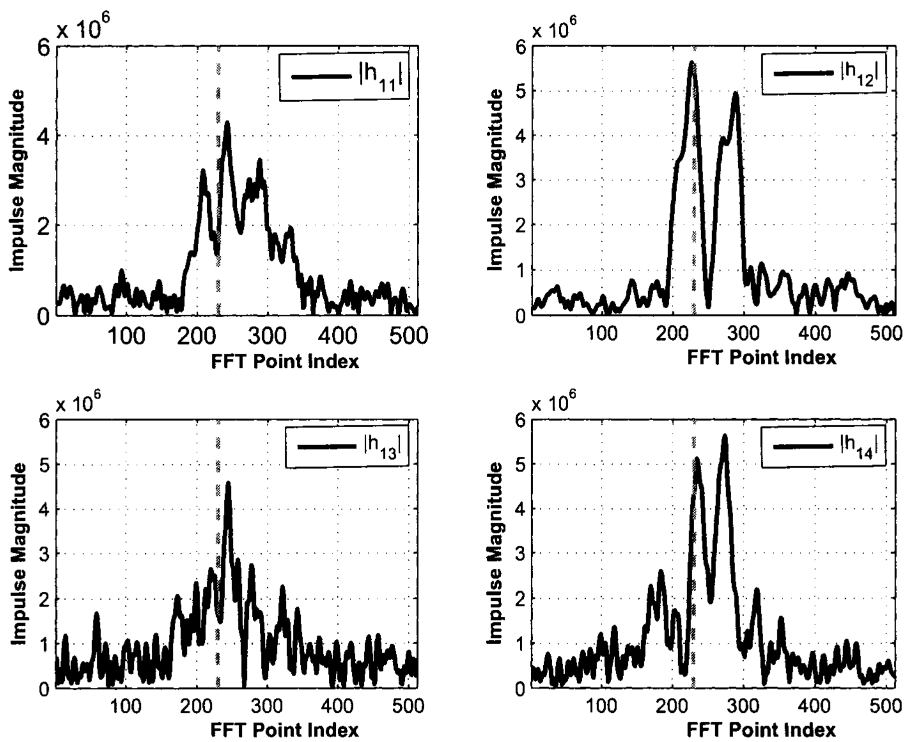

Figure 3.4: PSD of a single IR estimate at receiver one from all transmitters.

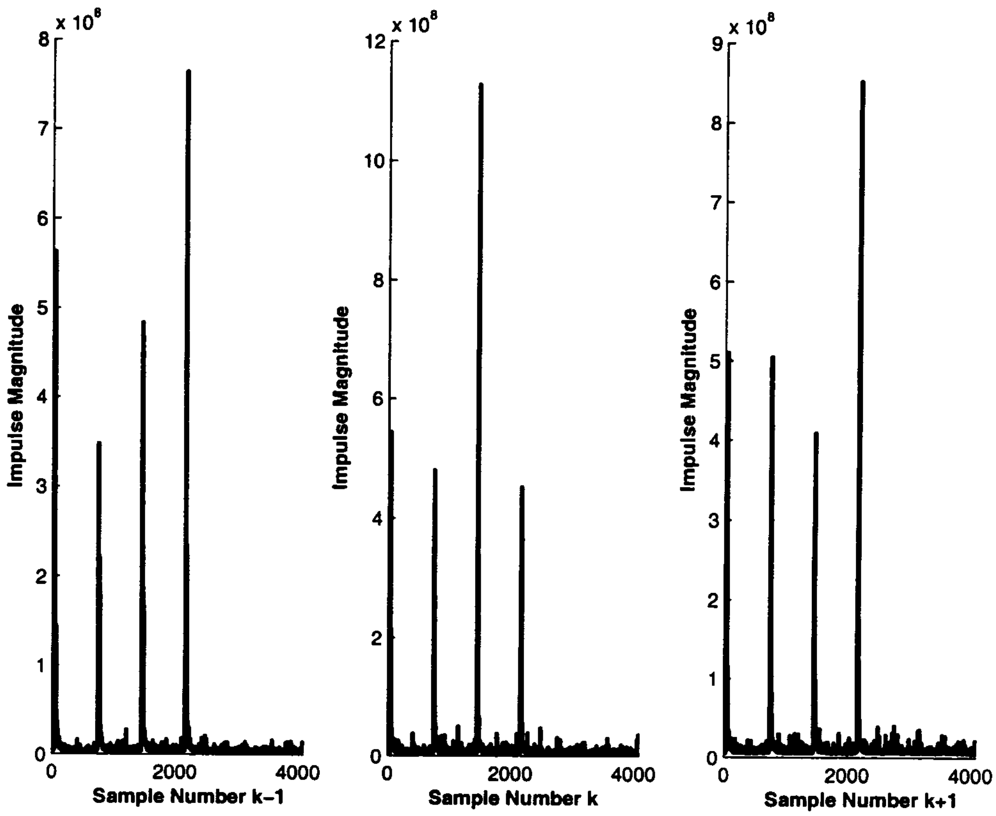

Figure 3.5: 4 × 4 MIMO unthresholded impulse response estimates (UIREs).

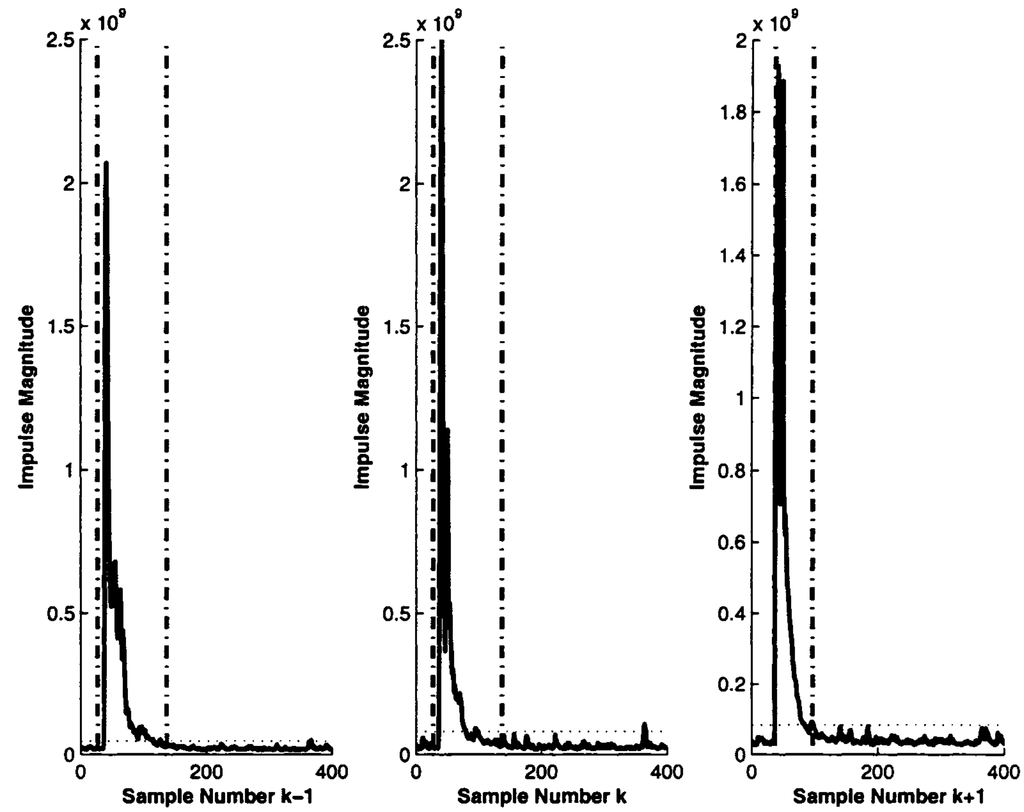

Figure 3.6: 4 $\times$ 4 MIMO thresholded impulse response estimates (TIREs).

3.2.3 Effect of Noise on Mutual Information

The routine presented here serves to determine how 'noisy' our TIREs are and its impact on mutual information calculations. Using information theory, noisy estimates of $\mathbf{H}$ increase entropy, thus affecting the mutual information. To estimate the effects of noise, consider the true channel matrix as

$$\mathbf{H} = \hat{\mathbf{H}} + \mathbf{E} \tag{3.3}$$

where $\hat{\mathbf{H}}$ is obtained from the measurements and $\mathbf{E} \sim \mathcal{CN}(0, \sigma_e^2 \mathbf{I})$. Then the argument of the $\log_2 \det(\cdot)$ function in Chapter 2 becomes

$$\left(\mathbf{I}_N + \frac{\gamma}{M}(\hat{\mathbf{H}}\hat{\mathbf{H}}^H + \mathbf{E}\mathbf{E}^H + 2\mathcal{R}\mathrm{e}(\hat{\mathbf{H}}\mathbf{E}^H))\right) \approx \left(\mathbf{I}_N + \frac{\gamma}{M}(\hat{\mathbf{H}}\hat{\mathbf{H}}^H + M\sigma_e^2\mathbf{I})\right). \tag{3.4}$$

While we don't know $\mathbf{E}$, we can estimate its covariance as

$$\mathcal{E}\{\mathbf{E}\mathbf{E}^H\} = M\sigma_e^2\mathbf{I} \tag{3.5}$$

and also

$$\mathcal{E}\{\hat{\mathbf{H}}\mathbf{E}^H\} = 0. \tag{3.6}$$

Applying (3.5) to a random measured sample of $\mathbf{H}^{(k)}$, we observe approximately a 0.03 bits/s/Hz difference at the median for the CDF estimate of mutual information, thus we expect the mutual information of the measured channel to lie between the two lines in Figure 3.7. The results indicate that our channel estimates, although not free of noise, have little effect on mutual information. We therefore do not need to correct any metrics obtained using $\mathbf{H}$ extracted from the TIREs.

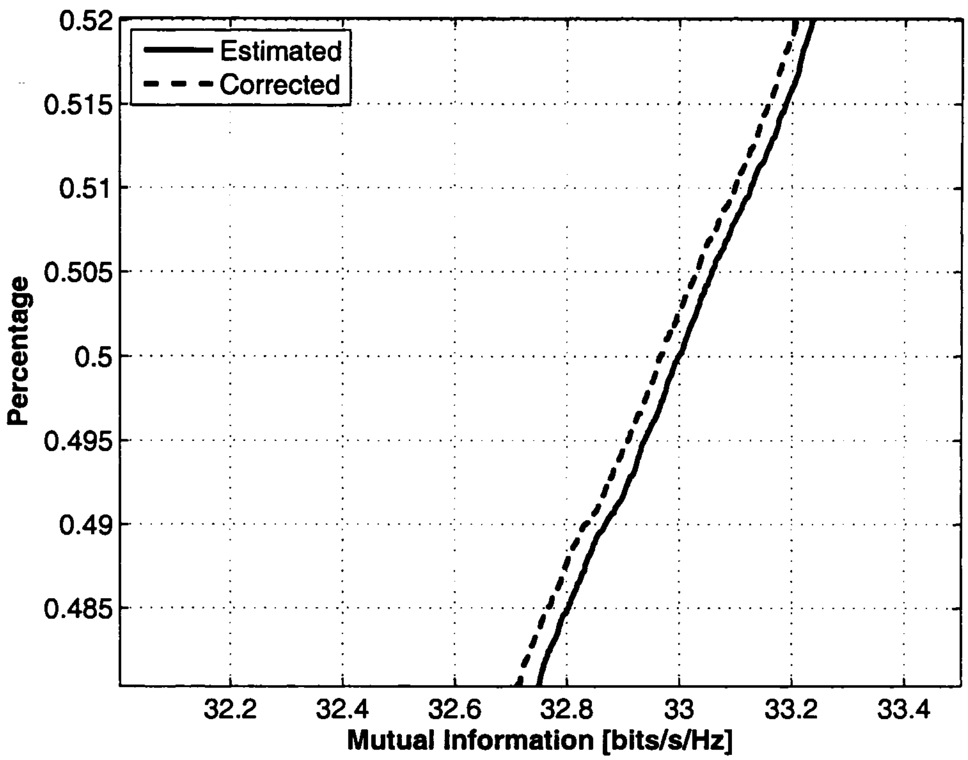

Figure 3.7: Mutual information cumulative distribution function (CDF) employing estimated noise cancelation for configuration with γ = 30 dB.

3.3 Urban MIMO Communications Channel

It is understood that the characteristics of real channels do not follow those predicted by theoretical models. Many signalling techniques have been developed assuming complex Gaussian channel distributions, $\mathbf{H} \sim \mathcal{CN}(0, \mathbf{I})$. However, the performance of the system, especially in the MIMO case, will be radically different in an urban environment for example, where the dominant effect on performance is multipath fading. Therefore, an accurate channel model would need dependencies that describe the channel completely.

Durgin [73] asserts that for realistic wireless channels, the reality is that a channel transfer function is described by 16 different dependencies, including the following:

Frequency The wireless channel depends on the transmitted frequency.

Time The wireless channel is time-varying.

Receiver Translation The wireless channel depends on the position movement (called translation) of the receiver antenna. In three-dimensional space, translation is actually three different scalar dependencies in the wireless channel.

Transmitter Translation What is true for the receiver is also true for the transmitter. The freedom to change transmitter position in three-dimensional space adds another three dependencies to a wireless channel representation.

Receiver Orientation Translation is only one type of spatial dependency. A receiver antenna may be reoriented in any direction in space, which changes the polarisation and gain pattern interaction of the receiver antenna with incoming radio waves. An antenna may be rotated in azimuth or elevation or be tilted laterally. Changes in orientation add up to three dependencies to a wireless channel representation.

Transmitter Orientation The radio channel also depends on the transmitter antenna orientation. This adds three more dependencies to the wireless channel.

Multi-Element Receiver The use of multiple antenna elements at the receiver adds one discrete dependency to a wireless channel.

Multi-Element Transmitter The use of multiple antenna elements at the transmitter adds another discrete dependency.

Depending on the configuration of the channel sounder, the effects of these dependencies can be analysed. Translation and orientation for transmitter/receiver, for example, was studied in [25]. Observed angle of arrival (AOA) is also dependant on translation and orientation. It was shown in [41] that the distribution of the angles of arrival of the multipath components in an urban microcell affects the diversity in a MIMO channel, and as a result, impacts system performance. Depending on the distribution, performance may worsen [4, 17, 25].

To properly describe site-specific propagation channels, these dependencies need to be quantified using a set of channel metrics. For a series of channel responses, $\mathbf{H}^{(k)}$, which is assumed to be ergodic over short intervals, we use the set of metrics discussed in the next section.

3.4 Channel Metric Selection

Using the thirteen metrics defined in Chapter 2, it is possible to characterise a narrowband MIMO channel given $\mathbf{H}^{(k)}$ [29, 41, 58]. However, mathematically and numerically, some metrics are redundant and therefore the number of functions needed can be reduced. They are summarised as follows:

- Average received signal strength, $P(\mathcal{H})$, and path-loss, $\alpha(\mathcal{H})$, are scaled copies of each other, and therefore either one can provide the same information.

- Channel capacity can be described using average mutual information, $\overline{I}(\mathcal{H})$, normalised average mutual information, $\overline{I}_s(\mathcal{H})$, and effective degrees of freedom, $\chi(\mathcal{H})$. With the propagation effects of the channel removed using $\alpha(\mathcal{H})$, mutual information is a useful metric. For example, work in [30] describes mutual information as a function of position along a street corridor.

- Effective degrees of freedom is a function of the average SNR, the number of transmit antennas M, and the eigenvalues of the autocorrelation matrix $\mathbf{HH}^H$, and will display similar properties as $\overline{I}(\mathcal{H})$. It is obtained by manipulating (2.10) such that the MIMO capacity can be written as a sum of $U = \min(N, M)$ equivalent SISO channels, each with gain λ_i [32].

- Effective rank, $\overline{R}(\mathcal{H})$, is insensitive to the effects of path-loss and quantifies the number spatial data pipes available in the channel to carry information.

- Multipath richness, φ, is a simple decomposition of $\overline{I}(\mathcal{H})$. However, this metric is not suited to a direct comparison with BER performance. The richness factor over the length of the run yields a 3-dimensional figure and cannot be compared easily to BER without using a 'slice' of φ. Performance was obtained using all spatial contributions. Richness shows the contributions to mutual information per eigenvalue basis.

- Normalised parallel channel gain, $\overline{CG}$, and normalised parallel channel capacity, $\overline{CC}$, reveals the same information as mutual information and effective degrees of freedom.

From these observations, we pick a subset of metrics to characterise narrowband MIMO channels summarised below:

1. Average signal strength: $P(\mathcal{H})$
2. Average mutual information (channel capacity): $\overline{I}(\mathcal{H})$
3. Normalised average mutual information: $\overline{I}_s(\mathcal{H})$
4. Effective rank: $\overline{R}(\mathcal{H})$
5. Diversity: $\Psi(\mathbf{R})$
6. Correlation: $\Phi(\mathbf{R})$

In the next chapter, we describe the outdoor measurement campaign and locations visited in Ottawa, Ontario, by CRC.

Chapter 4

Outdoor Measurement Campaign

This chapter presents the outdoor measurement portion of this study. Section 4.2 describes the tests performed and Section 4.3 describes the geographic profile of the measurement site.

4.1 Introduction

To illustrate the behaviour of different channels as a function of location, measurements from the CRC 2004 measurement campaign were selected. The route summary is listed in Table 4.1. From this point forward, a measurement route will be referred to by an identifier, e.g. AB35.

Table 4.1: Summary of Measurement Locations

Region	Date	Time	Route
Urban	March 30, 2004	12:38 pm	MQ30
Urban	March 30, 2004	12:33 pm	FA20
Suburban	April 5, 2004	12:18 pm	AB35
Suburban	April 5, 2004	12:08 pm	CC25
Suburban	April 5, 2004	12:22 pm	DD15
Suburban	April 5, 2004	12:03 pm	EF0
Rural	March 26, 2004	11:37 am	AB20

There was a vast amount of information available to process from CRC measurement campaigns with varying antenna configurations. The above collection of routes are sufficient to assess environmental factors based on location.

The three main environmental factors affecting a MIMO channel are channel complexity, external interference and stationarity [27]. The first is a function of the richness of scatterers, i.e. how they are spread in azimuth/elevation. The second is how the resolvable paths are affected by interferers. The third factor is how channel non-stationarity affects channel estimation error, limiting the useful period (or sample size) over which the channel can be estimated. We remind the reader we have assumed a consistency sample size using results from [39] defined in Chapter 2.

4.2 Description of the Outdoor Test

An extensive series of microcellular sounding runs were taken in three different locations in Ottawa, Ontario. The following is a description of each test that was performed.

The following is a list of the relevant test parameters, with values indicated.

1. Base Station Location
2. Base Station Antenna Height - 10 m to 14 m
3. Base Station Antenna
   - Type - Monopole
   - Polarisation - Vertical
   - Directivity - Omnidirectional
4. Coverage
   - Array Spacing - 1λ inter-element spacing

- Vehicle Speed - Variable and around 30 km/hr

5. Triggering Method - time triggered at 250 Hz

A route describes the distance traveled by the mobile receiver, while never covering the same street twice. The mobile traveled at normal speeds in an attempt to mimic typical user patterns. The delay time between two successive channel snapshots was determined by the triggering method [1,40]. The CRC testbed uses 250 Hz triggering.

Some response measurements are accompanied by global positioning system (GPS) coordinates which are appended to the header of each data block. Suburban routes, AB35, CC25, DD15, and EF0 have GPS information available, whereas urban and rural do not. It is obvious that GPS information is not easily accessible from within an urban center with rich scattering and obstruction from large buildings to the receiver. Aerial and topographical survey maps are available online and were used in conjunction with GPS information to plot vehicle position[1]. In the absence of GPS, we extrapolate the mobile position based on the sampling rate and speed of the mobile receiver as seen in Chapter 2. This method is not the best. However, it gives an approximation to the mobile position. The position of the mobile may also be estimated based on diversity and correlation parameters [58].

[1]This Matlab routine was contributed by Yvo DeJong, formerly of the CRC Radio Communications Technologies Group.

4.3 Site Description

In this section, we present descriptions for the three locations used for data analysis to be presented in Chapter 5.

4.3.1 Urban

CRC has logged many hours of outdoor measurements with different antenna spacing and geometry. In this report, only 2 routes are processed for urban analysis. The first measurement was along Slater St. from Lyon St. to Bank St. in Ottawa called MQ30 [58]. A second set of measurements, FA20, was obtained along Bank St. from Gloucester St. to Sparks St [41].

The base station was deployed at the Minto Place hotel (see Appendix A.1). The mobile receiver was driven along the routes shown in Figure 4.1. The immediate area around the transmitter was characterised by 2-5 to 10-30 storey buildings. The downtown area is relatively flat, however, some sections appear to slope upwards, which is typical of urban centers. MQ30 is characterised by a corridor of tall buildings and brief periods of open gaps, typical of urban height differences. Route FA20 had a tapering profile of lower structures and periods of taller buildings towards the end of the route. The gaps between the buildings and low roof edges would allow signals to propagate (by diffraction) into areas where no LOS would exist.

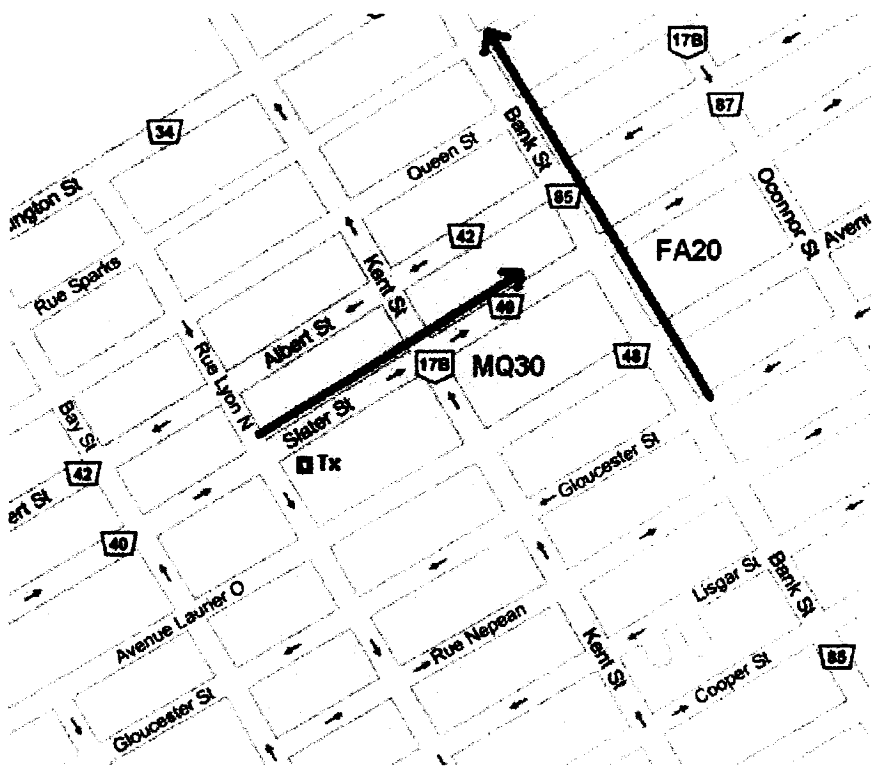

Figure 4.1: Location of transmitter and routes of receiver in urban Ottawa.

4.3.2 Suburban

A suburban neighborhood in Ottawa was measured in April of 2004. The site locations chosen by CRC were close to each other within 2-3 blocks (2 east-west by 3 north-south) in proximity to the transmitter.

In Kanata, the transmitter was deployed at a window of the Country Inn hotel at the corner of Terry-Fox Rd. and Katimavik Rd (see Appendix A.2). The mobile receiver was driven along the routes shown in Figure 4.2. The local area is characterised by an abundance of townhouses separated by trees or local structures. The four routes that make up the measurement campaign are: AB35, CC25, DD15 and EF0.

Like the urban measurements, the height of the transmitter is comparable to the height of structures in the area. We therefore expect the same mechanisms for radio propagation in an urban center to facilitate propagation for suburban. It is possible for there to be a 'knife-edge' characteristic when the launched signal encounters a large home or tall roof. In the case where no LOS exists, we expect diffraction to be largely responsible for signal propagation into regions CC25 and DD15.

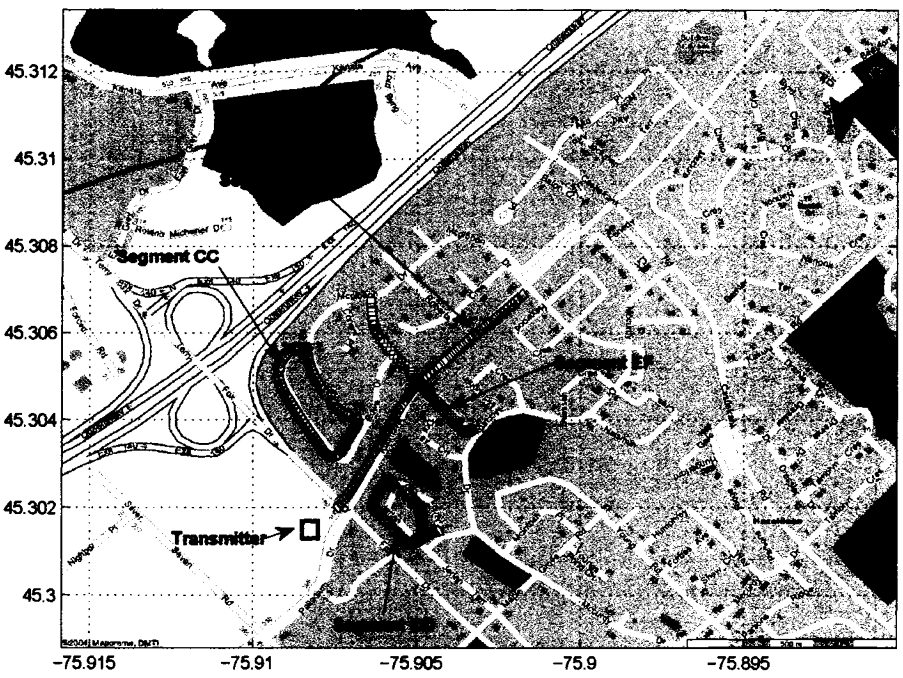

Figure 4.2: Location of transmitter and routes of receiver in suburban Ottawa.

4.3.3 Rural

The measurement route, AB20, was taken at the back of the CRC research campus (at 3701 Carling Ave.) along an access road intersecting Sandhill Rd. It is the most 'open' route taken, with no major buildings or objects. The lack of local scatterers or objects makes this measurement location typical of a rural area.

The transmitter was deployed at a 2^{nd}-floor laboratory window of building 2B (see Appendix A.3). The mobile receiver was driven along the routes shown in Figure 4.3. The mobile receiver traveled in a 'C'-shaped path. For a brief moment, the mobile receiver is in direct LOS with the transmitter. Once non-LOS is reached, the signals must diffract around a collection of buildings including the Canadian Space Agency's David Florida Lab (DFL) to reach the mobile. The DFL is the tallest structure in the area and is composed of varying height buildings joined together. The two tallest structures in the immediate area are two radar-based structures, i.e. terrestrial satellite uplink dishes, that are part of the Department of Defence.

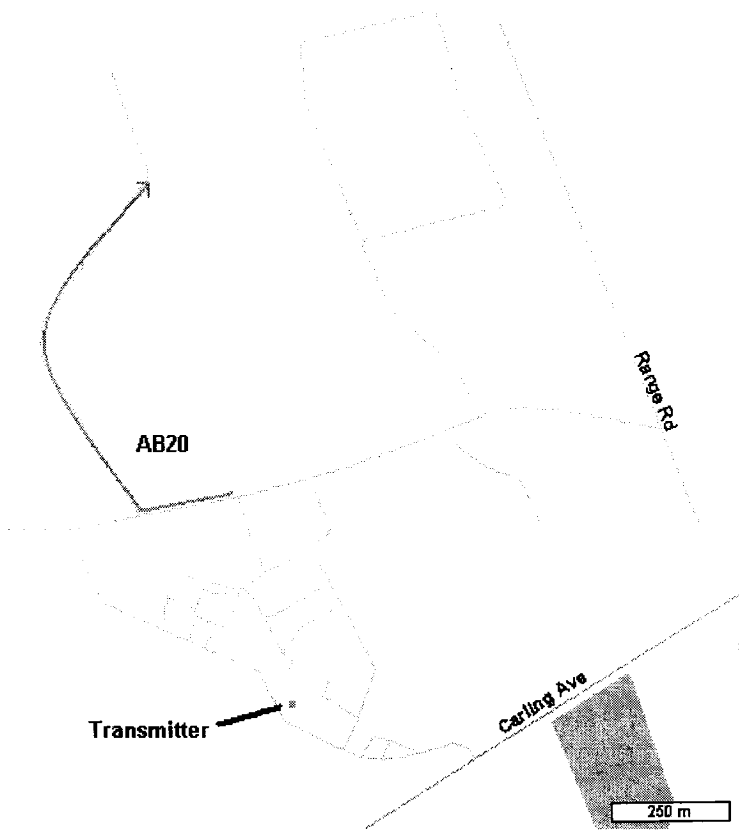

Figure 4.3: Location of transmitter and routes of receiver in rural Ottawa.

In the next chapter, we parameterise the channel measurements taken by CRC researchers in urban, suburban, and rural microcells. The parameterised channels are then analysed to understand the behaviour of the channel as a function of position in the environment.

Chapter 5

Channel Metric Results

This chapter presents the parameterised channel results for urban, suburban and rural Ottawa using the metrics described in Section 3.4. Experimental probing of the MIMO wireless channel shown previously, provided the raw data used to evaluate the following metrics: $P(\mathcal{H})$, $\overline{I}(\mathcal{H})$, $\overline{I}_s(\mathcal{H})$, $\overline{R}(\mathcal{H})$, $\Psi(\mathbf{R})$, and $\Phi(\mathbf{R})$ for all routes. Metric results are calculated using snapshots, defined by

$$\mathbf{H}^{(k)} = \mathbf{H}^{(K \cdot n)}|_{n=1,\ldots,K_{max}} \tag{5.1}$$

where K was given in Chapter 3, n is the sub-interval number and K_{max} is the maximum number of channel estimates such that $K_{max} \leq K \cdot n$.

5.1 Parameterisation of Urban Channels

The measurement routes in Urban Ottawa are shown in Figures 5.1 and 5.3. The processed metric results are presented in Figures 5.2 and 5.4 show the results for the urban environment. Note that $\overline{I}_s(\mathcal{H})$ and $\overline{R}(\mathcal{H})$ in FA20 remain fairly constant over the length of the route, as they discount variations in received signal power, $P(\mathcal{H})$ which also impact $\overline{I}(\mathcal{H})$. Results in [58] indicated a strong correlation between mobile position, diversity, and correlation. The inverse relationship between $\Psi(\mathbf{R})$ and $\Phi(\mathbf{R})$ is clear; these parameters also clearly show variation along the route. Locations where notable results occur for FA20 are indicated in Figure 5.1. Measurements show an increase in received signal power (Figure 5.2(a)) when crossing Laurier Ave. (A), Slater St. (B), Albert St. (C), and Queen St. (D).

As seen previously, the mutual information of a MIMO channel is related to the correlation through the eigenvalues of the channel's covariance matrix. Observing the diversity and correlation measures in Figures 5.2(e) and 5.2(f), there is a strong degree of correlation coinciding with mobile position. Points (A) through (D) show that correlation is strong when the mobile receiver is between major intersections. Referring to Figure 5.1, the mobile is in an area of high building density compared to that observed in MQ30.

It was reported in [41] that correlation for outdoor measurements displayed interesting properties contrary to the i.i.d. CG case. The traffic density for FA20 may have been a contributing factor to the high effective rank and high diversity at the intersections. Also, there was a higher building density at the corner of Slater St. and Bank St. compared to Queen St. where a drop in average signal strength and effective rank was observed.

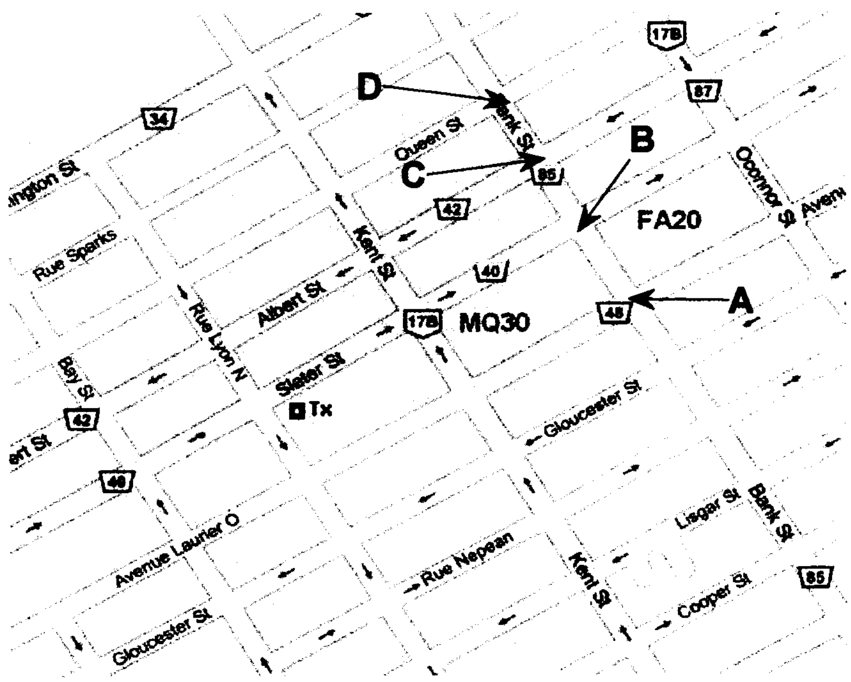

Figure 5.1: Points of interest on route FA20.

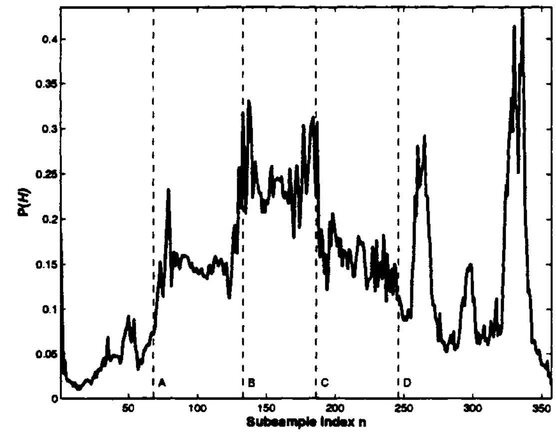

(a) Average Signal Strength

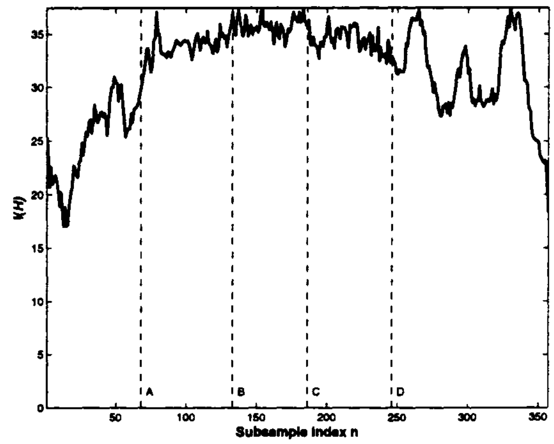

(b) Average Mutual Information ($\gamma = 30$ dB)

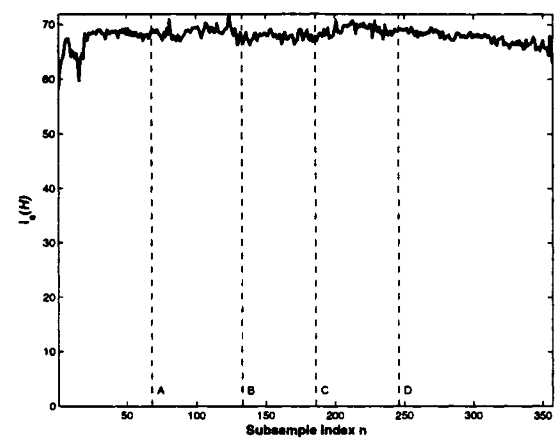

(c) Normalised Average Mutual Information ($\gamma = 30$ dB)

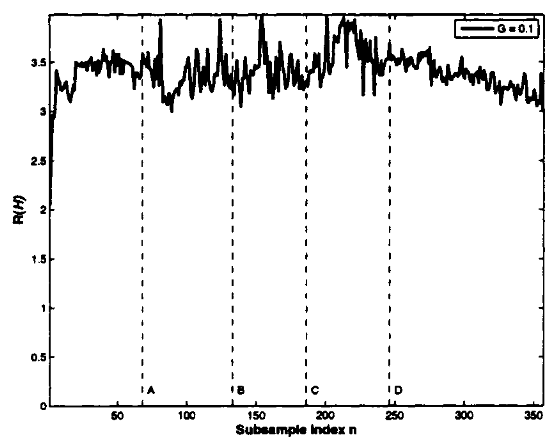

(d) Effective Rank ($G = 0.1$)

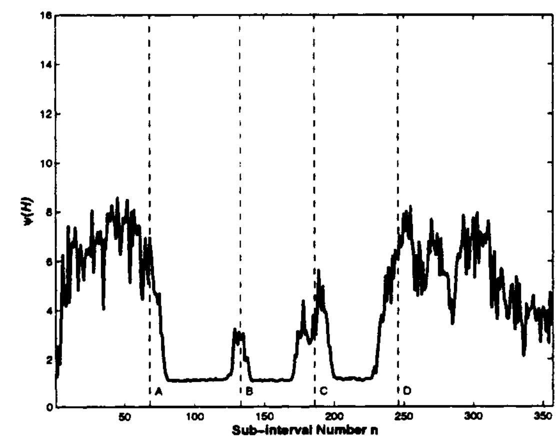

(e) Diversity

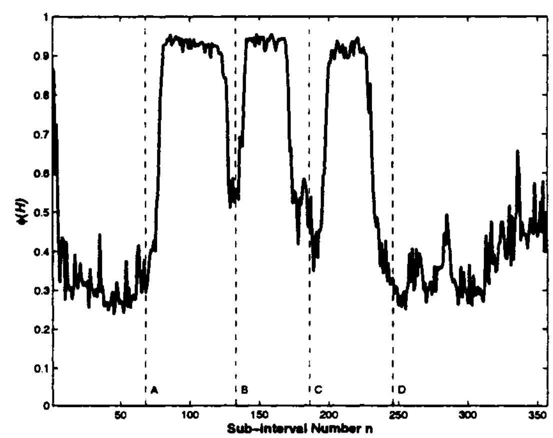

(f) Correlation

Figure 5.2: Parameterisation of FA20.

With MQ30, the mobile traveled the most direct path away from the transmitter. The effects of path loss are observed clearly as the average signal strength decreases as predicted by large-scale fading. Figure 5.3 indicates some interesting points along route MQ30. Diversity is high at the intersection of Lyon St. and Slater St. (A), and lowest when a strong specular component is received from the transmitter at (B). At the open intersection of Slater St. and Kent St. diversity increases, which is attributed to the presence of scatterers and diffraction at the building edges facing the area. As the separation between transmitter and mobile receiver increases, the effects of correlation dominate as mutual information decreases. Similar to FA20, correlation reaches its maximum when the Kent St.-Bank St. corridor is reached at (C) in Figure 5.4(f). At this point, the building density has increased considerably and the incoming signals have been heavily attenuated due to reflection and diffraction. In Figure 5.4(b), received signal strength is low despite effective rank (Figure 5.4(d)) indicating strong subchannels available to transport information. Overall, effective rank remains high, consistent with the propagation mechanisms responsible for signal propagation in an urban center. Along MQ30, the mutual information available in the channel degrades heavily due to the incoming signals being strongly correlated and low in signal power. At this point in the channel, power control would be necessary increase the information carrying ability of the channel.

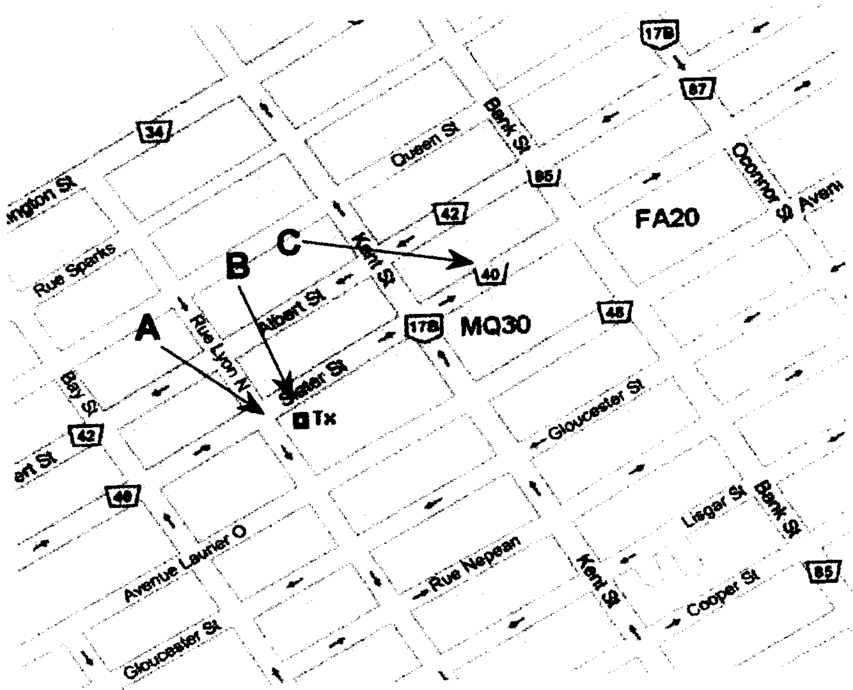

Figure 5.3: Points of interest on route MQ30.

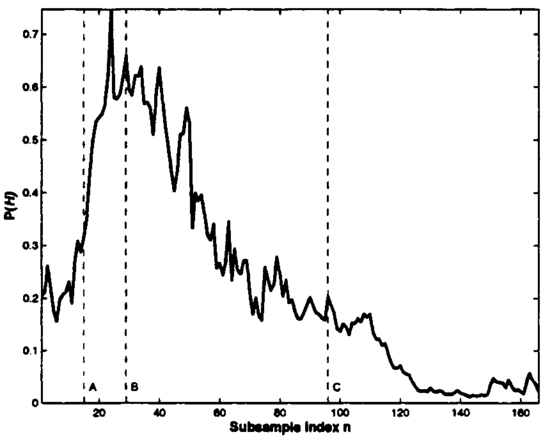

(a) Average Signal Strength

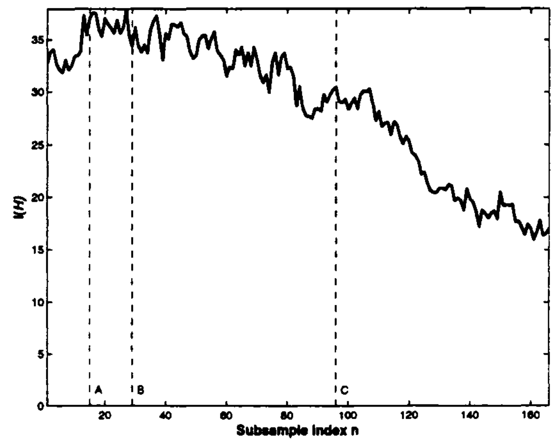

(b) Average Mutual Information (γ = 30 dB)

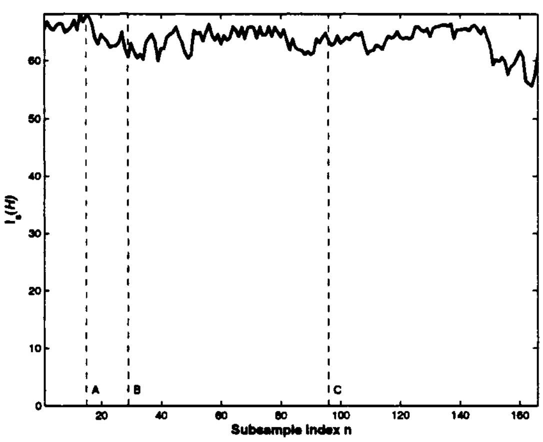

(c) Normalised Average Mutual Information (γ = 30 dB)

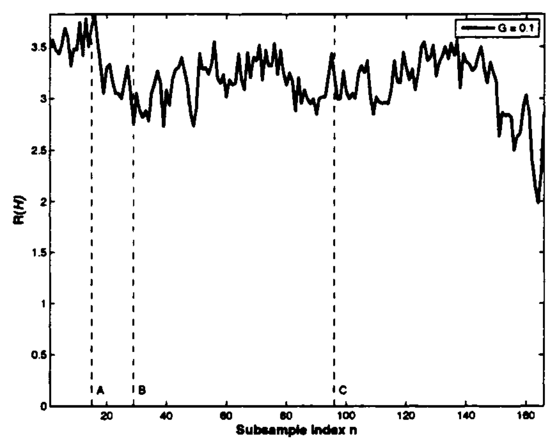

(d) Effective Rank (G = 0.1)

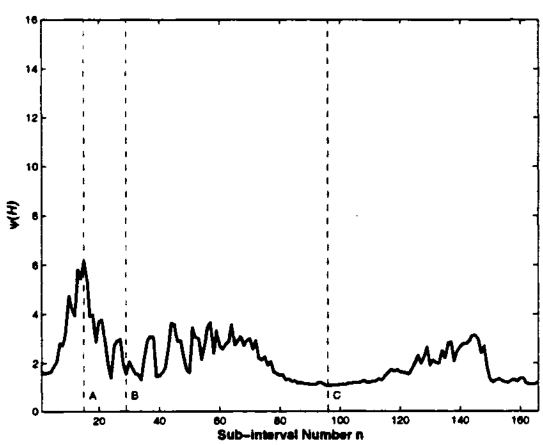

(e) Diversity

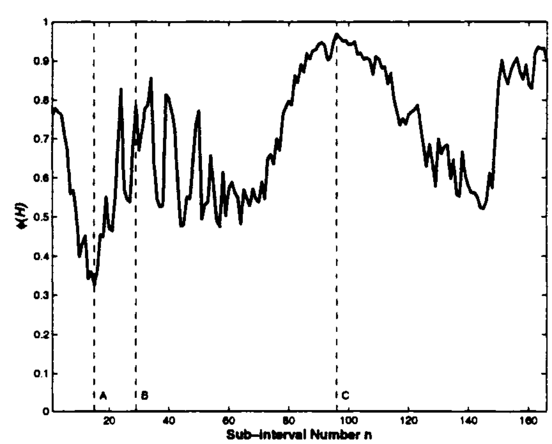

(f) Correlation

Figure 5.4: Parameterisation of MQ30.

5.2 Parameterisation of Suburban Channels

Figures 5.6 through 5.12 show the results for the suburban environment. The parameterised channels for suburban Ottawa behave differently when compared to the findings for urban routes FA20 and MQ30. Figure 5.5 indicates some interesting points along route AB35. It is the most direct trajectory away from the transmitter along Katimavik Rd. Contrary to what was observed for urban intersections, diversity is not high at Katimavik Rd. and Terry Fox Dr. (A) as seen in Figure 5.5 using an intensity plot for Φ. This is attributed to the more open geography, and lower traffic density.

Correlation remains high for the first half of the run and peaks coinciding with the passing of an open-area park at (B). After crossing the Davis Ave.-Curran St. intersection (C), the remaining incoming multipath components are weak but are still highly correlated despite a high effective rank over the same period. This result suggests that effective rank does not reveal any useful information in suburban environments. Mutual information (in Figure 5.6(b)) is high for the first 100m of the route due to the strong incoming specular components from the transmitter. A strong LOS is maintained until (A) is reached. After this, weak multipath components are responsible for the majority information throughput of the channel.

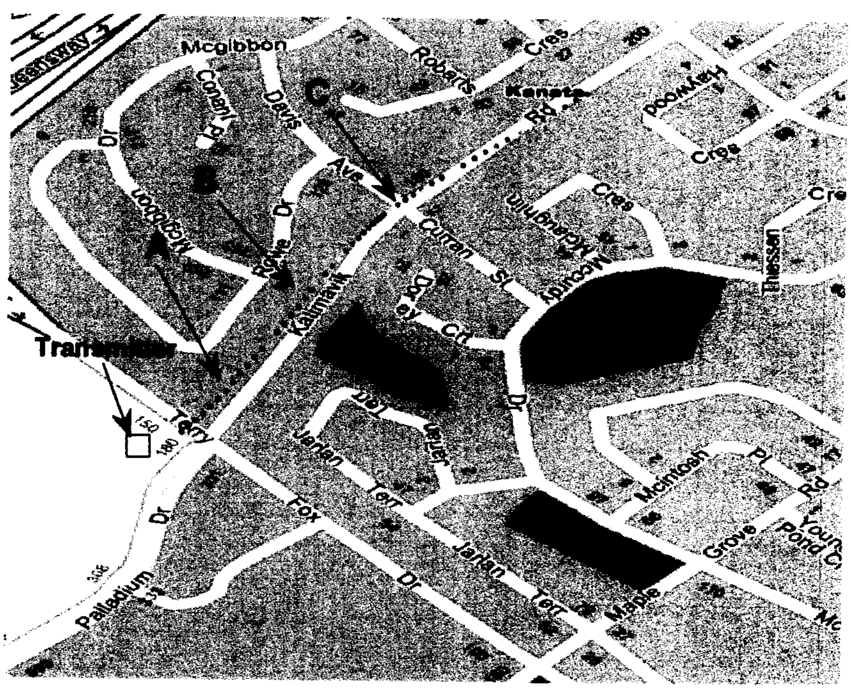

Figure 5.5: Points of interest on route AB35.

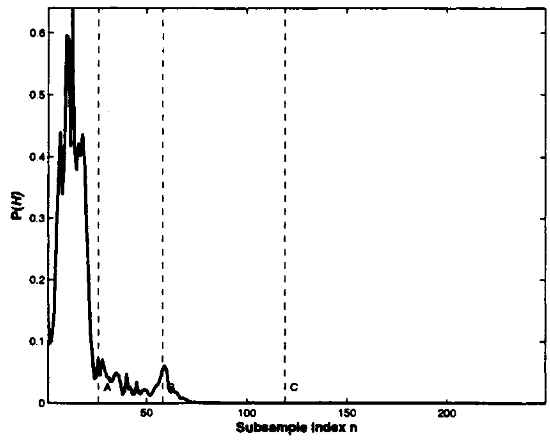

(a) Average Signal Strength

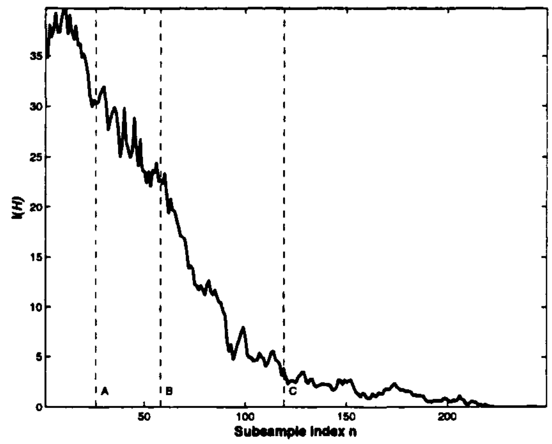

(b) Average Mutual Information (γ = 30 dB)

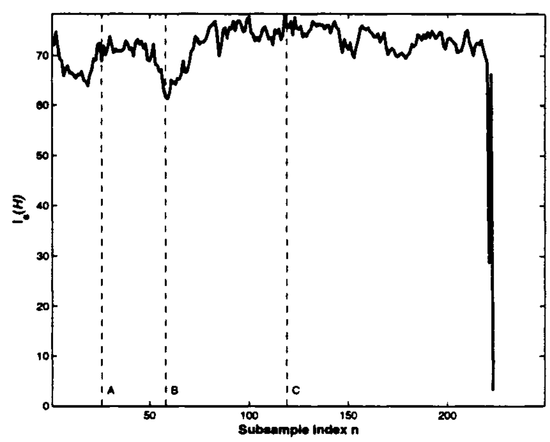

(c) Normalised Average Mutual Information (γ = 30 dB)

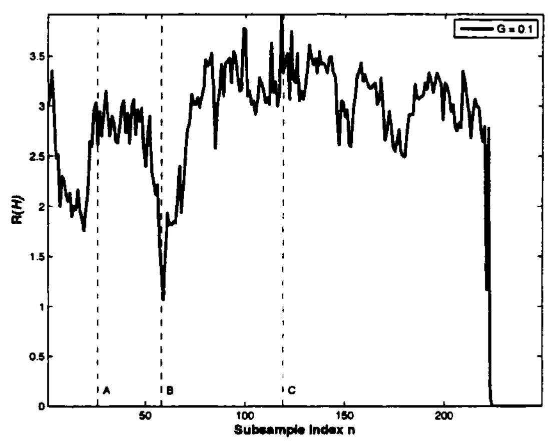

(d) Effective Rank (G = 0.1)

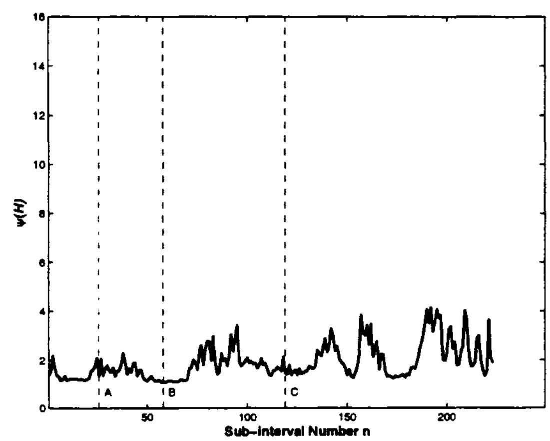

(e) Diversity

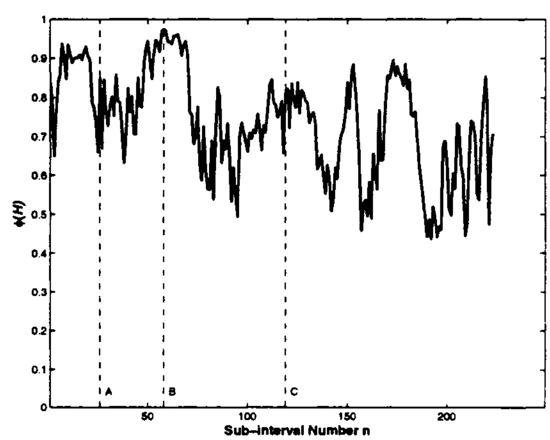

(f) Correlation

Figure 5.6: Parameterisation of AB35.

On CC25, the mobile receiver travels along a suburban loop formed by McGibbon Dr. and Rowe Dr. Figure 5.7 plots the results of Φ using GPS information along the route.

At the start of the route at (A), the axis of the array is perpendicular to the direction of the transmitter. Strong specular components arrive via the gaps between the houses that follow the bend around the first turn at (B). The diffraction at the roof-tops also produce signals that interact with scatterers, e.g. vehicles in driveways and rooftop antennas. From (B), the observed angular spread at the receiver is small, causing the signals to appear highly correlated.

After the turn at (B), the axis of the array is facing the direction of the transmitter until (C) is reached. The beam pattern of the array is highly directive at broadside, but resolution is poor near the axis. The incoming signals at the end of the array will catch the main lobe near its weakest spot. Thus, correlation has little impact when the incoming signal arrives along the axis of the array. Mutual information is high over the same interval, and highest at (C) where correlation is low.

At (D) and (E) diversity is low and average signal strength continues to decrease. Effective rank does behave much like diversity at urban intersections. Along McGibbon Dr. much of the received signal has been heavily attenuated at (F). The two main sources of signal power would be at the effective point sources formed at (E) and (A).

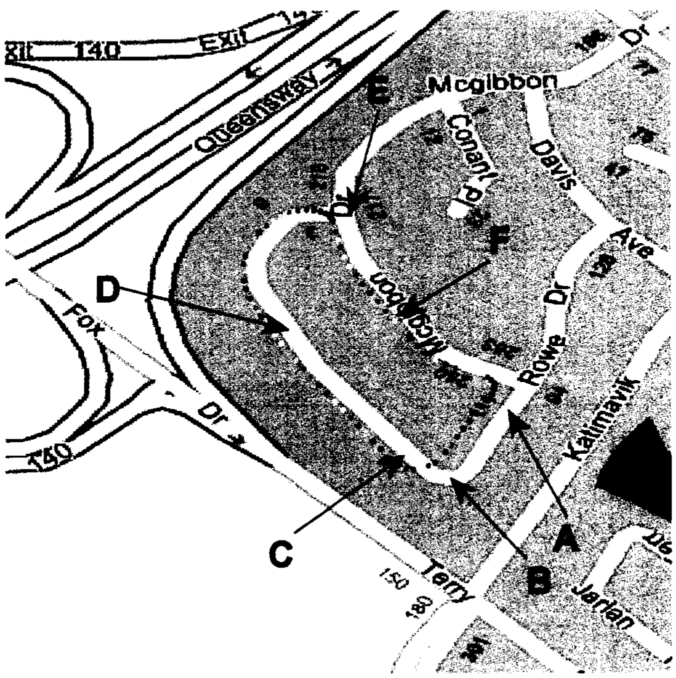

Figure 5.7: Points of interest on route CC25.

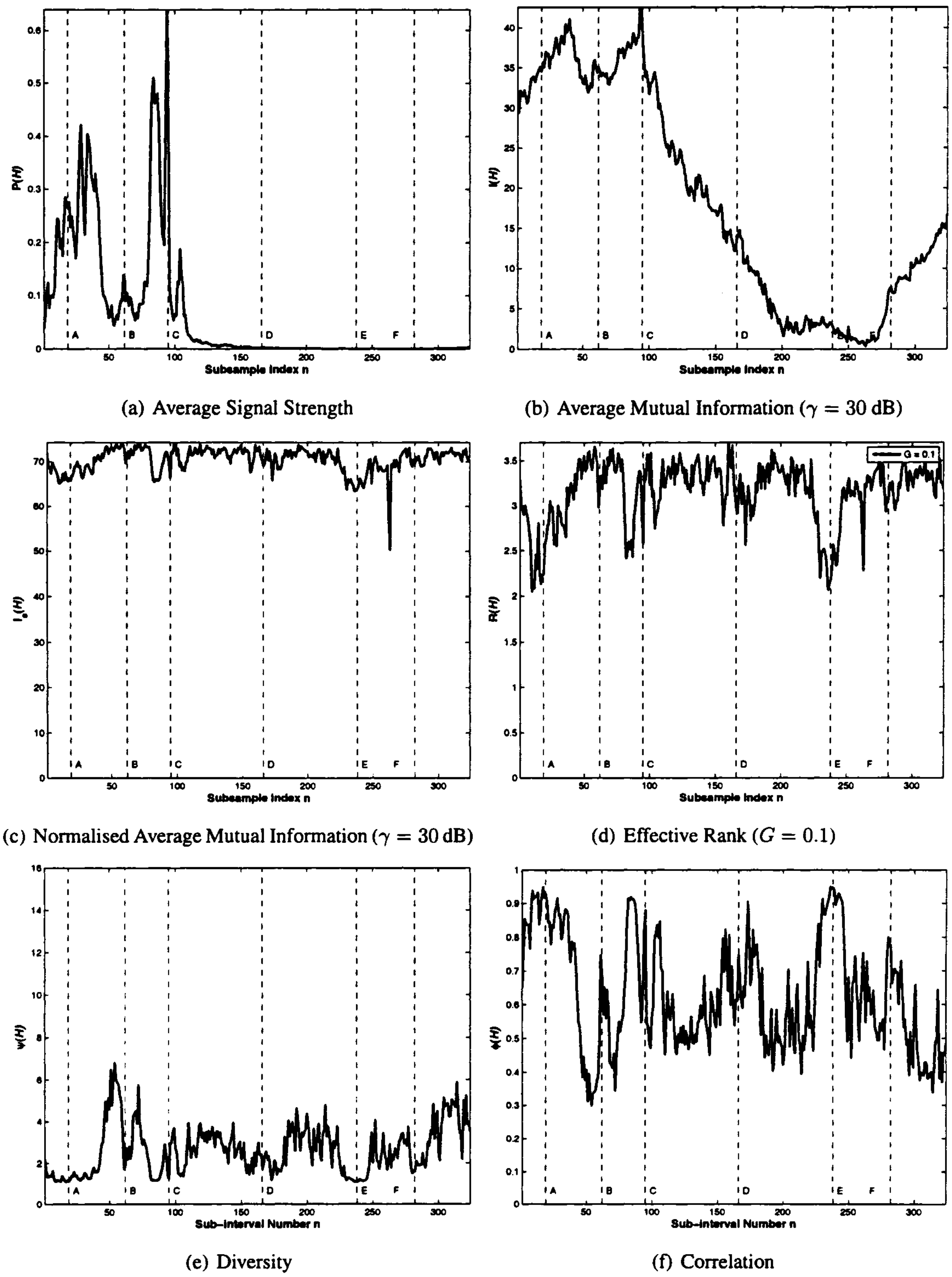

(a) Average Signal Strength

(b) Average Mutual Information ($\gamma = 30$ dB)

(c) Normalised Average Mutual Information ($\gamma = 30$ dB)

(d) Effective Rank ($G = 0.1$)

(e) Diversity

(f) Correlation

Figure 5.8: Parameterisation of CC25.

On DD15, the mobile takes a similar path to CC25. The observed correlation (see Figure 5.10(f)) is much lower throughout the route, though the results are much more interesting. Comparing the GPS markers with the correlation over position, some interesting results are observed where the orientation of the mobile changes. Figure 5.9 correlates the results for Φ with GPS position information for DD15. At (A) through (E) in Figure 5.10, it is observed that correlation is high when the mobile crosses an intersection. In [58] it was seen that correlation was low at an intersection. We note that there is a difference in the presence in local scatterers in urban and suburban environments. The contribution from local scatterers is significantly less in DD15, but the signals remain highly correlated.

Between (A) and (B), diversity and rank are high indicating a strong presence of multipath components. One possible explanation for this is the incoming signals acting as a point source from (C). For the same observations in CC25, the observed angular spread of the incoming specular components is small.

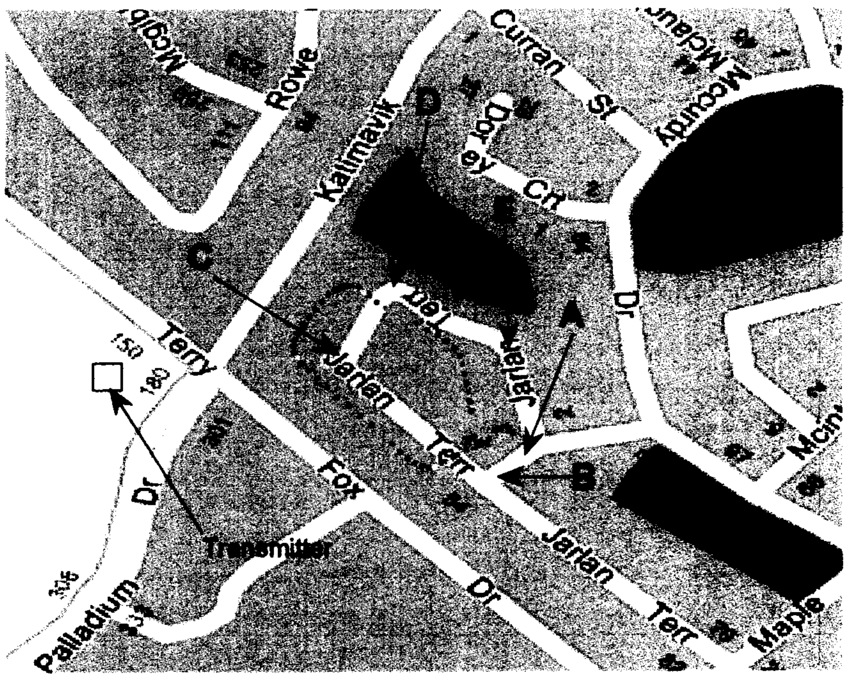

Figure 5.9: Points of interest on route DD15.

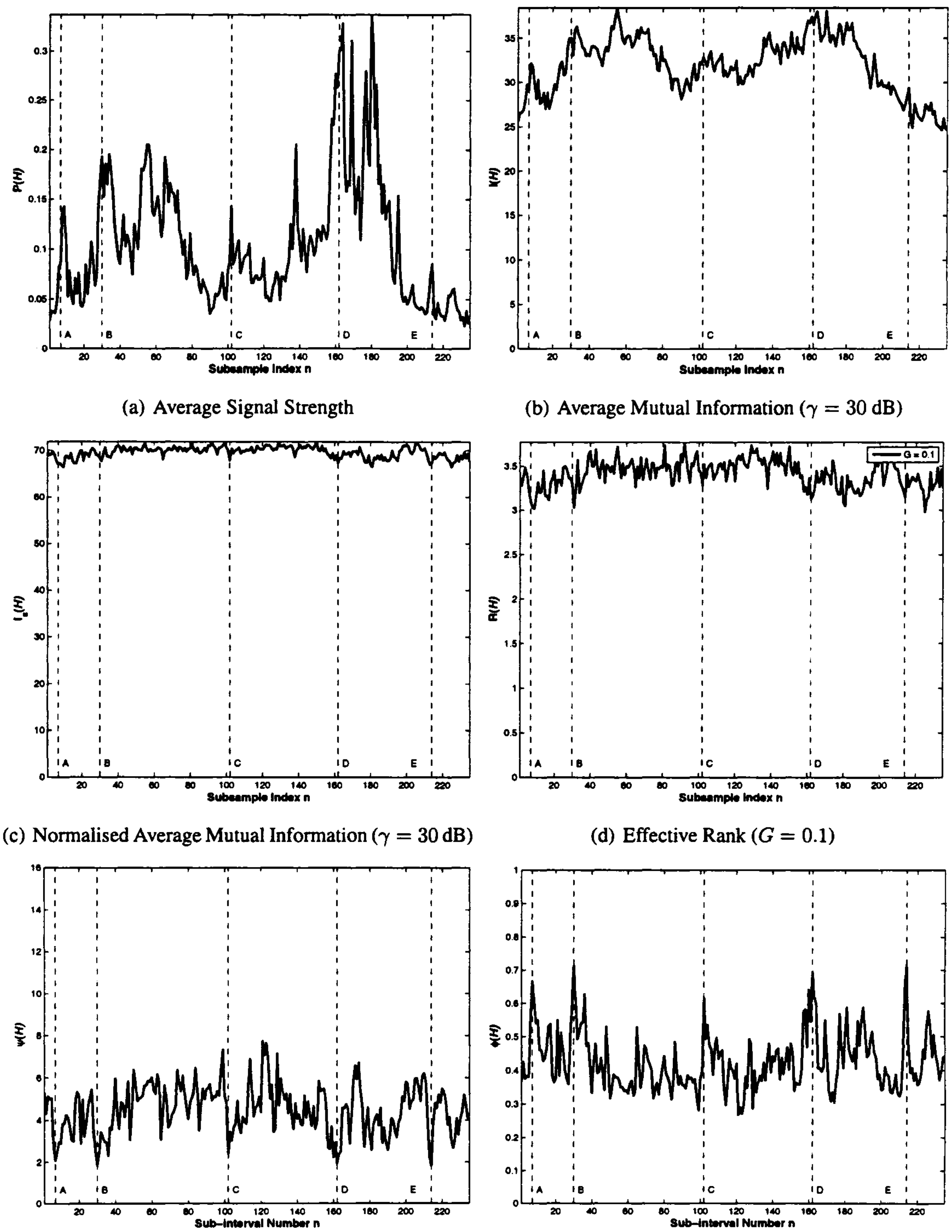

(a) Average Signal Strength

(b) Average Mutual Information (γ = 30 dB)

(c) Normalised Average Mutual Information (γ = 30 dB)

(d) Effective Rank (G = 0.1)

(e) Diversity

(f) Correlation

Figure 5.10: Parameterisation of DD15.

On the last route EF0 the mobile travels parallel to the orientation of the transmitter array. The previous two routes showed the opposite trend for diversity-correlation at an intersection. Figure 5.11 shows the results for Φ with GPS position information for EF0. Mutual information and average received signal power both peaked at (A), the intersection of Katimavik Rd. and Davis Ave.-Curran St. At the same time effective rank was low and correlation was high indicating that there was a significant contribution of multipath components from the direction of the transmitter. Once at the intersection, the diffraction off the houses caused the signals to reach the broadside of the array where it was is most responsive to the observed angular spread.

Mutual information reached its highest point at (B) coinciding with the passing of Rowe Dr. It is possible for signals arriving along Rowe Dr. and Davis Ave. to be reflected/scattered thus giving the illusion of having a transmitter nearby. Towards the end of the route at (C) average normalised mutual information, effective rank and correlation showed an interesting result.

The rich scattering at (B) serves as an effective point source, though, no multipath existed at that point. The resulting signal would bee transmitted in many directions. Diffraction into the narrow corridor near (C) reduced these to an effective strong specular component arriving at the array broadside. The results in Figure 5.12 do capture interesting properties in the suburban radio channel that are quite different than those observed in the urban case.

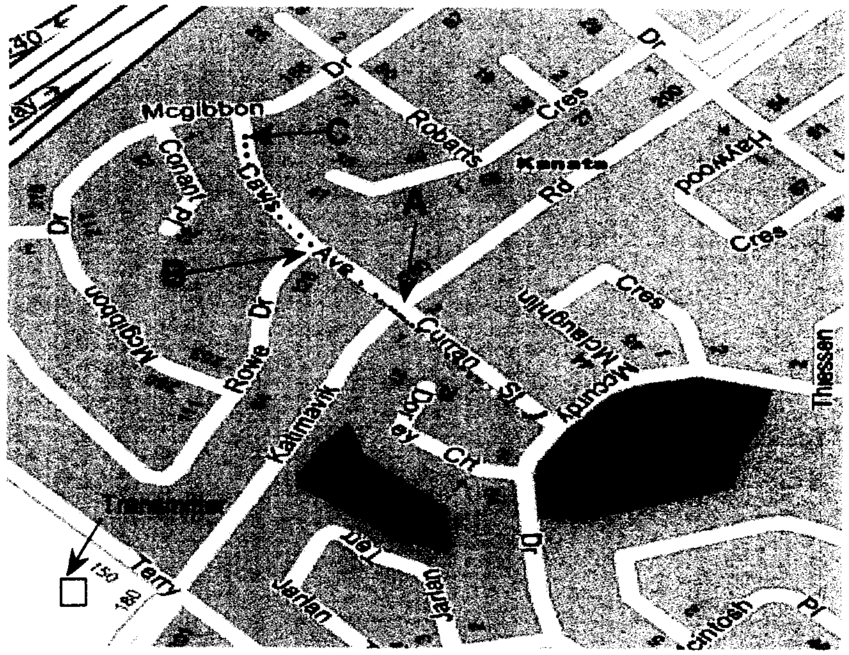

Figure 5.11: Points of interest on route EF0.

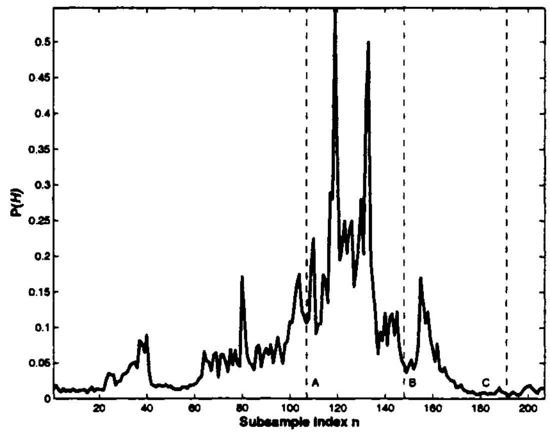

(a) Average Signal Strength

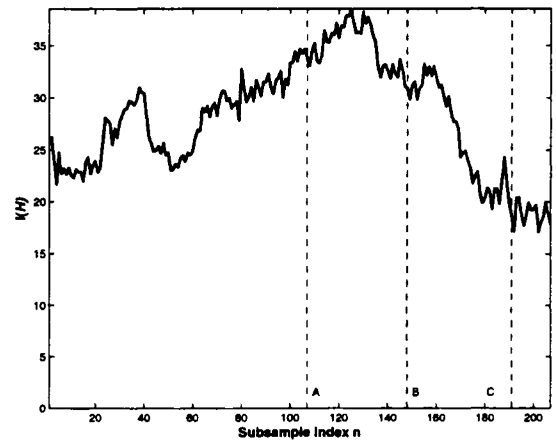

(b) Average Mutual Information (γ = 30 dB)

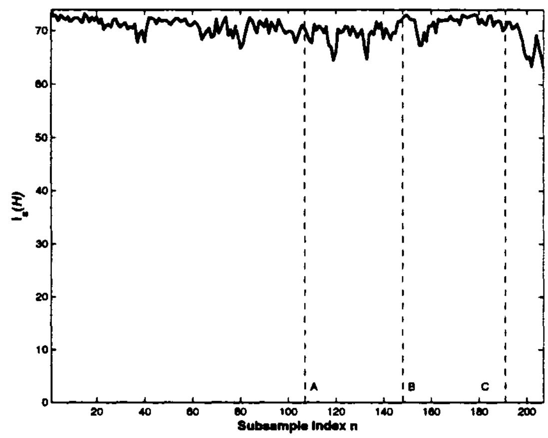

(c) Normalised Average Mutual Information (γ = 30 dB)

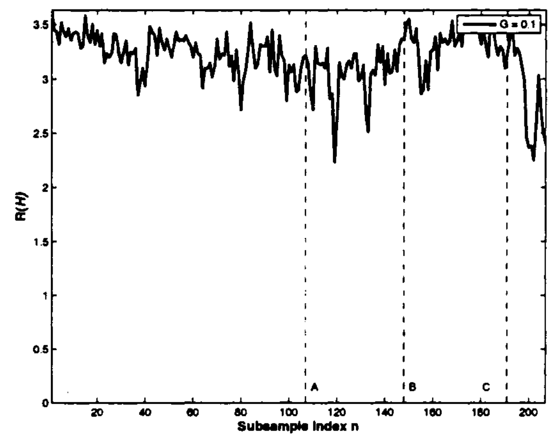

(d) Effective Rank ($G = 0.1$)

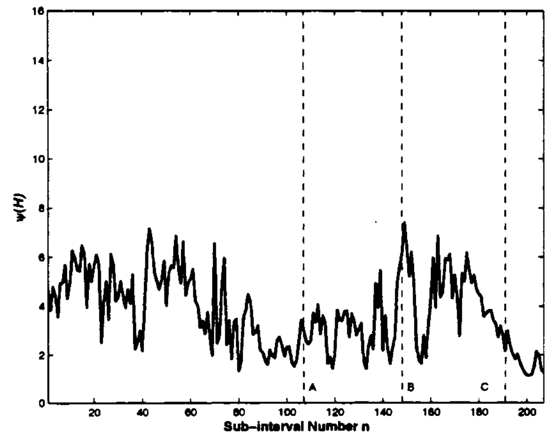

(e) Diversity

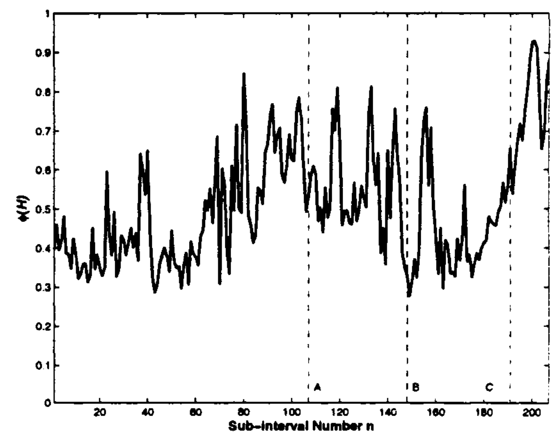

(f) Correlation

Figure 5.12: Parameterisation of EF0.

5.3 Parameterisation of Rural Channels

Figure 5.14 shows the results for the rural environment. The parameterised channels for rural Ottawa behave similarly to those observed for suburban Ottawa. Figure 5.13 indicates some interesting points along route AB20. In Figure 5.14(a), the sharp decline in average signal strength for AB20 was attributed to free-space path-loss. At the start of AB20, the fluctuations in diversity and correlation are attributed to the presence of terrestrial satellite uplink dishes and storage structures that are in proximity to the first turn at (A).

The orientation of the mobile receive array was also an important factor in the receiving of multipath signals. Once the first turn was made by the mobile, small changes in diversity and correlation were observed. The broadside of the receive array would be facing the direction of the transmitter. Thus, the incoming signals would appear correlated for small angular spread and be heavily attenuated after interacting with the buildings found directly in the transmitter's path (circles). Many of the signals reaching the receiver from the transmitter were produced by diffraction and reflection.

Mutual information was observed to remain stationary once the turn had been made and the mobile traversed the most direct route away from the transmitter (A to B). With the effects of path-loss removed, the normalised average mutual information (see Figure 5.14(c)) is directly related to the amount of diversity in the channel. At (C), normalised average mutual information shows that correlation impacts the amount of information available in the channel. The incoming components, though small in signal power, are highly correlated due to the local environment. After passing (C), the mobile enters a region where hills are on both sides of the route.

In the next chapter, we compare the metric results based on location and correlate these results to the BER in the channel.

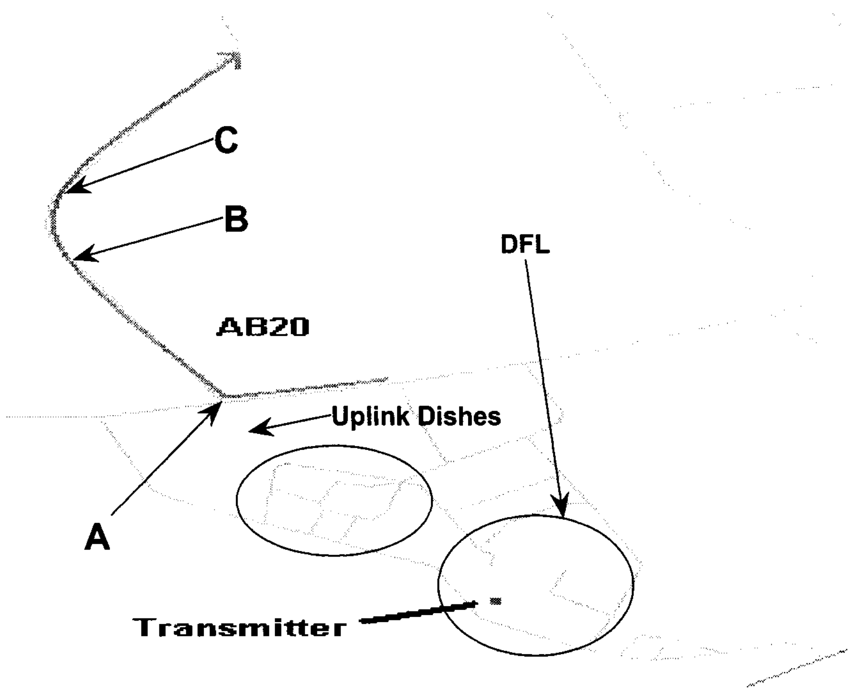

Figure 5.13: Points of interest on route AB20.

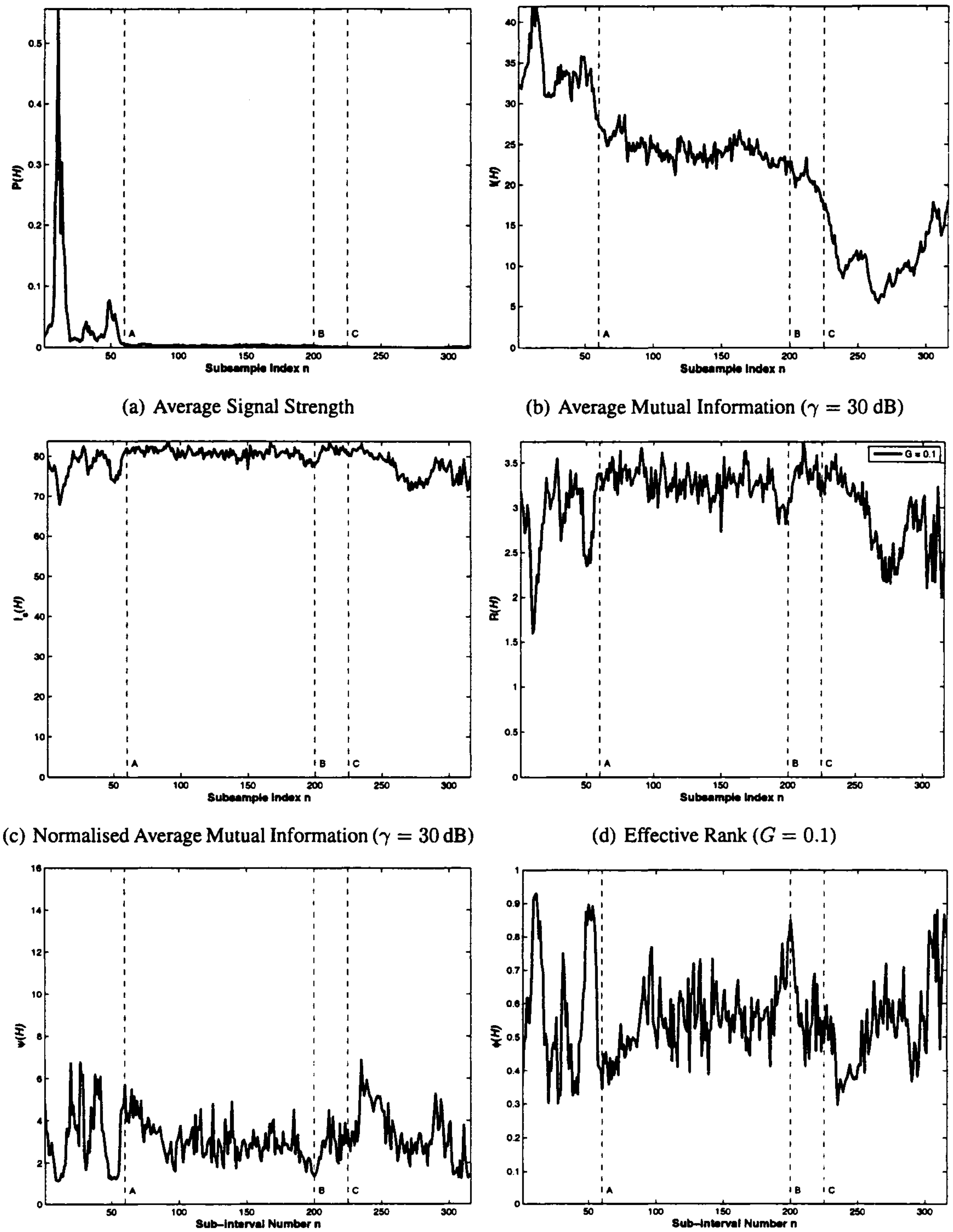

(a) Average Signal Strength

(b) Average Mutual Information (γ = 30 dB)

(c) Normalised Average Mutual Information (γ = 30 dB)

(d) Effective Rank (G = 0.1)

(e) Diversity

(f) Correlation

Figure 5.14: Parameterisation of AB20.

Chapter 6

Performance Prediction

In this chapter, the normalised data collected using the CRC testbed is processed to predict the BER performance of different MIMO Space-Time architectures[1]. The prediction technique consists of 4 basic steps: 1) simulate BER performance, 2) compare BER to metric(s), 3) apply regression, and 4) fitness testing.

6.1 BER Performance of all Routes

To illustrate the benefits of STBC and V-BLAST have for high data rate communications in real environments, we simulate their BER performance using measured data. A simulation was conducted using the framework outlined Chapter 2 for $N = M = 4$; 2 bits/s/Hz and 8 bits/s/Hz respectively for V-BLAST and STBC over a specified operating range of SNR.

Figure 6.1 shows the simulated BER results for urban Ottawa for V-BLAST and STBC. The results for FA20 and MQ30 show that STBC and V-BLAST perform differently when correlation is high at a given SNR. Generally, performance is better in V-BLAST when correlation is low, but strongly related to signal strength and mutual information as observed earlier. Clearly, the type of MIMO technique used in an urban environment depends on correlation.

[1]These techniques do not require the knowledge of the channel at the transmitter.

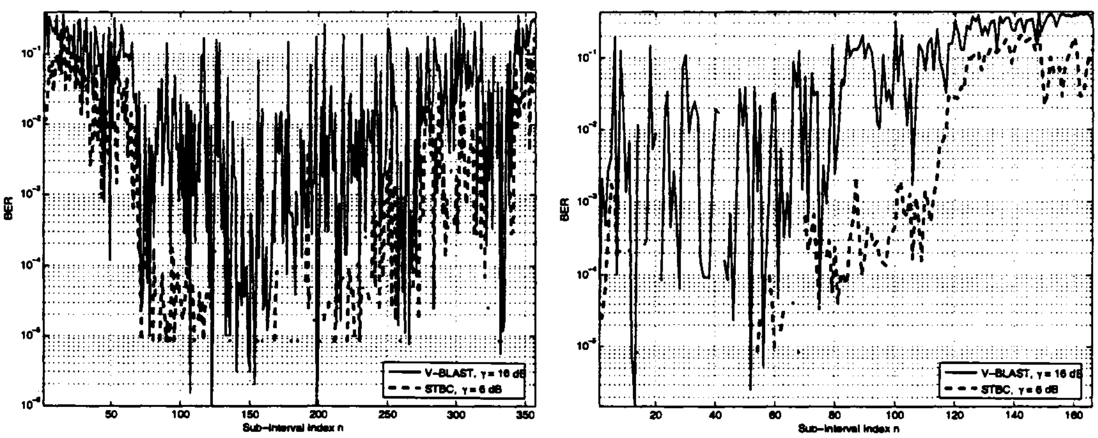

(a) FA20

(b) MQ30

Figure 6.1: BER performance over time for urban Ottawa.

Figure 6.2 shows the BER results for suburban Ottawa for V-BLAST and STBC at their respective SNR. The correlation over route AB35 was high and STBC performance was expected to improve. Performance for V-BLAST degrades as the received signal power decreases and correlation increases. For STBC, it is signal strength alone that appears to impact performance.

On CC25, performance for both MIMO techniques is relatively good. Performance for V-BLAST is worse at the start where the correlation is high. STBC performance trend matches that of V-BLAST when the mobile starts the second portion of its run. There is a significant loss of signal strength and performance of both techniques degrade.

On DD15, although the trajectory of the mobile was similar to CC25, the performance trend was the same. Performance of STBC improved over the regions where correlation was high.

On EF0, the best performance of V-BLAST was observed when the mobile was far from the intersection of Katimavik Rd. and Davis Ave.-Curran St. STBC performance degraded near the end of the run despite there being a high correlation but signal strength was low.

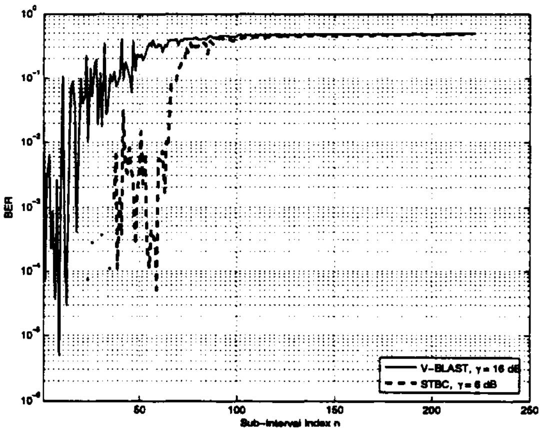

(a) AB35

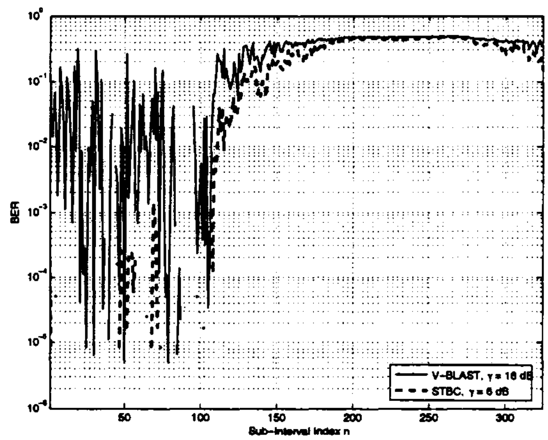

(b) CC25

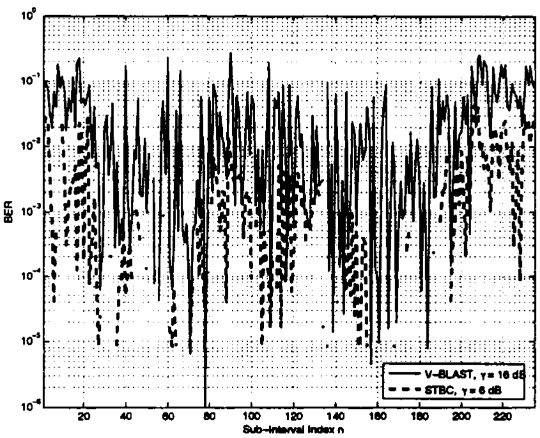

(c) DD15

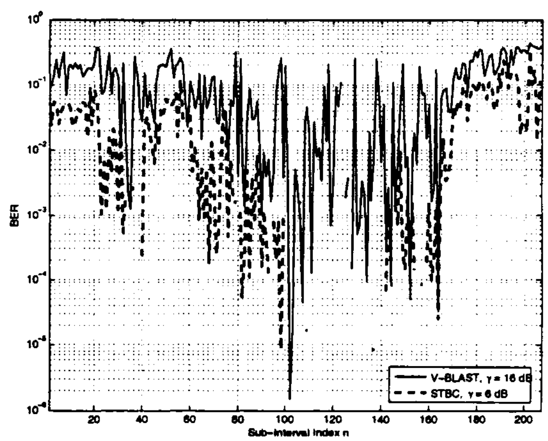

(d) EF0

Figure 6.2: BER performance over time for suburban Ottawa.

Figure 6.3 shows the BER results for rural Ottawa for V-BLAST and STBC. The correlation observed along AB20 was high, i.e. $\Phi > 0.6$, for a majority of the route. The performance of V-BLAST follows a similar trend. It is important to note that in both cases, performance is relatively constant over the region where the mobile is traveling away from the transmitter. The results do indicate that the performance of V-BLAST and STBC is strongly linked to the amount of correlation in the channel and the average received signal strength.

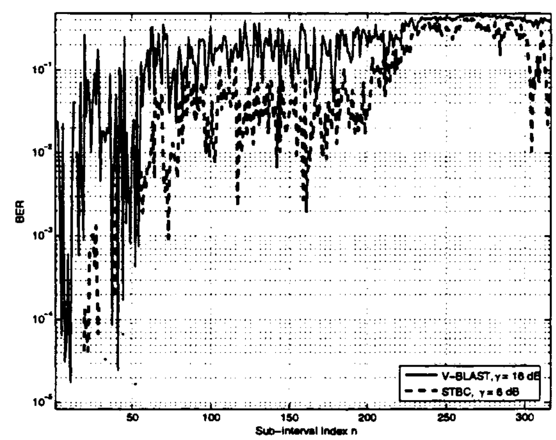

Figure 6.3: BER performance over time for rural Ottawa.

6.2 Methodology of Prediction

Previous work [27, 74] had used only the mutual information to define good channels. It is not the only possible metric of performance. Performance prediction, such as the technique presented in this thesis, uses the metrics defined in Chapter 3 to estimate the performance of two space-time architectures.

Few studies exist that use real measurement data to predict the BER results for MIMO transmission schemes. Performance prediction in this thesis is a three part process: 1) the parameterised metric information is plotted against the BER for different simulated MIMO techniques, 2) a first order linear regression is applied to the result, and 3) the fit of the first order regression is tested. The two most common fitness metrics are normalised mean-square error (NMSE) and coefficient of correlation. These simple metrics give an indication of how accurately the predictor trendline from regression fits the measured/simulated data. We use linear estimation since there are a limited number of data points obtained from simulation, *i.e.*, only points between 10^{-4} and 10^{-1} were considered.

6.2.1 Linear Regression

The best-fit predictor was obtained using the 'polyfit(x,$\bar{\text{t}}$,n)' function in Matlab. The operation finds the coefficients of a polynomial $p(\text{x} = BER)$ of degree n that fits the target data, $\bar{\text{y}}$. The result is given by

$$p(\text{x}) = p_n x^n + p_{n-1} x^{n-1} + \ldots + p_2 x^2 + p_1 x^1 + p_0 \quad (6.1)$$

where $p = \bar{\text{y}}$ for the calculations carried out in this thesis. A first-order fit, $n = 1$, was used. Equation (6.1) operates over the supplied BER information for a particular MIMO scheme and metric values $\bar{\text{y}}$ obtained by channel parameterisation.

6.2.2 Goodness of Fit

In order to determine how good our predictors are, a goodness of fit measure for each data set is computed. Specifically, we compare the vector of target values for regression ($\bar{\text{y}}$), i.e. metrics as a function of BER, to the vector of output from regression ($\bar{\text{t}}$). The two goodness of fit measures are 1) normalised mean-squared error ($\hat{e}$), and 2) coefficient of correlation (κ).

The first is a simple error minimisation computation given by

$$\hat{e} = \frac{\mathcal{E}\{(\bar{\text{t}} - \bar{\text{y}})^2\}}{\text{var}(\bar{\text{t}})} \quad (6.2)$$

where $\hat{e} = 0$ is a perfect match. The second is also useful in determining the relationship between the metric and estimate. For a given set of variables, we use κ to give us the linear relationship between these variables. It is defined in terms of their covariance and standard deviations, denoted by $\sigma_{\bar{t}}$ and $\sigma_{\bar{y}}$, given by

$$\kappa = \frac{\text{cov}(\bar{t}, \bar{y})}{\sigma_{\bar{t}}\sigma_{\bar{y}}} \tag{6.3}$$

where $-1 \leq \kappa \leq 1$. The coefficient of correlation provides a quick and easy way to view the correlation between two variables. If there is no relationship then $\kappa = 0$ and if there is a perfect positive match $\kappa = 1$. If there is an inverse relationship, where one set of variables increases while the other decreases, then κ will be negative.

6.3 BER versus Metrics

In Figure 6.4, the comparison of BER performance to metrics is displayed for V-BLAST [56] and Jafarkhani's STBC [67]. Tables 6.1 and 6.2 summarise the fitness metrics for route AB20 using V-BLAST and STBC. Not all metrics are suitable for prediction, as very few of them demonstrate an observable trend. The following conclusions can be made:

- Diversity $\Psi(\mathcal{H})$, and correlation $\Phi(\mathcal{H})$, are poor predictors;
- Normalised parallel channel gain $\overline{CG}(\mathcal{H})$, normalised parallel channel capacity $\overline{CC}(\mathcal{H})$, and average signal strength $P(\mathcal{H})$ are weak predictors;
- Effective rank $\overline{R}(\mathcal{H})$ is not suitable for prediction; and
- Mutual information $\overline{I}(\mathcal{H})$ is a good predictor, but not well suited for high SNRs.

Table 6.1: Summary of fitness for Figure 6.4(a)

Fitness	Ψ	Φ	R	P	I	$\overline{CC}$	$\overline{CG}$
$\hat{e}$	0.824	0.824	0.915	0.796	0.385	0.832	0.712
κ	0.406	0.406	0.269	0.439	0.781	0.396	0.528

Table 6.2: Summary of fitness for Figure 6.4(b)

Fitness	Ψ	Φ	R	P	I	$\overline{CC}$	$\overline{CG}$
$\hat{e}$	0.992	0.993	0.981	0.506	0.141	0.994	0.808
κ	4.02×10^{-2}	2.78×10^{-2}	0.116	0.701	0.926	1.58×10^{-2}	0.433

As observed in Figure 6.4, effective rank has a distribution that 'groups' at levels bounded between 1 and $U = \min(N, M)$. The clustering of points at any given level will dominate the slope of the regression line. Therefore, effective rank, regardless of the type of MIMO scheme, is a poor performance predictor.

The fitness metrics indicate that the regression of mutual information is a good indicator of V-BLAST and STBC BER performance. V-BLAST performance is very poor for any $\gamma < 8$ dB so that no regression can be applied. Similarly, average received signal power was also a weak predictor. We consider received signal power to be a natural extension to mutual information and omit its analysis.

If mutual information is a good predictor, then the eigenvalue decomposition of the argument of the argument of it may also be a good performance indicator. The eigenvalues of $\mathrm{R} = \mathcal{E}\{\mathrm{HH}^H\}$ are plotted against the BER for V-BLAST and STBC for route AB20 in Figures 6.5 and 6.6 for BERs lower than 10^{-1} (vertical dashed line). We remind the reader that $\lambda_1 \leq \lambda_2 \leq \lambda_3 \leq \lambda_4$ is the convention used in this thesis for a 4×4 system. Tables 6.3 through 6.6 summarise the goodness of fit for the regression lines in Figures 6.5 and 6.6.

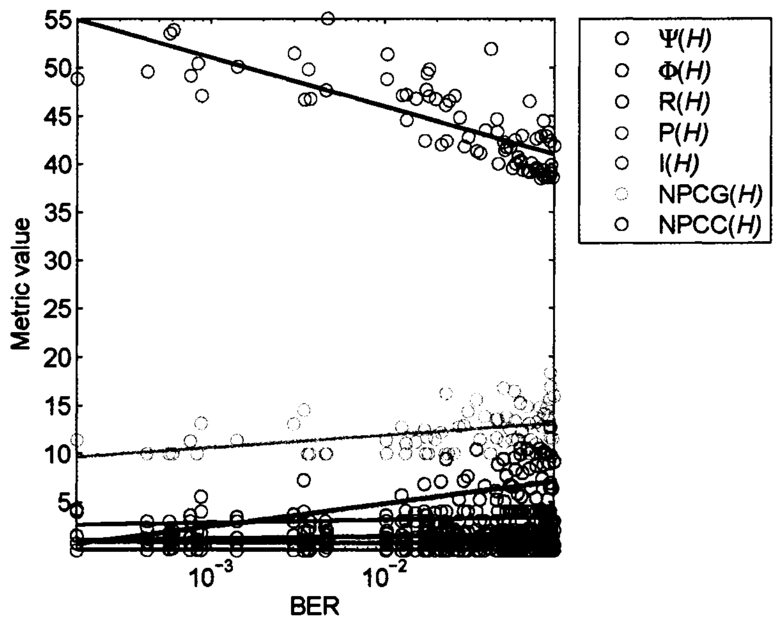

(a) V-BLAST, $\gamma = 16$ dB

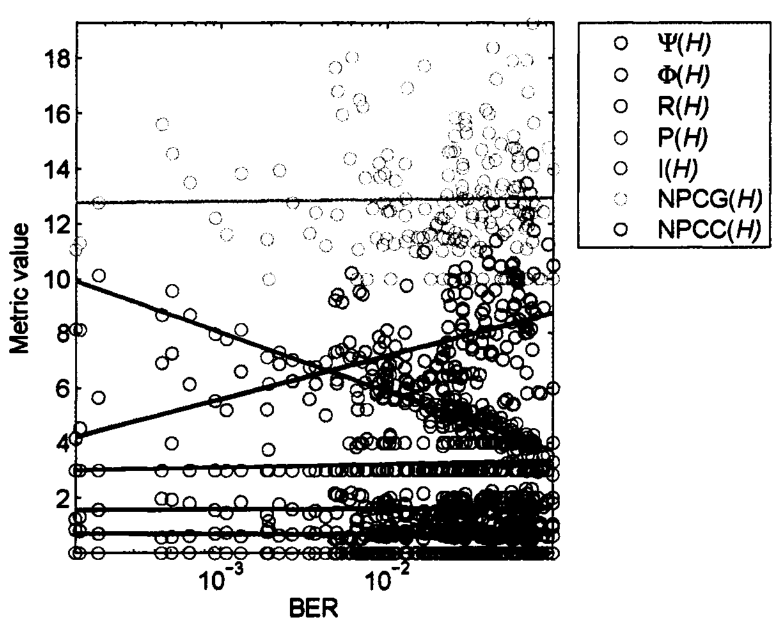

(b) STBC, $\gamma = 6$ dB

Figure 6.4: AB20 BER versus metric comparison where regression (solid) and metric data (circle) are the line types.

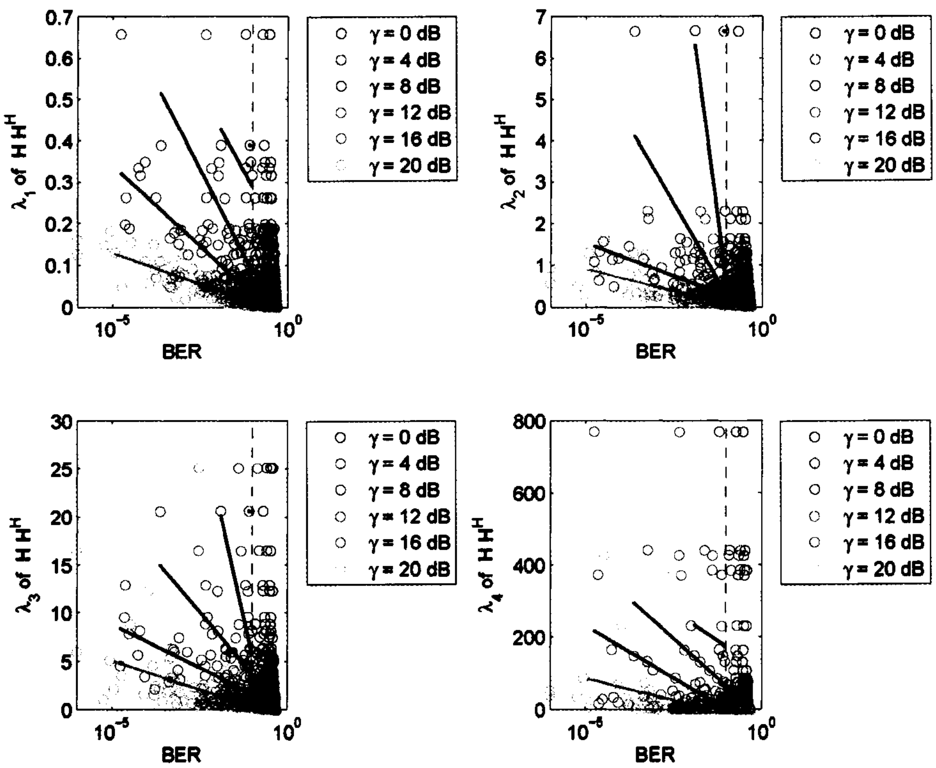

Figure 6.5: BER versus λ for AB20 using V-BLAST.

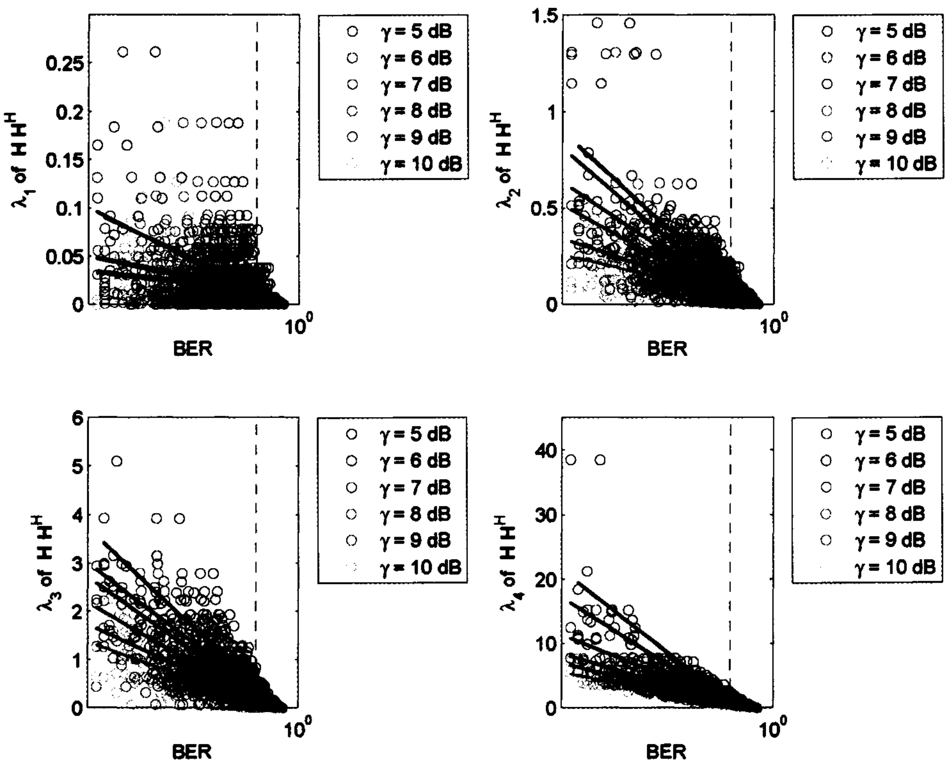

Figure 6.6: BER versus λ for AB20 using STBC.

Table 6.3: Normalised mean-square error ($\hat{e}$) fitness for V-BLAST on route AB20

γ (dB)	0	4	8	12	16	20
λ_1	-	-	0.817	0.462	0.324	0.383
λ_2	-	-	0.133	0.482	0.521	0.502
λ_3	-	-	0.265	0.685	0.778	0.831
λ_4	-	-	0.884	0.889	0.760	0.839

Table 6.4: Coefficient of correlation (κ) fitness for V-BLAST on route AB20

γ (dB)	0	4	8	12	16	20
λ_1	-	-	0.285	0.722	0.820	0.784
λ_2	-	-	0.922	0.707	0.687	0.703
λ_3	-	-	0.838	0.538	0.461	0.405
λ_4	-	-	7.29×10^{-2}	0.280	0.48	0.39

Table 6.5: Normalised mean-square error ($\hat{e}$) fitness for STBC on route AB20

γ (dB)	5	6	7	8	9	10
λ_1	0.853	0.798	0.948	0.935	0.972	0.970
λ_2	0.551	0.532	0.557	0.570	0.687	0.765
λ_3	0.408	0.447	0.431	0.496	0.570	0.596
λ_4	0.218	0.272	0.110	0.125	0.146	0.156

Table 6.6: Coefficient of correlation (κ) fitness for STBC on route AB20

γ (dB)	5	6	7	8	9	10
λ_1	0.377	0.445	0.216	0.244	0.150	0.156
λ_2	0.668	0.682	0.663	0.653	0.556	0.481
λ_3	0.768	0.742	0.753	0.708	0.654	0.633
λ_4	0.884	0.852	0.943	0.935	0.934	0.918

While one might expect one eigenvalue to be a good predictor for both MIMO technologies, the results are quite interesting. It is observed that 1) the smallest eigenvalue is the best predictor of V-BLAST BER performance and 2) the largest eigenvalue is the best predictor for STBC performance given simulations using measured channel data.

The receive probability of error is strongly linked to the minimum distance d_{min} of the elements of the received vectors of $\mathbf{X}$ as seen in Chapter 2. Burel [28] showed that the relationship between the minimum distance and the smallest singular value of $\mathbf{H}$, σ_{min}, given by

$$d_{min} \geq \sigma_{min} d_0 \tag{6.4}$$

where d_0 is the minimum distance between the elements of $\mathcal{S} = \{\mathbf{s}_i\}$, the set of all possible transmitted vectors. The above result shows that a large value of σ_{min}, where $\lambda = \sigma^2$, assures a large value of d_{min}. A large value of d_{min}, i.e. a large minimum singular value (or eigenvalue), assures a low probability of error for a given spatial modulation scheme [31].

The largest eigenvalue, λ_{max}, is also useful for characterising channel behaviour. In [31] it was stated that the performance of diversity transmission is influenced by the Frobenius norm of the channel, given by

$$||\mathbf{H}||_F^2 = \sum_{i,j} |h_{ij}|^2. \tag{6.5}$$

The eigenvalues are also related to (6.5) by

$$||\mathbf{H}||_F^2 = \sum_{i} \lambda_i. \tag{6.6}$$

In (6.6) it is seen that with respect to correlation, the eigenmode corresponding to λ_{max} carries a significant portion of power. Thus, 'good' channels convey as much power as possible regardless of channel rank.

Collectively, the normalised mean-square error and coefficient of correlation indicate that the smallest and largest eigenvalues of $\mathbf{R} = \mathcal{E}\{\mathbf{H}\mathbf{H}^H\}$ are the best choices for predicting BER performance for V-BLAST and STBC, respectively.

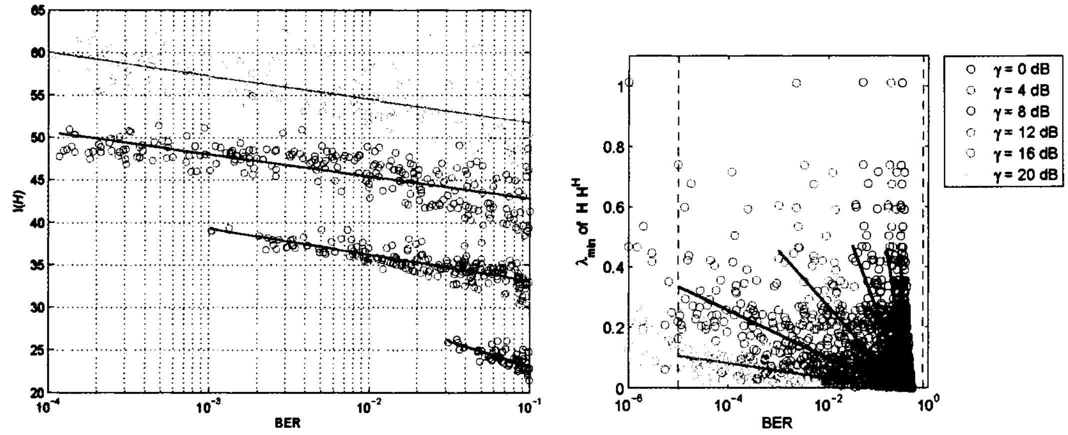

(a) $\overline{I}(\mathcal{H})$ (b) λ_{min}

Figure 6.7: V-BLAST performance prediction of FA20.

6.4 Results

It was demonstrated previously that mutual information and the associated largest and smallest eigenvalues are good BER performance predictors for a given MIMO technique. Using measurement data from all routes (Chapter 4-5) and simulated BER results (Chapter 6), the performance prediction is carried out for different microcells in Ottawa. Prediction is shown for V-BLAST and STBC over the useable operating SNRs from Chapter 2, i.e. 0-20 dB for V-BLAST and 5-10 dB for STBC.

6.4.1 V-BLAST

V-BLAST detector performance was evaluated using mutual information, $\overline{I}(\mathcal{H})$ and the smallest eigenvalue, λ_{min}. Note that all plots do not appear in this section. The plots with fewer data points, i.e., MQ30, AB35 and CC25 can be found in Appendix B. The plots using λ_{min} uses vertical dashed lines to indicate the regions of regression.

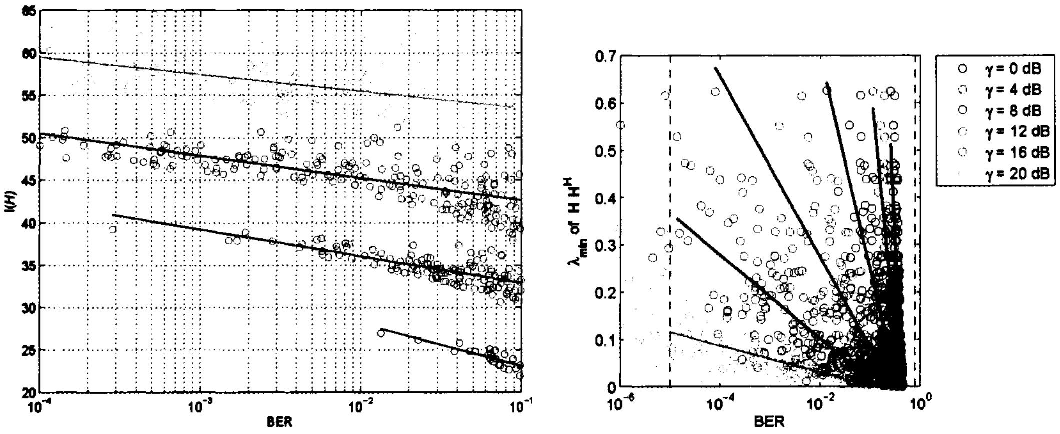

(a) $\overline{I}(\mathcal{H})$ (b) λ_{min}

Figure 6.8: V-BLAST performance prediction of DD15.

Figure 6.7 shows the performance prediction for FA20 using $\overline{I}(\mathcal{H})$ and λ_{min}. The results show that predictions for V-BLAST are good above SNRs of 8 dB using mutual information. At SNRs lower than 8 dB, no information can be obtained due to poor performance. The best overall fit for spatial multiplexing is achieved at 20 dB.

Figures 6.8 and 6.9 show the performance prediction for routes DD15 and EF0. The prediction for DD15 shows the same trend as observed in FA20 for $\gamma \geq 8$ dB. The best fit is observed for 12 dB. Performance cannot be determined for 0 and 4 dB using V-BLAST since performance is too poor.

In Figure 6.9 the prediction result is somewhat similar to DD15. Geographically, the routes are different but the BER prediction results are very similar, i.e., the slopes of the regression lines (solid) are only a few decimal places different.

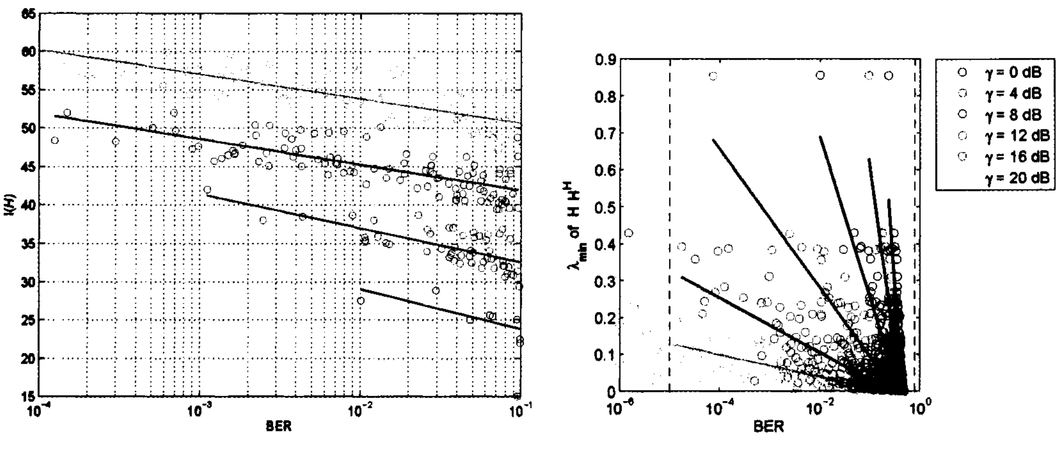

(a) $\overline{I}(\mathcal{H})$ (b) λ_{min}

Figure 6.9: V-BLAST performance prediction of EF0.

Figure 6.10 shows the performance prediction for AB20. The results for rural Ottawa follow those of urban and suburban. V-BLAST performance is only comparable for $\gamma \geq 8$ dB and the best prediction is available at high SNRs. The spacing between regression lines appears to be smaller when compared to FA20 or DD15 possibly attributed to the lack of data points in the set. It was observed earlier that the received signal power for AB20 dropped significantly as the mobile approached the end of the route.

6.4.2 STBC

Jafarkhani's STBC [67] was evaluated using mutual information, $\overline{I}(\mathcal{H})$, and the largest eigenvalue, λ_{max}. The same presentation as found in Section 6.4.1 is followed here; the other plots can be found in Appendix C. The regression regions are also indicated by vertical dashed lines.

Figure 6.11 shows the performance prediction for FA20 using $\overline{I}(\mathcal{H})$ and λ_{max}. The results for STBC are more pronounced than those observed with V-BLAST. The regression of mutual information appears to be very tight for low SNRs.

Figure 6.12 and 6.13 show the performance prediction for routes DD15 and EF0. The

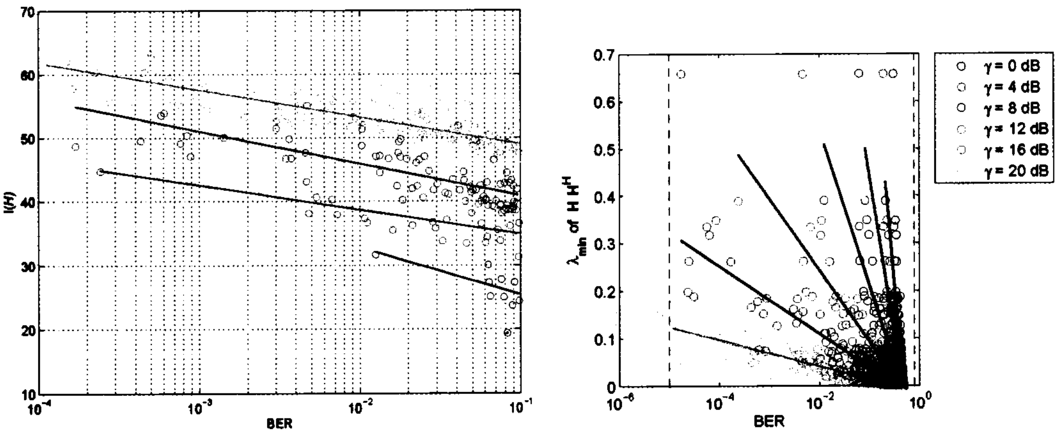

(a) $\bar{I}(\mathcal{H})$ (b) λ_{min}

Figure 6.10: V-BLAST performance prediction of AB20.

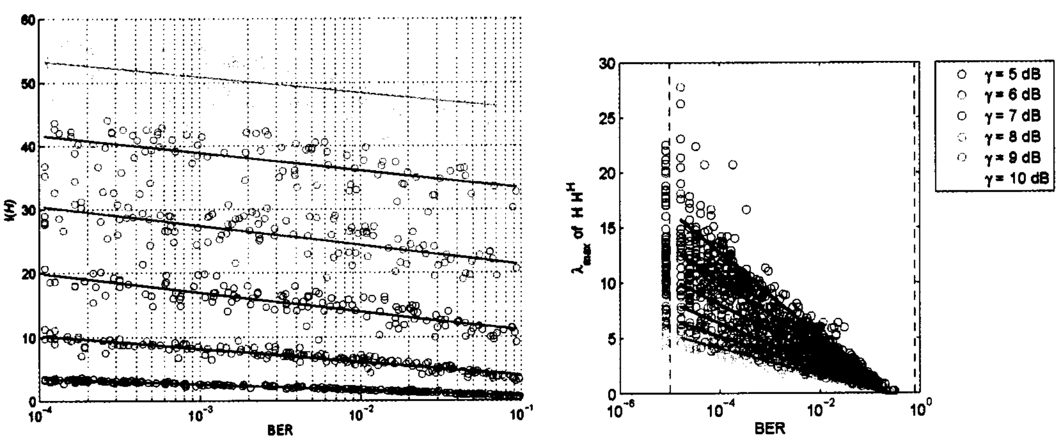

(a) $\bar{I}(\mathcal{H})$ (b) λ_{max}

Figure 6.11: STBC performance prediction of FA20.

results for DD15 and EF0 appear to look similar in terms of their regression for mutual information. Prediction using λ_{max} shows a slightly different result. In both cases, the best range of result is given for $\gamma = 5$ dB. The best fit appears to be over AB20 where the observed correlation was high and comparable to EF0. At low SNRs the regression line is indeed very tight for mutual information and the largest eigenvalue.

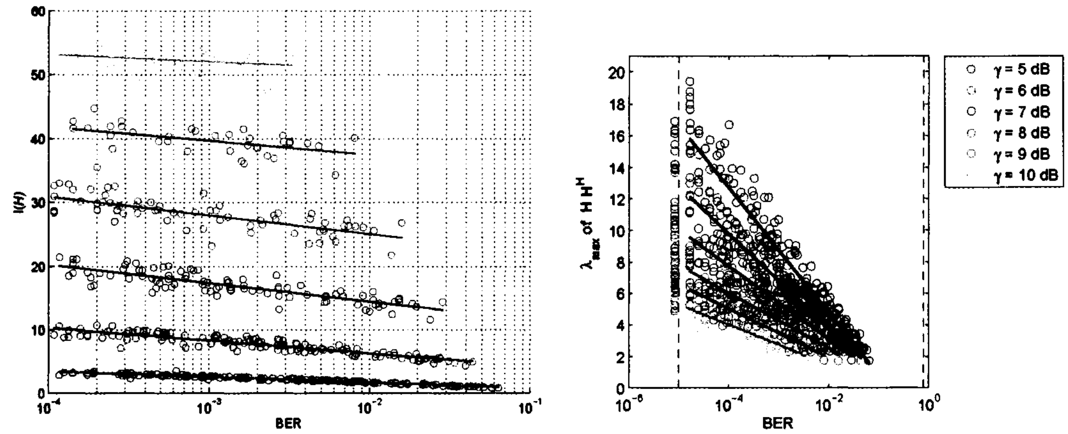

(a) $\overline{I}(\mathcal{H})$ (b) λ_{max}

Figure 6.12: STBC performance prediction of DD15.

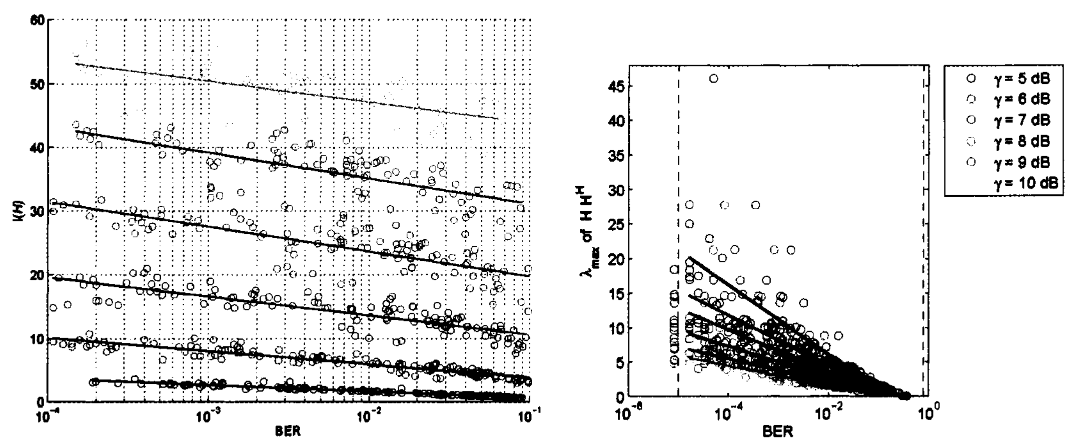

(a) $\overline{I}(\mathcal{H})$ (b) λ_{max}

Figure 6.13: STBC performance prediction of EF0.

6.4.3 Regression Slope versus SNR

The BER prediction results are interesting as they lend insight into estimation of the performance of MIMO techniques in an environment. However, mutual information, or the upper bound on achievable data rates for the channel, are not key parameters of interest as observed.

The relative slopes of the predictions using mutual information and eigenvalues indicate

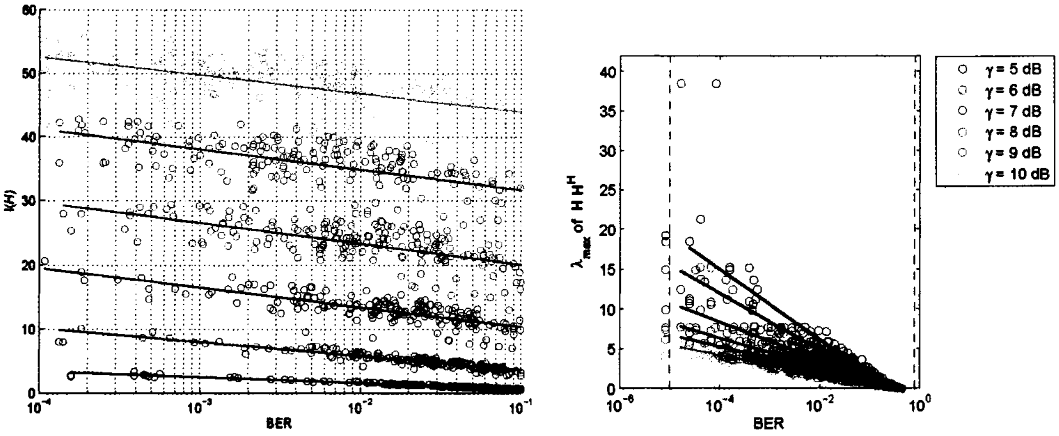

(a) $\bar{I}(\mathcal{H})$ (b) λ_{max}

Figure 6.14: STBC performance prediction of AB20.

that a slight relation may exist. Figures 6.15 and 6.16 show the results of a comparison between MIMO technique SNR and slope of the applied regression. Using mutual information, results indicate a slight correlation between the regression slope and SNR. Only portions of the operating SNR appear to demonstrate a trend, i.e., $\gamma \geq 12$ dB for V-BLAST and $\gamma \leq 7$ dB for STBC.

Using the eigenvalues, λ_{min} and λ_{max}, the plots indicate that a strong correlation exists, i.e. the slope is almost linear indicating that the eigenvalues are independent of location. The same is not true for mutual information. It is clear that a link between BER performance and parameters of the MIMO channel exist. Analysis using higher-order metrics and regressions may result in better estimations of BER performances. However, results indicate that system designers need to consider using both the channel eigenvalues and mutual information when deploying a MIMO communications system.

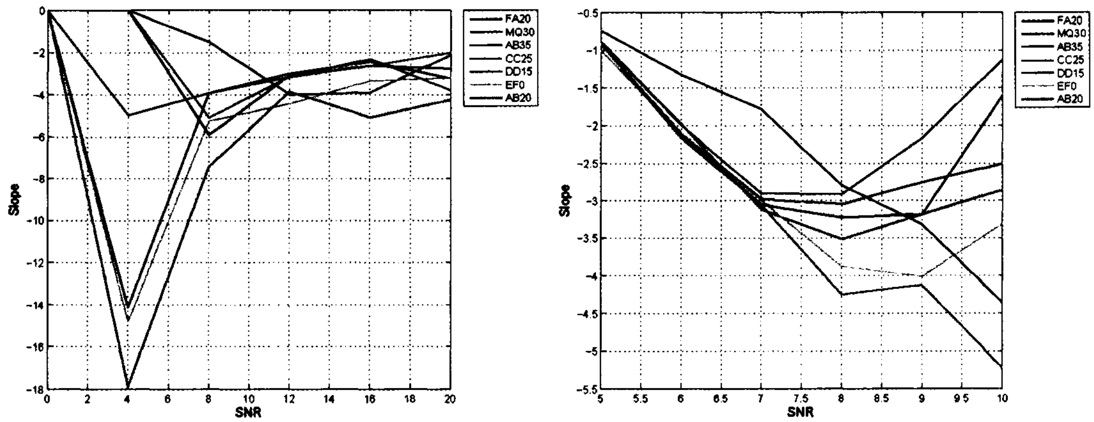

(a) V-BLAST

(b) STBC

Figure 6.15: Slope versus SNR using $\overline{I}(\mathcal{H})$.

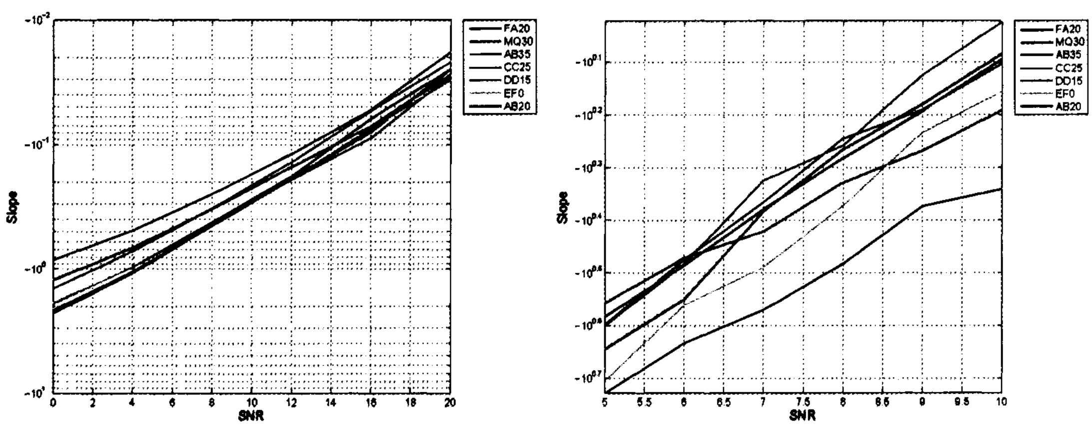

(a) V-BLAST

(b) STBC

Figure 6.16: Slope versus SNR using λ_{min} and λ_{max}.

Chapter 7

Conclusions

This thesis has presented a characterisation of outdoor MIMO channels. The data from an extensive outdoor measurement campaign was analysed and used to simulate the BER performance of different MIMO techniques. CRC has logged a vast amount of measurement hours in cataloging the mobile radio channel. The BER performance of V-BLAST and STBC was found to be linked to the eigenvalues [75–77] of the channel and less on the available mutual information.

7.1 Summary of the Thesis

Chapter 1 provided an introduction to the thesis, including the motivation for a robust wireless system, the need for accurate and detailed characterisations of the channel and a literature survey. The chapter concludes with the contributions and structure of this thesis.

In Chapter 2, a short review of the radio channel, including propagation characteristics, signal fading distributions, and appropriate channel scattering models was given. The chapter includes a survey of quantitative descriptors, i.e., channel metrics, found in the literature for radio channel qualifications followed by a summary of space-time architecture and block coding schemes used in this thesis.

Chapter 3 described the system model utilised for channel sounding, including an appropriate mathematical channel model. A well known method for channel impulse response extraction [72] was used, including a method for estimating noise and subtracting its contribution from mutual information. The final portion of this chapter was dedicated to determining the appropriate subset of channel metrics suitable for characterising performance of a mobile radio channel, i.e., V-BLAST and orthogonal STBC using QPSK modulation.

Chapter 4 described the outdoor measurement campaign in Ottawa, measurement setup, and presented a detailed description for each location.

Chapter 5 presented the parameterisation of all routes using the metrics given in Chapter 3, and discussed the trends associated with the mobile position in the local environment.

Chapter 6 described the method used to determine which metrics are suited to predict BER performance using measured data, i.e. eigenvalues preferred over mutual information. The possible candidates were subjected to a fitness test to determine the best and weak BER predictors for V-BLAST and STBC. Contrary to statements made in [2, 27, 32, 78] mutual information is not the strongest MIMO performance predictor.

7.2 MIMO Technique Conclusions

There are a few general conclusions about MIMO techniques that were observed based on the results from Chapter 6. They are as follows:

Channel Model A double scattering channel model is a useful tool for simulating outdoor conditions in the mobile radio channel.

Performance Not all MIMO techniques are suited to a particular location. It was observed that V-BLAST and STBC performance depended on amount of correlation present in the channel. It was observed in Chapter 2 that V-BLAST performance degrades with correlation and STBC improves with it. With block coding, correlation improved the effective SNR, while the code structure exploited temporal diversity to main performance in low rank conditions. The same is not true for V-BLAST due to high spatial correlation.

Mobile position Using the metrics and simulated BER results, it is possible to estimate the mobile position in the channel using diversity or correlation [58].

The performance of MIMO transmission is linked to the channel behaviour. It was reported in [41] that the channel characteristics impact the eigenvalue distribution of the channel's autocorrelation matrix, thus affecting mutual information and the performance of V-BLAST and STBCs.

7.3 Location Conclusions

There are a number of location conclusions which can be drawn:

LOS and non-LOS Depending on the placement of the transmitter in an environment, a strong specular component may exist which can impact performance. In the urban case, a strong dominant component was observed where diversity was low which coincided with the mobile position being inline with the transmitter.

Multipath effects In an urban street corridor, multipath tunneling affects system performance. A strong signal propagates down the street, multipath components reflected off buildings are attenuated, resulting in a dominant component along the street. Thus, high correlation is observed.

Mobile position In an urban center, it was found that diversity may be used to extrapolate position. The opposite is true for correlation and suburban environments.

Correlation For the urban case, there is a high amount of scatterers at an intersection including buildings. However, in suburban areas, there are fewer scatterers present leading to higher correlation. The small angular spread in urban corridors gives rise to high correlation.

7.4 Channel Metric Conclusions

In MIMO communication systems, there exist many different channel parameterisations to quantify channel behaviour over time. However, only a few of these parameters can be used to describe BER performance. Three classes of predictors are: poor, weak and strong.

Poor predictors Channel metrics such as diversity and correlation are poor indicators in predicting values for BER performance of different MIMO techniques. However, they are linked to the position of the mobile in the channel. Effective rank is not suitable for prediction of BER performance due to the resulting distribution observed in this thesis, i.e. $R=\{1,2,3,4\}$.

Weak predictors Normalised parallel channel gain and normalised parallel channel capacity are weak predictors. A small trend was observed in the BER comparison for the MIMO techniques however the goodness of fit measures indicated that these metrics rated poorly when fitted by regression.

Strong predictors Mutual information, average signal strength and the channel eigenvalues were good metrics for performing BER prediction.

The best predictors are discussed next in least to best ability to predict performance of a given MIMO technique.

Mutual information The amount of mutual information available in the channel proved to be a good predictor of BER performance. The results from fitness testing showed that its ability to predict a trend in the channel was good. However, results showed that its usefulness for a given technique was limited at high and low SNRs.

Smallest eigenvalue The smallest eigenvalue was found to have an impact on V-BLAST BER performance, linked to the minimum distance between received signal vectors. V-BLAST performance relies on the channel links being uncorrelated and a certain value of λ_{min} could guarantee this [28]. It was seen that performance could be predicted but only with a high SNR.

Largest eigenvalue The largest eigenvalue was found to have an impact on STBC BER performance. Correlation increases the largest eigenvalue which raises the average SNR of the received signal and thus improves STBC performance.

Although effective rank and normalised averaged mutual information are insensitive to path loss, it was found after then removing the effects of path-loss, both performed poorly as predictors. Also, high received signal power does not guarantee good performance, as observed with MQ30 and AB20. The best BER prediction so far has been demonstrated using the eigenvalue decomposition of the spatial correlation matrix over available mutual information. This prediction was also independent of the location of the mobile in the environment. Performance of V-BLAST was linked to the smallest eigenvalue, λ_{min}, while STBC performance was linked to the largest eigenvalue, λ_{max}.

7.5 Future Work

In this thesis we have looked at the characterisation of a 4×4 wireless MIMO channel in a variety of outdoor locations. There exists the possibility of extending the scope of this work to a 8×8 system as described in [40]. Many other research topics can be carried out as an extension of this research, such as the following:

Future analysis A more sophisticated evaluation needs to be carried out, i.e. taking a combination of channel metrics to get a better prediction.

Higher order metric analysis A second order linear regression analysis could reveal other valuable metrics for channel characterisation.

More testing Further testing of the predictions could be carried out in other environments to see if the results found in this research are reliable.

MIMO techniques Spatial multiplexing and STBC are not the only types of MIMO techniques that exist [61]. Eigenbeamforming, for example, is another type of technique [41, 48] that could be explored using the results in this thesis.

Perhaps comparing the trade-off between diversity and spatial-multiplexing could be explored. The MIMO techniques V-BLAST and STBC were kept separate in this thesis. However, research in [61] looked at combining spatial multiplexing and STBC using correlated fading channels. The research presented in this thesis could be applied to predict performance of a new and possibly better MIMO technique.

Appendix A

Route Maps

This appendix provides satellite maps for the routes used in this thesis. Some of these images are available online via the Google Maps portal interface.

Figure A.1: Transmitter range of view from Minto Place.

Figure A.2: Satellite map for suburban Ottawa; Transmitter indicated in red and measurement points of interested in blue. © Google, NAVTEQ Imagery, 2005.

Figure A.3: Satellite map for rural Ottawa; Route indicated by red arrow and transmitter indicated by circle. © Google, NAVTEQ Imagery, 2005.

Appendix B

V-BLAST Performance Prediction Results

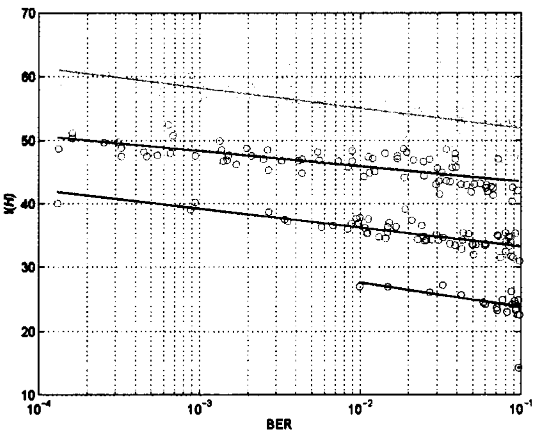

(a) $\bar{I}(\mathcal{H})$

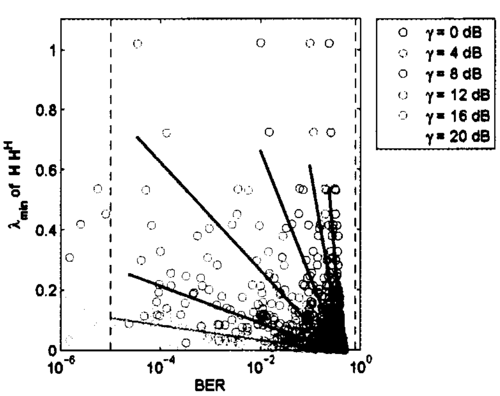

(b) λ_{min}

Figure B.1: V-BLAST performance prediction of MQ30.

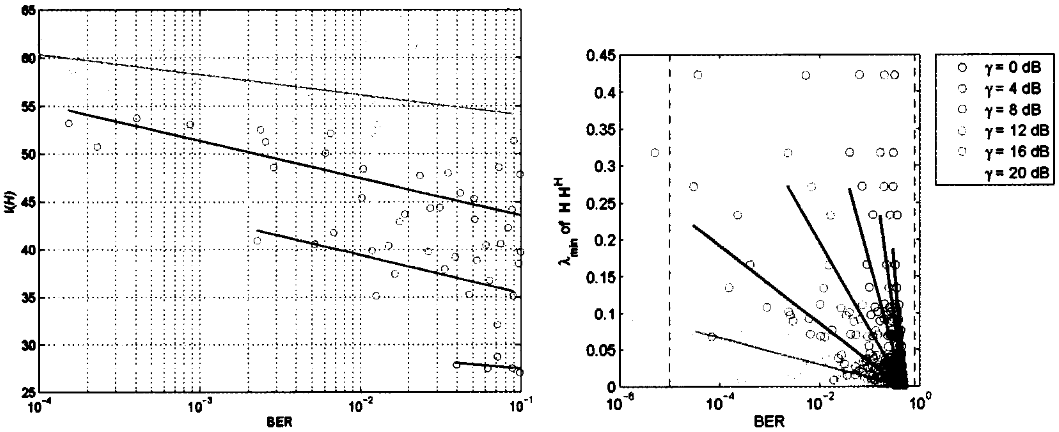

(a) $\overline{I}(\mathcal{H})$ (b) λ_{min}

Figure B.2: V-BLAST performance prediction of AB35.

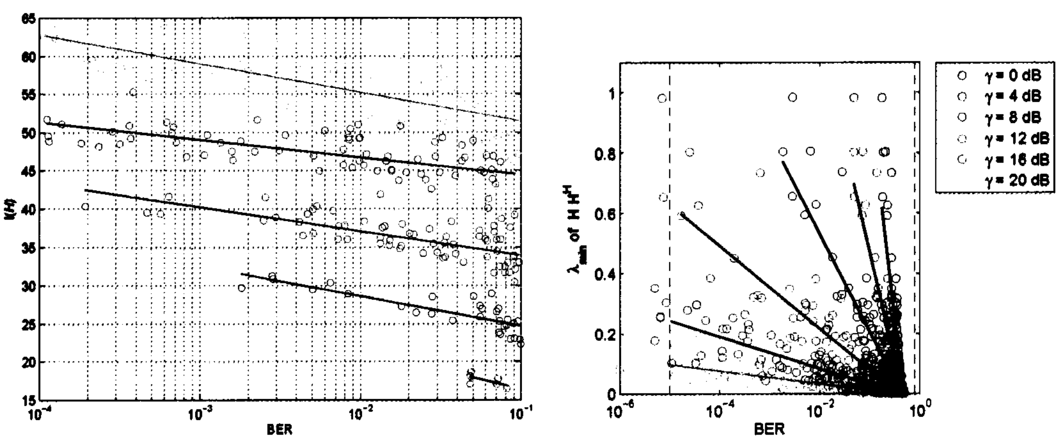

(a) $\overline{I}(\mathcal{H})$ (b) λ_{min}

Figure B.3: V-BLAST performance prediction of CC25.

Appendix C

STBC Performance Prediction Results

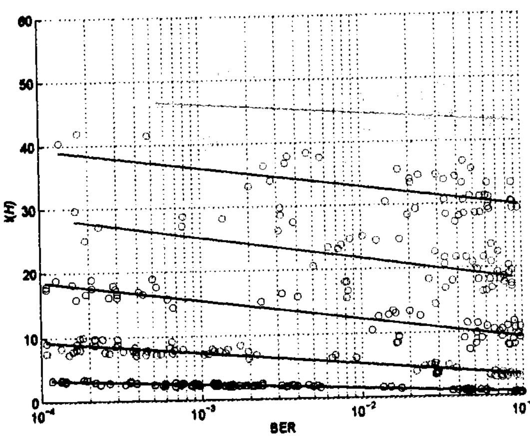

(a) $\mathcal{I}(\mathcal{H})$

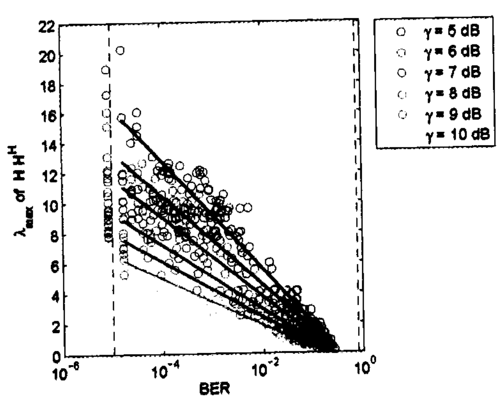

(b) λ_{min}

Figure C.1: STBC performance prediction of MQ30.

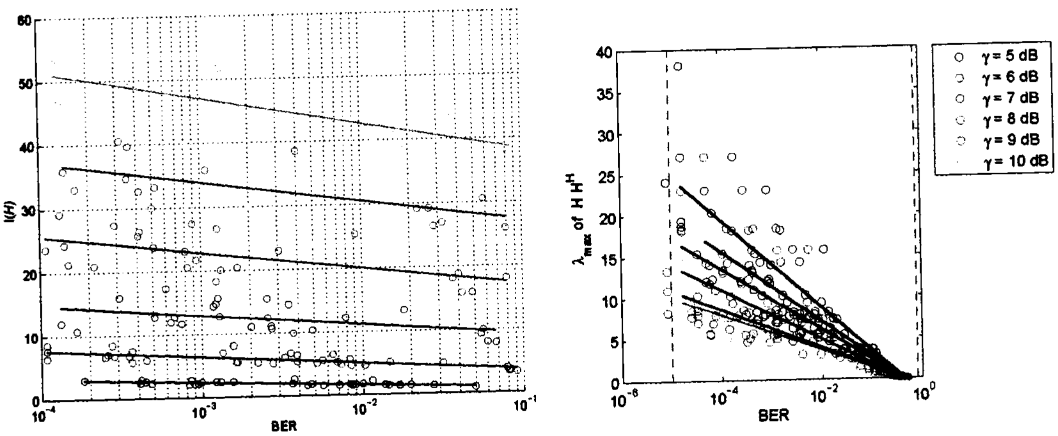

(a) $\bar{I}(\mathcal{H})$ (b) λ_{min}

Figure C.2: STBC performance prediction of AB35.

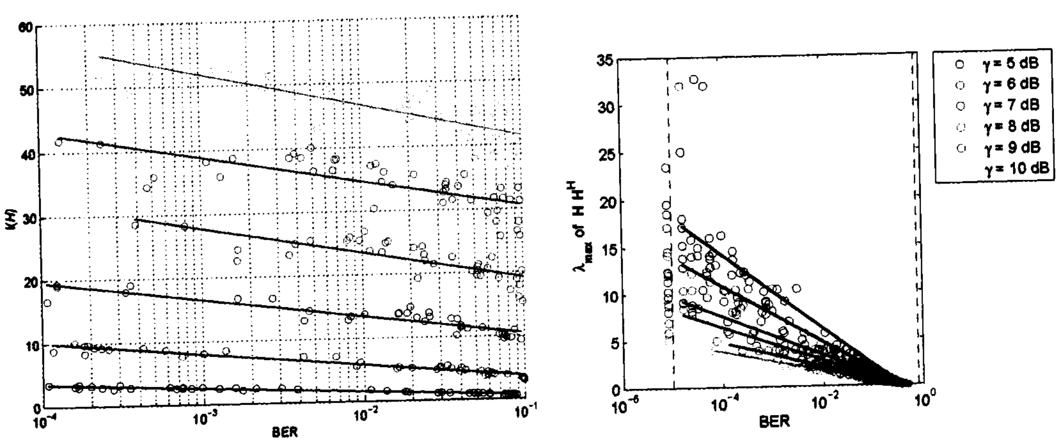

(a) $\bar{I}(\mathcal{H})$ (b) λ_{min}

Figure C.3: STBC performance prediction of CC25.

Bibliography

[1] J. Wallace and M. Jensen, "Spatial characteristics of the MIMO wireless channel: experimental data acquisition and analysis," in *Proc. ICASSP 2001 - IEEE Int. Conf. Acoust. Speech and Signal Processing*, vol. 4, (Salt Lake City, Utah), pp. 2497–2500, May 2001.

[2] J. Ling, D. Chizhik, P. Wolinansky, R. Valenzuela, N. Costa, and K. Huber, "MIMO measurement in Manhattan," in *Proc. PIMRC 2002 - IEEE 13th Int. Symp. on Pers., Indoor and Mobile Radio Commun.*, vol. 4, (Lisboa, Portugal), pp. 1631–1635, Sept. 2002.

[3] S. Howard, H. Inanoglu, J. Ketchum, M. Wallace, and R. Walton, "Results from MIMO channel measurements," in *Proc. PIMRC 2002 - IEEE 13th Int. Symp. on Pers., Indoor and Mobile Radio Commun.*, vol. 4, (Lisboa, Portugal), pp. 1932–1936, Sept. 2002.

[4] A. Molisch, "Effect of far scatter clusters in MIMO outdoor channel models," Tech. Rep. TR-2003-38, Mitsubishi Electric Research Laboratory, May 2003.

[5] D. Gesbert, H. Bolcskei, D. Gore, and A. Paulraj, "Outdoor MIMO wireless channels: Models and performance prediction," *IEEE Trans. Commun.*, vol. 50, pp. 1926–1934, Dec. 2002.

[6] U. Martin, "Spatio-temporal radio channel characteristics in urban macrocells," in *IEE Proc. Radar, Sonar and Navigation*, vol. 145, pp. 42–49, Feb. 1998.

[7] A. Kuchar, J.-P. Rossi, and E. Bonek, "Directional macro-cell channel characterization from urban measurements," *IEEE Trans. Antennas Propagat.*, vol. 48, pp. 137–146, Feb. 2000.

[8] P. Pajusco, "Experimental characterization of DOA at the base station in rural and urban area," in *Proc. VTC 1998 Spring IEEE 48th Vehicular Technology Conf.*, vol. 2, (Ottawa, Canada), pp. 993–997, May 1998.

[9] M. Toeltsch, J. Laurila, A. Molisch, K. Kalliola, P. Vainikainen, and E. Bonek, "Spatial characterization of urban mobile radio channels," in *Proc. VTC 2001 Spring - IEEE 53rd Vehicular Technology Conf.*, vol. 1, (Rhodes, Greece), pp. 399–403, May 2001.

[10] H. Asplund and J.-E. Berg, "Estimation of scatterer locations from urban array channel measurements at 1800 MHz," in *Proc. Radio Vetenskap och Kommunikation (RVK'99)*, (Karlskrona, Sweden), pp. 136–140, June 1999.

[11] G. Foschini and M. Gans, "On limits of wireless communications in a fading environment when using multiple antennas," *Wireless Personal Communications*, vol. 6, pp. 311–335, 1998.

[12] I. Telatar, "Capacity of multi-antenna Gaussian channels," *European Transactions on Telecommunications (ETT)*, pp. 585–595, Nov. 1999.

[13] A. Goldsmith, S. Jafar, N. Jindal, and S. Vishwanath, "Capacity limits of MIMO channels," *IEEE J. Select. Areas Commun.*, vol. 21, pp. 684–702, June 2003.

[14] B. Sklar, "Rayleigh fading channels in mobile digital communication systems part I: Characterization," *IEEE Commun. Mag.*, pp. 136–146, Sept. 1997.

[15] E. Biglieri, J. Proakis, and S. Shamai, "Fading channels: information-theoretic and communications aspects," *IEEE Trans. Inform. Theory*, vol. 44, pp. 2619–2692, Oct. 1998.

[16] M. Ozdemir, E. Arvas, and H. Arslan, "Dynamics of spatial correlation and implications on MIMO systems," *IEEE Commun. Mag.*, vol. 42, pp. S14–S19, June 2004.

[17] D.-S. Shiu, G. Foschini, M. Gans, and J. Kahn, "Fading correlation and its effect on the capacity of multielement antenna systems," *IEEE Trans. Commun.*, vol. 48, pp. 502–513, Mar. 2000.

[18] C.-N. Chuah, D. N. Tse, J. Kahn, and R. Valenzuela, "Capacity scaling in MIMO wireless systems under correlated fading," *IEEE Trans. Inform. Theory*, vol. 48, pp. 637–650, Mar. 2002.

[19] M. Ivrlač, W. Utschick, and J. Nossek, "Fading correlations in wireless MIMO communications systems," *IEEE J. Select. Areas Commun.*, vol. 21, pp. 819–827, June 2003.

[20] M. Ivrlač, T. Kurpjuhn, C. Brunner, and W. Utschick, "Efficient use of fading correlations in MIMO systems," in *Proc. VTC 2001 Fall - IEEE 54th Vehicular Technology Conf.*, vol. 4, (Atlantic City), pp. 2763–2767, Oct. 2001.

[21] M. Ivrlač and J. Nossek, "On the impact of correlated fading for MIMO-systems," in *Proc. ISCAS 2002 - IEEE Int. Symp. on Circuits and Systems*, vol. 3, (Scottsdale, Arizona), pp. 655–658, May 2002.

[22] C. Oestges, B. Clerckx, D. Vanhoenacker-Janvier, and A. Paulraj, "Impact of diagonal correlations on MIMO capacity: application to geometrical scattering models," in *Proc. VTC 2003 Fall - IEEE 58th Vehicular Technology Conf.*, vol. 1, (Orlando, Florida), pp. 394–398, Oct. 2003.

[23] H. Shin and J. Lee, "Capacity of multiple-antenna fading channels: Spatial fading correlation, double scattering, and keyhole," *IEEE Trans. Inform. Theory*, vol. 49, pp. 2636–2647, Oct. 2003.

[24] D. Chizhik, G. Foschini, M. Gans, and R. Valenzuela, "Keyholes, correlations, and capacities of multielement transmit and receive antennas," *IEEE Trans. Wireless Commun.*, vol. 1, pp. 361–368, Apr. 2002.

[25] L. Xin and N. Zai-ping, "Impact of array orientation on performance of MIMO wireless channels," in *Proc. ICCCAS 4004 - Int. Conf. on Communications, Circuits and Systems*, vol. 1, (Chengdu, China), pp. 254–257, June 2004.

[26] M. Ivrlač and J. Nossek, "Quantifying diversity and correlation in Rayleigh fading MIMO communication systems," in *Proc. ISSPIT 2003 - IEEE 3rd Sig. Proc. and Information Technology*, (Darmstadt, Germany), pp. 158–161, Dec. 2003.

[27] D. Bliss, K. Forsythe, I. Hero, A.O., and A. Yegulalp, "Environmental issues for MIMO capacity," *IEEE Trans. Signal Processing*, vol. 50, pp. 2128–2142, Sept. 2002.

[28] G. Burel, "Statistical analysis of the smallest singular value in MIMO transmission systems," in *Proc. ICSSIP 2002 - Int. Conf. on Signal, Speech and Image Processing*, (Skiathos Island, Greece), Sept. 2002.

[29] J. Heath, R.W. and K. Dandekar, "Characterizations of narrowband MIMO channels," in *Proc. ISWC 2002 - Int. Symp. on Wireless Comm.*, (Victoria, BC), 2002.

[30] K. Dandekar, S. Kawale, L. Dong, and R. Heath, "Electromagnetic characterization of MIMO communication systems," *Submitted to IEEE Transactions on Vehicular Technology*, 2002.

[31] J. Heath, R.W. and A. Paulraj, "Characterization of MIMO channels for spatial multiplexing systems," in *Proc. ICC 2001 - IEEE Int. Conf. Commun.*, vol. 2, (Helsinki, Finland), pp. 591–595, June 2001.

[32] F. Bohagen, P. Orten, and G. Oien, "Construction and capacity analysis of high-rank line-of-sight MIMO channels," in *Proc. WCNC 2005 - IEEE Wireless Commun. and Networking Conf.*, vol. 1, (New Orleans, LA), pp. 432–437, Mar. 2005.

[33] S. Chan-Taw, "Performance analysis of linear detectors using partial decision techniques in multiple antenna systems," Master of Science, University of Ottawa, Ottawa, Ontario, Canada, Dec. 2005.

[34] S. Haykin and M. Moher, *Modern Wireless Communications.* Upper Saddle River, NJ: Prentice Hall, 2005.

[35] W. Jakes, *Microwave Mobile Communications.* New York: Wiley, 1974.

[36] T. Rappaport, *Wireless Communications: Principles and Practice.* New Jersey: Prentice Hall, 2002.

[37] D. Bliss, A. Chan, and N. Chang, "MIMO wireless communication channel phenomenology," *IEEE Trans. Antennas Propagat.*, vol. 52, pp. 2073–2082, Aug. 2004.

[38] G. Foschini, "Layered space-time architecture for wireless communication in a fading environment when using multiple antennas," *Bell Labs Technical Journal*, vol. 1, pp. 41–59, Sept. 1996.

[39] R. Bultitude, T. Willink, M. Herben, and G. Brussard, "Detection of changes in the spectra of measured CW mobile radio data for space wave modelling applications," in *Proc.*

QBSC 2000 - Queen's University Biennial Symp. on Communications, (Kingston, Ontario, Canada), pp. 90–94, May 2000.

[40] C. Squires, T. Willink, and B. Gagnon, "A flexible platform for MIMO channel characterisation and system evaluation," in *Proc. WIRELESS 2003 - 15th Int. Conf. on Wireless Commun.*, (Calgary, Alberta, Canada), July 2003.

[41] T. Willink, "Measurement-based analysis of MIMO system performance in urban microcells," Tech. Rep. CRC-RP-2005-002, Communications Research Centre, Ottawa, Canada., Sept. 2005.

[42] R. Bultitude, G. Brussard, M. Herben, and T. Willink, "Radio channel modeling for terrestrial vehicular mobile applications," in *Proc. ICAP/JINA Millennium Conf. on Antennas and Propagation*, (Davos, Switzerland), Apr. 2000.

[43] P. Smith, L. Garth, and S. Loyka, "Exact capacity distributions for MIMO systems with small number of antennas," *IEEE Commun. Lett.*, vol. 7, pp. 481–483, Oct. 2003.

[44] S. Loyka and A. Kouki, "New compound upper bound on MIMO channel capacity," *IEEE Commun. Lett.*, vol. 6, pp. 96–98, Mar. 2002.

[45] Q. Zhang, X. Cui, and X. Li, "Very tight capacity bounds for MIMO-correlated Rayleigh-fading channels," *IEEE Trans. Wireless Commun.*, vol. 4, pp. 681–688, Mar. 2005.

[46] Y. Murakami, K. Kobayashi, M. Orihashi, and T. Matsuoka, "Analysis of BER performances using channel matrix eigenvalue in MIMO systems under Rayleigh and Rician fading channels," in *Proc. PIMRC 2004 - IEEE 15th Int. Symp. on Pers., Indoor and Mobile Radio Commun.*, vol. 2, (Barcelona, Spain), pp. 1126–1130, Sept. 2004.

[47] B. Getu and J. Andersen, "BER and spectral efficiency of a MIMO system," in *Proc. WPMC 2002 - Wireless Pers. Multimedia Commun.*, vol. 2, (Honolulu, Hawaii), pp. 397–401, Oct. 2002.

[48] T. Willink, "Improving power allocation to MIMO eigenbeams under imperfect channel estimation," *IEEE Commun. Lett.*, vol. 9, pp. 622–624, July 2005.

[49] J. Andersen and J. Nielsen, "Multipath richness–a measure of MIMO capacity in an environment," Tech. Rep. COST 273 TD-04-157, Duisburg, Germany, Sept. 2004.

[50] M. Gans, N. Amitay, Y. Yeh, H. Xu, T. Damen, R. Valenzuela, T. Sizer, R. Storz, D. Taylor, W. MacDonald, C. Tran, and A. Adamiecki, "Outdoor BLAST measurement system at 2.44 GHz: calibration and initial results," *IEEE J. Select. Areas Commun.*, vol. 20, pp. 570–583, Apr. 2002.

[51] P. Eggers, "Dual directional channel formalisms and descriptions relevant for Tx-Rx diversity and MIMO," Tech. Rep. COST 273 TD-03-044, Barcelona, Spain, Jan. 2003.

[52] J. Wallace and M. Jensen, "MIMO capacity variation with SNR and multipath richness from full-wave indoor FDTD simulations," in *Proc. AP-S 2003 - International Symposium Digest*, vol. 2, (Columbus, Ohio), pp. 523–526, June 2003.

[53] C. Squires, G. Colman, and T. Willink, "A performance comparison of diversity strategies for interference and jamming mitigation," in *Proc. WIRELESS 2005 - 17th Int. Conf. on Wireless Commun.*, (Calgary, Alberta, Canada), pp. 433–438, July 2005.

[54] A. Dogandzic and J. Jin, "Estimating statistical properties of MIMO fading channels," *IEEE Trans. Signal Processing*, vol. 53, pp. 3065–3080, Aug. 2005.

[55] P. Kyritsi, "Correlation measures for MIMO systems," Tech. Rep. COST 273 TD-02-037, Espoo, Finland, May 2002.

[56] G. Golden, C. Foschini, R. Valenzuela, and P. Wolniansky, "Detection algorithm and initial laboratory results using V-BLAST space-time communication architecture," *Elect. Lett.*, vol. 35, pp. 14–16, Jan. 1999.

[57] C. Shen, H. Zhuang, L. Dai, and S. Zhou, "Detection algorithm improving V-BLAST performance over error propagation," *Elect. Lett.*, vol. 39, pp. 1007–1008, June 2003.

[58] G. Downes, T. Willink, and C. D'Amours, "Capacity limitations of real MIMO channels and their impact on system performance," in *Proc. WIRELESS 2005 - 17th Int. Conf. on Wireless Commun.*, (Calgary, Alberta, Canada), pp. 100–104, July 2005.

[59] V. Tarokh, N. Sheshadri, and A. Calderbank, "Space-time codes for high data rate wireless communication: performance criterion and code construction," *IEEE Trans. Inform. Theory*, vol. 44, pp. 744–765, Mar. 1998.

[60] Y. L. C. de Jong and T. Willink, "Iterative tree search detection for MIMO wireless systems," *IEEE Trans. Commun.*, vol. 53, pp. 930–935, June 2005.

[61] H. Skjevling, D. Gesbert, and N. Christophersen, "Combining space-time block codes and multiplexing in correlated MIMO channels: An antenna assignment strategy," in *Proc. NORSIG 2003 - 6th Nordic Signal Processing Symposium*, (Bergen, Norway), Oct. 2003.

[62] S. Alamouti, "A simple transmit diversity technique for wireless communications," *IEEE J. Select. Areas Commun.*, vol. 10, pp. 1451–1458, Oct. 1998.

[63] L. He and H. Ge, "A new full-rate full-diversity orthogonal space-time block coding scheme," *IEEE Commun. Lett.*, vol. 7, pp. 590–592, Dec. 2003.

[64] P. Luo and H. Leib, "Full-rate full-diversity space-time code for four-transmit-antenna systems," *IEEE Trans. Wireless Commun.*, vol. 4, pp. 1974–1979, Sept. 2005.

[65] L. Dalton and C. Georghiades, "A full-rate, full-diversity four-antenna quasi-orthogonal space-time block code," *IEEE Trans. Wireless Commun.*, vol. 4, pp. 363–366, Mar. 2005.

[66] H. Van Trees, *Optimum Array Processing*. New York: Wiley, 2002.

[67] H. Jafarkhani, "A quasi-orthogonal space-time block code," *IEEE Trans. Commun.*, vol. 49, pp. 1–4, Jan. 2001.

[68] T. Willink, B. Gagnon, Y. De Jong, and R. Bultitude, "A MIMO measurement and demonstration system for advanced space-time signalling techniques," in *Proc. ANTEM 2002*, (Montreal, QC), July 2002.

[69] K. Kalliola, H. Laitinen, K. Sulonen, L. Vuokko, and P. Vainikainen, "Directional radio channel measurements at mobile station in different radio environments at 2.15 GHz," in *Proc. EPMCC 2001 - 4th European Personal Mobile Communications Conference*, (Vienna, Austria), Feb. 2001.

[70] M. Jensen and J. Wallace, *Space-Time Processing for MIMO Communications*, ch. MIMO Wireless Channel Modeling and Experimental Characterization. Wiley, 2005.

[71] P. Goud Jr., R. Hang, D. Truhachev, and C. Schlegel, "A portable MIMO testbed and selected channel measurements," *EURASIP Journal on Applied Signal Processing*, Nov. submitted for publication.

[72] T. Willink, "Extraction of impulse responses from MIMO measurement data - mark I," Tech. Rep. RRCT-TJW-04-01, Communications Research Centre, Ottawa, Canada., May 2004.

[73] G. Durgin, *Space-Time Wireless Channels*. New Jersey: Prentice Hall, 2003.

[74] A. Swindlehurst, G. German, J. Wallace, and M. Jensen, "Experimental measurements of capacity for MIMO indoor wireless channels," in *IEEE Workshop on Sig. Proc. Adv. in Wireless Comm.*, pp. 30–33, 2001.

[75] R. Gozali and B. Woerner, "On robustness of space-time block codes of spatial correlation," in *Proc. VTC 2002 Spring - IEEE 55th Vehicular Technology Conf.*, 2002.

[76] R. Gozali and B. Woerner, "Theoretic bounds of orthogonal design transmit diversity over independent and correlated fading channels," in *Proc. ISIT 2002 - IEEE Int. Symp. on Inform. Theory*, (Lausanne, Switzerland), 2002.

[77] R. Gozali, R. Mostafa, R. Palat, R. Nory, B. Woerner, and J. Reed, "On performance of orthogonal STBC in indoor and outdoor MIMO wireless channels using analysis, simulation and measurement campaign," *IEEE J. Select. Areas Commun.*, 2002.

[78] J. Wallace, M. Jensen, A. Swindlehurst, and B. Jeffs, "Experimental characterization of the MIMO wireless channel: Data acquisition and analysis," *IEEE Trans. Wireless Commun.*, vol. 2, pp. 335–343, Mar. 2003.